STUDIES ON AXIAL ELONGATION AND TERMINATION OF SEGMENTATION IN THE VERTEBRATE EMBRYO

Annalisa Vezzaro

University College London

and

Cancer Research UK London Research Institute

PhD Supervisor: Dr David Ish-Horowicz,FRS

A thesis submitted for the degree of

Doctor of Philosophy

University College London

September 2011

Declaration

I Annalisa Vezzaro confirm that the work presented in this thesis is my own. Where information has been derived from other sources, I confirm that this has been indicated in the thesis.

Abstract

The vertebrate body is segmented along the anteroposterior axis into repetitive structures, the vertebrae, which derive from embryonic precursors called somites. During development, periodic somite formation is driven by a molecular oscillator, the segmentation clock. Segmentation and elongation of the body axis depend on a population of progenitor cells located at the tail end of the embryo that contributes to axial tissues, including somitic tissue, until the entire embryonic body and the correct number of somites is produced. Although much is known about somite production, it is not known how segmentation and axial elongation come to an end.

In this thesis, I show that termination of chick axial elongation is associated with decline of signals required for maintenance of progenitor cells, implying that down-regulation of these signals triggers depletion of the progenitors. I also show that somite formation decreases as axial elongation comes to an end, suggesting that slow down of the segmentation clock causes somite formation to cease.

I have also explored whether the dose of specific genes is limiting in determining the final somite number in mouse, and I have found that heterozygous mutations of selected genes of the Wnt signalling pathway form fewer somites, indicating that Wnt gene activity might be limiting in controlling the definitive somite number.

I have also investigated the role of *Greb1*, a gene that our laboratory identified as being selectively expressed in the tail region where progenitors reside. I provide evidence that *Greb1* controls axial morphogenesis of the zebrafish embryo by regulating movements required for normal convergence and extension of the embryonic axis during gastrulation. My results possibly provide a link between progenitor contribution to axial elongation and cell movements in the tail.

Acknowledgement

I thank Cancer Research UK for generously funding my PhD, and Sally Leevers, Erin Fortin, Sabina Ebbols and David Bacon for the excellent academic support offered in the past four years.

I am indebted to David Ish-Horowicz, my supervisor, who taught me a lot about science and life. Thank you, David.

I thank my second and third supervisors, Holger Gerhardt and Julian Lewis, for their encouragement during our thesis committee meetings.

A very special thank-you to the current and past members of the Developmental Genetics and Vertebrate Development laboratories: Mark, Ned, Rippei, Sheena, Sophie, Babis, Barbara, Chris, Christina, Emmanuel, Krzysztof, Michael, Ravindra, Cristian, Christian, Maxine, Robert, Adam, Anja, Claudia, Chris, Darren, Despina, Emre, John, Linda, Phil, Russell. Thank you all for your friendship and for the endless scientific and emotional support.

I am most grateful to Anja, Babis, Ned, Rippei, Sophie for their patience in reading this thesis, and for giving many helpful comments on different chapters.

I thank members of the Developmental Biology super-group.

I thank Anne Weston, Lucy Collinson, Mike Bennett, Tim Mohun, Peter Jordan and Daniel Zicha for their expertise and help in various microscopy techniques, and I thank people who provided me reagents and gave helpful advice, especially Marie-Cristine Ramel.

I thank people from the different LRI core facilities, especially David Phillips, Graham Clark, Vicky Dearing, Bradley Spencer-Dene, Clare Watkins, Ian Oliver, July Bee, Scott Lighterness, Gavin Kelly, Probir Chakravarty, and Richard Mitter.

Three people have been exceptionally important to me in the past four years and in my life: my mum, my dad and my boyfriend. This achievement would have never been possible without your valuable support, patience and love.

Thank you to the rest of my family, to my friends in Italy: Fabio, Chiara, Fede, Mary, Ceci, Ale, Matte, Ila and Marzietta, and to my friends in London, in particular to Cecile, Katharina and Nanni who have made this a wonderful chapter of my life. I thank many others who I have surely forgotten.

Finally, I would like to thank two people who fought to be here to see this achievement, but unfortunately could not make it. Thank you to my grandma and grandpa.

Table of Contents

Table of figures

List of tables

Abbreviations

CLE= caudal lateral epiblast

CNH= chordoneural hinge

E= embryonic day (for mouse)

HH= Hamburger and Hamilton embryonic stage (for chick)

HPF= hours post fertilisation (for zebrafish)

HREM= high resolution episcopic microscopy

micro-CT= micro-computed tomography

PCP= planar cell polarity

RA= retinoic acid

SCD= spondylocostal dysostosis

SEM= scanning electron microscopy

STD= spondylothoracic dysostosis

TBM= tail bud mesoderm

VER= ventral ectodermal ridge

Chapter 1. Introduction

The vertebrate body is segmented along the anteroposterior axis into repetitive structures, such as the vertebrae. The vertebrae, the ribs, their associated muscles and the back skin derive from embryonic precursors called somites. Pairs of somites, which are blocks of mesodermal cells, form in an anterior-to-posterior sequence from the presomitic mesoderm (PSM) (the mesodermal tissue that flanks the neural tube) with a period that is species specific. Periodic somite formation is controlled by a molecular oscillator, called segmentation clock, which drives cyclic gene expression in the PSM with the same periodicity as somite formation (Pourquie, 2011).

During development, somitogenesis (the process which leads to somite formation) is tightly associated with axial elongation: as new somites form at the anterior of the PSM, new axial tissues (including somitic tissue) are produced at the posterior end of the embryo, replenishing the PSM and contributing to the lengthening of the body axis. The production of axial tissues depends on a population of progenitor cells, termed axial progenitors, located in the primitive streak (a midline structure which is the site of gastrulation and germ layer formation in chick and mouse, the sites of frog and zebrafish gastrulation are the blastopore lip and the margin, respectively) at early developmental stages, and in the tail bud (the posterior extremity of the embryonic tail) later in development (Cambray and Wilson, 2002, Cambray and Wilson, 2007, McGrew et al., 2008, Davis and Kirschner, 2000, Kanki and Ho, 1997). To date, much work has focused on the mechanisms that contribute to somite formation and axial elongation, but with less understanding on the mechanisms that cause termination of these two processes.

This thesis describes my studies into some of the molecular mechanisms that control the final somite number and the definitive body axis length of embryos of different vertebrate species.

In this introduction, I first give details of the origin, formation and patterning of the somitic tissue and of the other axial tissues derived from the axial progenitors, presenting studies performed in different vertebrate species. Second, I illustrate the

molecular mechanisms underlying somite formation and axial elongation, providing examples of human diseases caused by the malfunctioning of such mechanisms.

1.1 Origin of the somites

1.1.1 Prospective somitic mesoderm forms by morphogenetic movements

During gastrulation, the formation of the three germ layers: the mesoderm, the ectoderm and the endoderm is linked to cell movements occurring in the primitive streak of chick and mouse and in corresponding regions of zebrafish and frog embryos (margin and blastopore lip, respectively) (Solnica-Krezel, 2005) (see Figure 1.1).

The early chick embryo exhibits a superficial single-cell thick epithelium, the epiblast, which will give rise to the embryo proper. Underlying the epiblast, is the presumptive endodermal layer, the primary hypoblast. The secondary hypoblast marks the prospective posterior of the blastoderm. During avian and murine gastrulation, cells of the epiblast ingress through the primitive streak, leading to formation of the three germ layers (ectoderm, mesoderm and endoderm), including the mesoderm in an anterior-to-posterior sequence (Solnica-Krezel, 2005). The cells which ingress early give rise to the most anterior mesoderm (axial and paraxial), those which ingress later give rise to the posterior mesodermal tissue, including the prospective somitic mesoderm (Lawson et al., 1991).

During development, the primitive streak undergoes a series of morphological changes, some of which depend on convergent extension movements. Convergent extension movements are required for proper narrowing and elongation of the body axis, and such narrowing and elongation is achieved by cell intercalation. Within the mesoderm, cell intercalation is promoted by formation of oriented mediolateral protrusions which are used by cells to exert traction on each other (see Figure 1.2) (Keller, 2002). For example, convergent extension movements promote narrowing and elongation of the primitive streak (Lawson and Schoenwolf, 2001). After having first elongated and formed the Hensen's node at its anterior end (the Hensen's node or node or organizer is a bulbous mass of cells which directs the development of the embryonic axis), the

primitive streak then regresses, its remnant and the node becoming incorporating into the tail bud. It has been shown that the tail bud retains gastrulation-like movements and organizer's properties, driving formation of different tissues, including the most posterior somitic tissue (Knezevic et al., 1998).

Failure of morphogenetic movements at gastrulation results in severe axial defects, including absence of the somites, as observed in mouse mutants for *Fgf8*. *Fgf8* is expressed in the primitive streak of the gastrulating embryo and its gene product is a well-known regulator of mesoderm formation (Sun et al., 1999). FGF signalling acts upstream of *Brachyury* to control cell movements (Sun et al., 1999). Similarly to *Fgf8*, *Brachyury* is expressed in the primitive streak (Beddington et al., 1992). It is also expressed in the mesoderm emerging from the streak, the head process and the notochord (Wilkinson et al., 1990). Embryonic patterning defects of *Brachyury* mutants include: absent/abnormal somites posterior to the seventh pair; kinked neural tube, apparently absent notochord (Gruneberg, 1958). A central feature of *Brachyury* mutants is the thickening of the primitive streak, resulting from accumulation of mesoderm cells near the primitive streak. Remarkably, it has been suggested that this is caused by defective cell movements (e.g. mesoderm cells emerging from the primitive streak and lacking *Brachyury* are compromised in their ability to move away from the primitive streak) (Beddington et al., 1992).

In the zebrafish and in the frog, prospective somitic cells move/converge towards the margin or blastpore, respectively, resembling the movements of chick and mouse prospective somitic cells towards the primitive streak (Solnica-Krezel, 2005). Following convergence, prospective somitic tissue invaginates and elongates along the anteroposterior axis of zebrafish and frog embryos, until gastrulation terminates (see Figure 1.2). The somitic mesoderm, which invaginates until this stage, forms the most anterior somites, whereas formation of more posterior somites depends on movements occurring in the tail region (Kanki and Ho, 1997). Kanki et al. (1997) have shown that some of the cell movements in the tail bud resemble the cell movements at the gastrulation site, suggestive of a continuing process between early and late embryonic stages.

Cell intercalation and convergent extension movements, implicated in narrowing and elongation of the body axis of different vertebrates, are regulated by components of the non-canonical Wnt pathway (see Figure 1.2). The non-canonical Wnt pathway is molecularly similar to the Planar Cell Polarity pathway (PCP) that controls polarity of epithelial cells in flies (Tada and Kai, 2009). In the non-canonical Wnt pathway, Wnt5 and Wnt11 ligands bind to Frizzled (Fz), a seven-pass transmembrane receptor, which transduces the Wnt signal through Dishevelled (Dsh), a cytoplasmic signalling protein. The Wnt/Fz signalling activates members of the Rho family which mediates rearrangements of the cytoskeleton, to drive intercalation (Myers et al., 2002b). The non-canonical Wnt pathway also includes Strabismus, a transmembrane protein, and Knypek, a heparan sulfate proteoglycan that seems to potentiate the Wnt11 signalling (Jessen et al., 2002, Topczewski et al., 2001, Myers et al., 2002b). Deregulation of any of the members of this pathway results in a failure of convergent extension, as is also observed for over-expression or down-regulation of *Wnt11* and *Wnt5* (Makita et al., 1998, Moon et al., 1993). Accordingly, *silberblick* and *pipetail,* zebrafish mutants of *Wnt11* and *Wnt5*, respectively, exhibit a broader and shorter axis (Heisenberg et al., 2000, Kilian et al., 2003). Downstream of Wnt ligands, loss of function of Fz2 causes convergent extension defects; both inhibition and induction of Dsh affect cellular protrusion leading to a failure in convergent extension; over-expression of a dominant negative form of Rok2, a Rho kinase, interferes with cell movements (Sumanas et al., 2001, Wallingford et al., 2000, Marlow et al., 2002). *trilobite* (a mutation of *Strabismus*) and *knypek* zebrafish mutants present defects in gastrulation movements, their body axis being shortened and broadened (Jessen et al., 2002, Topczewski et al., 2001). A similar phenotype has been observed in the mouse mutant for *loop-tail*, an orthologue of *Strabismus*, suggestive of a conserved role for non-canonical Wnt genes between lower and higher vertebrates (Kibar et al., 2001).

Notably, convergent extension has been shown to mediate the formation of somitic derivatives, such as the muscles. *knypek;trilobite* double mutants form fewer slow muscle fibres as a consequence of defective movements required for specifying and maintaining slow muscle precursors, the adaxial cells (Yin and Solnica-Krezel, 2007). Thus, morphogenetic movements seem to influence the origin and the successive development of the somites.

Figure 1.1 Morphogenetic movements during chick and zebrafish gastrulation.

Figure a is a graphic depiction of a chick embryo at the primitive streak stage. The anterior end of the embryo is at the top, where the Hensen's node is located, the posterior end of the embryo is at the bottom. The primitive streak represents the site of gastrulation of the embryo. During gastrulation, cells from the epiblast, the outer layer of the embryo, ingress through the primitive streak. The ingression movements contribute to formation of the three germ layers: prospective mesodermal and endodermal cells at the surface of the embryo get internalised beneath the prospective ectodermal cells. Once internalised, cells move away from the streak contributing to elongation of the axis.
Figure b represents a zebrafish embryo at the shield stage (side view). The ventral margin of the embryos is on the left, and the dorsal margin is on the right, the animal pole is at the top and the vegetal pole is at the bottom, the border between the two is the blastoderm margin (black line). During gastrulation, internalisation movements at the level of the margin (red arrow) contribute to formation of the inner mesoderm and endoderm, and the outer ectoderm. As the three germ layers form, convergence (green arrows) and extension (blue arrows) movements promote narrowing and elongation of the embryo. Figure adapted from (Myers et al., 2002b).

Figure 1.2 Convergent extension movements, cell intercalation and the non-canonical Wnt pathway.
Figure a represents a zebrafish embryo at the beginning of the gastrulation period, at the end of the gastrulation period and at the segmentation stage. Convergence (green arrows) and extension (blue arrows) mediolaterally narrow and anteroposteriorly elongate the embryonic axis. Figure adapted from (Myers et al., 2002b).
Figure b represents radial and mediolateral intercalation of cells within a tissue. Narrowing and elongation of the body axis occurs by radial intercalation first, where cells intercalate one another perpendicular to the plane of the tissue, and then by mediolateral intercalation, where cells intercalate one another mediolaterally with the plane of the tissue. As a result of radial and mediolateral intercalation, the tissue is thinner, narrower and longer. Figure adapted from (Keller, 2002).
Figure c is a graphic depiction of the non-canonical Wnt pathway. Wnt ligands bind to the Frizzled receptor, which transduces the signal through Dishevelled, activating members of the Rho family. This activation mediates rearrangements of the cytoskeleton, driving cell intercalation. Figure adapted from (Myers et al., 2002b).

1.1.2 A population of resident progenitor cells contributes to the production of presomitic and somitic tissue

In the chick and in the mouse, after the prospective somitic cells ingress into the primitive streak, a subset of cells forms a population of resident progenitors that are first located in the node/primitive streak and later (from ~E10.5 in mouse and from ~HH15 in chick) in their derivative, the chordoneural hinge (CNH), located in the tail bud of the embryo. The population of resident progenitors, called axial progenitors, contributes to the PSM, the somites and the other axial tissues (neural tube and notochord). The progenitors resident in the node/primitive streak contribute to the most anterior PSM and somites, while the progenitors resident in the CNH are believed to contribute to more posterior PSM and somites (~ last 25/35 somites in chick/mouse) (for a review, see Wilson et al., 2009). Thus, the axial progenitors, first located in the node/primitive streak and later in the CNH, contribute to the presomitic and somitic tissue along the entire anteroposterior body axis (Cambray and Wilson, 2002, Cambray and Wilson, 2007, McGrew et al., 2008).

Studies in the frog and in the zebrafish suggest that presomitic and somitic tissue of lower vertebrates is produced by progenitor cells in a similar way to higher vertebrates (Davis and Kirschner, 2000, Kanki and Ho, 1997). Some of the findings regarding the existence and the features of such progenitors are presented below.

1.1.2.1 Progenitor cells in higher vertebrates

Selleck et al. (1991) have produced a detailed fate map of the chick node by marking small group of cells within the node with a lipophilic cell marker. This fate map shows that, at HH4, the epiblast of the medial part of the node contains prospective notochord and neural tube cells. The medial part of the node contains prospective notochord cells only, while the lateral and posterior part of the node contains prospective somitic cells. They have also analysed the cell lineage of individual cells contained in the node, by

injecting a vital dye into single cells. They show that, between HH3 and HH9, single cells, which reside between the regions known to contribute to the notochord only or to the somites only, give rise to progeny of both notochord and somites. These results indicate that the node contains resident cells with extensive differentiation potential.

A related fate map generated for the mouse node/primitive streak is consistent with that of the chick (Wilson and Beddington, 1996). Unlike the chick study, the mouse study does not examine the cell lineage of single cells (previous studies support the existence of multipotent single cells in the mouse epiblast (Lawson et al., 1991)). However, the mouse fate map reveals that, at E8.5, cells contained in the node and in the primitive streak are retained in these regions and in their derivatives (the tail bud) for the subsequent 24-48 hours, suggestive of a resident population of cells at early and late primitive streak stages (Wilson and Beddington, 1996).

The exact location of such resident population at late mouse embryonic stages (when the primitive streak regresses and the tail bud arises) has been defined. By lineage tracing of groups of cells, Cambray et al. (2002, 2007) show that cells derived from the caudal end of the node and from the rostral part of the primitive streak, a region called node-streak border, are later incorporated into the CNH, a region in the tail bud of the embryo (see Figure 1.3). Thus, the CNH is a derivative of the node-streak border, and, similarly to the node-streak border, it contains resident cells with extensive differentiation potentials (e.g. these cells contribute to PSM, somites, neural tube and notochord). In contrast, cells of the tail bud mesoderm, which is located posterior to the CNH, exhibit limited differentiation potentials (e.g. these cells contribute to somites only). Similar conclusions have been reported for the chick CNH/tail bud mesoderm region (McGrew et al., 2008).

The lineage studies presented above do not provide evidence on the fate of single progenitors, thus the labelled group of cells might represent a mixed population of cells. To investigate the fate of single progenitors, a genetic single-cell labelling in utero has been performed in the mouse, allowing long-term tracing and retrospective analysis of all clonal descendants from the gastrulation stage to the tailbud stage (Tzouanacou et al., 2009). The study shows that neural ectoderm and mesoderm derive from a common single progenitor that persists throughout axial elongation.

Besides the node/primitive streak and the CNH, other regions have been identified as source of axial tissues, such as the caudal lateral epiblast (CLE) (for a review, see Wilson et al., 2009). The CLE is located on either side of the primitive streak, and extends from the node-streak border for half of the length of the primitive streak in the chick or even longer in the mouse. The CLE contains progenitors of some of the neural tube tissue and of some of the somitic tissue, and it contributes somewhat to the CNH (Wilson et al., 2009). Therefore, the node/primitive streak and the epiblast first, and the CNH later are the sites of resident axial progenitors in the chick and in the mouse embryos.

Axial progenitors exhibit stem cell-like properties. From all the studies reported above, axial progenitors clearly exhibit extensive differentiation potentials (Selleck and Stern, 1991, Lawson et al., 1991, Cambray and Wilson, 2002, Cambray and Wilson, 2007, McGrew et al., 2008) (Tzouanacou et al., 2009). It seems possible that axial progenitors are also able to self-renew. Thus, axial progenitors are retained in the progenitors' region for a long period of time (Wilson and Beddington, 1996) (Cambray and Wilson, 2002, Cambray and Wilson, 2007, McGrew et al., 2008) and serial heterochronic grafts of cells from E12.5 CNH into E8.5 CNH repopulate the CNH and also contribute to axial tissues (Cambray and Wilson, 2002). Therefore, these studies provide evidence for the origin of axial tissues from a stem cell population.

Figure 1.3 Location of axial progenitors in the vertebrate embryo.

Figure a is the dorsal view of a chick embryo at the tail bud stage. Key structures/tissues are indicated.
Figure b is a sagittal section through the tail end of the same chick embryo. Axial progenitors are located in the CNH (red box), which marks the end of the neural tube and the notochord, and which is anterior to the tail bud mesoderm. Figure adapted from (Wilson et al., 2009).

1.1.2.2 Progenitor cells in lower vertebrates

Although less exhaustive than that for the mouse and for the chick, there is also evidence regarding the existence of axial progenitors in the frog and in the zebrafish.

Davis et al. (2000) have marked groups of 9 cells in different regions of the frog tail, including the CNH (which derives from the blastopore lip, the correspective of the primitive streak), and they have showed that the dorsal CNH contains progeny of the neural tube, the notochord and the somites. Similar results were obtained when smaller groups of cells (3 cells only) were marked at later embryonic stages, implying that the frog CNH maintains its extensive differentiation potential over time.

Kanki et al. (1997) have individually labelled 105 cells in the prospective tail bud of the zebrafish embryo and the fate of these cells has been followed as axial elongation progresses. The tail bud tissue of the zebrafish derives from the margins (gastrulation sites of the zebrafish embryo), specifically the anterior half of the tail bud derives from the dorsal margin and the posterior half of the tail bud derives from the ventral margin. Kanki et al. have showed that only the cells derived from the dorsal margin contribute to the neural tube, the notochord and the somites, while the cells derived from the ventral margin are limited in their differentiation potential (e.g. they only contribute to somites). However, no single cell contributes to more than one tissue. Although there is little evidence for the existence of single multipotent progenitors during frog and fish tail development, at least at the embryonic stages analysed, these studies show that specific regions of the frog and the zebrafish tail have the potential to contribute to more than one axial tissue. Remarkably, recent advances in the microscopy field, such as the development of scanned light sheet microscopy, have allowed filming and analysis of the entire course of the zebrafish embryogenesis at the cellular level (Keller et al., 2008). Thus, this microscopy technique should allow one to identify specific cells that participate to axial growth and to study their contributions to individual germ layers.

1.1.3 Axial progenitors contribute to the notochordal and neural tissues

The axial progenitors represent the source of various tissues, including the notochord and the neural tube (Cambray and Wilson, 2002, Cambray and Wilson, 2007, McGrew et al., 2008, Davis and Kirschner, 2000, Kanki and Ho, 1997) (Tzouanacou et al., 2009) Although the embryonic development of the notochord and the neural tube is not the primary focus of this thesis, these two axial structures will be frequently mentioned in the next chapters, as they play essential roles in the formation of the vertebrate body axis. For example, signalling molecules secreted by the notochord to the surrounding tissues, including the somites, are known to provide fate information and to contribute to correct patterning of those tissues (STEMPLE, 2005). A brief overview on the development and function of the notochord and the neural tube is presented below.

1.1.3.1 The notochord

The notochord is an embryonic midline structure that is positioned between the neural tube and the gut. In vertebrates, the antecedent of the notochord is the chordamesoderm, which originates from the organizer (the node in chick and mouse and its correspectives in zebrafish and frog). During gastrulation, the narrowing and lengthening of the chordamesoderm, driven by morphogenetic movements and cellular rearrengements, leads to formation of the notochord (Stemple, 2005). At later stages, the mature notochord is composed of an extracellular thick sheath and intracellular vacuoles. The notochordal cells exert pressure against the sheath, making the notochord a stiff rod of tissue.

The stiffness of the notochord is essential for one of its main functions: the axial support (Stemple, 2005). Although the notochord is a transient structure (eventually contributing to intervertebral discs), it is considered the axial skeleton of the embryo

until the vertebrae form. Mutations of genes required for notochord development, result in severe embryonic malformations (e.g. axis truncation) which negatively affect locomotion of some animal species (Stemple et al., 1996). The most representative mutation is that of the mouse gene *Brachyury (T*) or its zebrafish orthologue *No tail (Ntl)* (Beddington et al., 1992, Halpern et al., 1993), (Gruneberg, 1958). At early embryonic stages, *T/Ntl* is expressed in the prospective notochord and in the prospective mesoderm. Accordingly, mutants of *T* or *Ntl* lack a differentiated notochord and do not form enough mesoderm, the tail part of the body being truncated.

The notochord has also a role in patterning of the surrounding tissues (Stemple, 2005). Interestingly, in the zebrafish *Ntl* mutant the absence of the notochord causes defective somitic morphology (Halpern et al., 1993). Together, these observations indicate that the notochord plays essential roles in vertebrate development, being both a support for the axial skeleton and a source of fate information for other axial tissues, including the somites (Stemple, 2005). Another tissue whose patterning is influenced by the signals derived from the notochord is the neural tube, as it is explained below.

1.1.3.2 The neural tube

The neural tube is the embryonic precursor of the central nervous system that comprises the brain and the spinal cord. During development, the nervous system arises from the ectodermal cells that lie over the midline of the embryo. The ectoderm thickens to form the neural plate that subsequently invaginates and forms the neural tube. As development progresses, brain vesicles appear at the anterior end of the neural tube and the spinal cord forms in more posterior regions(Bronner-Fraser and Fraser, 1997).

The establishment of neuronal diversity depends on the mechanisms that operate in space and in time during development (Lumsden and Krumlauf, 1996),(Jessell, 2000). Dorsoventral and anteroposterior patterning of the neural tube and brain depend on inductive signals that define the spatial pattern of the expression of transcription factors along the axis. For example, in the ventral neural tube, the neuronal fate along the dorsoventral axis depends on the Shh-mediated patterning of Nkx-, Dbx-, Pax-, and Irx-

class homeodomain proteins (Briscoe et al., 2000). In the hindbrain, the neuronal fate along the anteroposterior axis (i.e. rhombomere pattern) depends on the Krox/RA-mediated expression of Hox proteins, responsible of providing positional values (Lumsden and Krumlauf, 1996). Thus, neural progenitors at different axial positions acquire different molecular identities (i.e. the progenitors differentiate into roof plate cells, commissural neurons and neural crest cells dorsally, and into floor plate, motor neurons and interneurons ventrally).

The establishment of the dorsoventral patterning of the neural tube is tightly linked to the signals coming from the notochord (Stemple, 2005). It has been shown that the notochord can induce ectopic floor plate differentiation, and that removal of the notochord results in absence of the floor plate (Placzek et al., 1990, Dodd et al., 1998). Specifically, Placzek et al. have demonstrated that the expression of a floor plate-specific chemoattractant is induced in the neural tube by an ectopic notochord. On the contrary, the expression of the same chemoattractant is lost in the neural tube after removal of the notochord (Placzek et al., 1990). Among the signalling molecules derived from the notochord, Shh has been shown to be necessary and sufficient for the differentiation of the floor plate (Roelink et al., 1994, Chiang et al., 1996).

Establishment of the dorsoventral patterning of the neural tube also includes the induction of different neuronal types in different dorsoventral regions. Shh together with 9-cis-retinoic acid (RA) are required for inducing specific subsets of interneurons and motor neurons in the neural tube (Maden, 2006).

RA acts several other times during the development of the nervous system. Genetic studies performed in the mouse embryo have shown that the dose of RA has to be tightly controlled over the embryonic period for normal functioning of the nervous system after birth. Both excessive and limited levels of RA in the embryo cause spinal cord defects in the newborn, such as spina bifida, which is due to an incomplete closure of the embryonic neural tube at its posterior end. Indeed, spina bifida is one of the most common congenital diseases in humans (Abu-Abed et al., 2001, Niederreither et al., 1999).

1.2 Periodic formation and spatial distribution of the somites

After the formation of the prospective somitic mesoderm by morphogenetic movements, the first somite pair appears at the anterior end of the PSM. Subsequent pairs of somites form along the anteroposterior axis in a periodic fashion. The period of somite formation is characteristic for each vertebrate species: 30 minutes in the zebrafish, 90 minutes in the chick, 120 minutes in the mouse and 4-5 hours in human, leading eventually to a species specific number of somites: 31 somites in the zebrafish, 52 somites in the chick, 65 somites in the mouse and 35-37 somites in human. In all vertebrates, periodic somite formation is under the control of the segmentation clock, a molecular oscillator that acts in the PSM (Pourquie, 2011). The clock is linked to the determination front, at which PSM cells undergo a transition that leads to somite formation. The position of the determination front is defined by a system of opposing gradients: a FGF/Wnt posterior- to-anterior gradient, and a RA anterior-to-posterior gradient (Pourquie, 2011). Thus, the segmentation clock and the determination front control formation of the somites in time and space, as first postulated by Cooke and Zeeman in their "clock and wavefront" theoretical model (Cooke and Zeeman, 1976).

Some of the studies that have contributed to the current understanding of the segmentation process are presented below.

1.2.1 The segmentation clock

Palmeirim et al. (1997) have shown that c-*Hairy1*, which encodes a transcription factor of the Notch signalling pathway, is expressed in an oscillatory fashion in the chick PSM. c-*Hairy1* expression switches on and off cyclically in the PSM, at a period that coincides to that of somite formation. These observations were the first to support the existence of an oscillator that drives periodic gene expression in the PSM to set the pace of somite formation.

Cyclic gene expression appears like a wave of gene expression that sweeps across the field of the PSM cells. Thus it cannot be fixed in terms of segment-specific cell lineage. Moreover, cyclic expression in the PSM is maintained even after tissue transection and tissue explant, implying that the cyclic pattern does not require movement of material or propagation of signals (Palmeirim et al., 1997). The cyclic pattern is rather a result of a wave of gene expression timing: individual cells at different anteroposterior levels along the PSM are in different phases of the oscillating cycle. This anteroposterior profile reflects the pattern of the cyclic gene expression wave that repeats itself with every newly forming somite. The entire multicellular PSM oscillates at a regular period that corresponds to that of somite formation and the smallest oscillating unit is a single cell (for a review see (Oates et al., 2012)).

Following the study of Palmeirim et al., other cyclic genes were identified in the mouse and in the zebrafish PSM as well as in the chick PSM. Those genes belong to the Notch, Fgf, and Wnt signalling pathways (Figure 1.4). The conservation of individual cyclic genes within each pathway and between different species is limited to the Notch pathway (Palmeirim et al., 1997),(Dequeant et al., 2006),(Krol et al., 2011).

The Delta-Notch signalling pathway is a well-studied cell-cell communication pathway, implicated in development and disease. The transmembrane receptor Notch on the signal-receiving cell is activated by its ligand, Delta, a transmembrane protein on the signal-sending cell. The activation of Notch triggers cleavages in the Notch receptor that release the Notch intracellular domain which translocates to the nucleus and binds to the transcription factor of the CBF1/Su(H)/LAG1 family (CSL), activating transcription of Notch target genes (Lai, 2004)

Notch signalling is evolutionary conserved between vertebrates. *Hairy*-related genes have been identified in the chick (*c-Hairy1* and *c-Hairy2*), in the mouse (*Hes7*) and in the zebrafish (*Her1* and *Her7*). Dynamic Notch signalling is also seen in invertebrates (Palmeirim et al., 1997, Bessho et al., 2001, Oates and Ho, 2002, Jouve et al., 2000, Holley et al., 2002, Stollewerk et al., 2003). Thus, it seems possible that *Her/Hes* genes are good candidates to act at the core of the segmentation clock.

Hes/Her genes encode transcriptional repressors, which negatively feedback on the promoter of their own genes. Mathematical models have revealed that oscillations can

be generated by negative feedback loops, only if certain delays are included in such loops (e.g. the delays involved in transcription and translation) (Lewis, 2003, Lewis, 2008). Thus, the period of the oscillations and somite formation could be generated by delayed negative feedback loops.

Mutations of *Hes/Her* genes and of other components of the Notch signalling pathway affect oscillations, somite formation, and ultimately organisation of the axial skeleton (Bessho et al., 2001, Conlon et al., 1995, Evrard et al., 1998). In the mouse, *Hes7* mutants exhibit disturbed oscillatory behaviour of various cyclic genes. In *Hes7* mutants, the somites are irregular in shape and size, with poor definition of the borders. Accordingly, the vertebrae and ribs are fused and their size is reduced (Bessho et al., 2001). A similar phenotype has been observed in mutants of *Lfng*, which is a target and a negative regulator of the Notch pathway (Evrard et al., 1998, Dale et al., 2003).

It is not clear whether *Hes/Her* genes or other genes, belonging to the Notch pathway, represent the master oscillator that drives oscillations within the Notch pathway and in other signalling pathways. *Hes7* regulates oscillations of genes of the Notch and Fgf signalling pathways, suggesting that *Hes7* is the master oscillator (Bessho et al., 2001) (Niwa et al., 2007). However, Niwa et al. (2007) have shown that oscillations of *Hes7* are under the control of the Notch and Fgf signalling pathways. Specifically, Fgf signalling initiates *Hes7* oscillations in the posterior PSM and Notch signalling propagates *Hes7* oscillations in the anterior PSM. These evidences argue against *Hes7* being the master oscillator.

Alternatively, Wnt or Notch oscillators might be the masters. In the hypomorphic *Wnt3a vestigial tail* mutants, cyclic expression of Notch and Wnt components is lost and somite formation is disrupted, indicating that the Wnt pathway is upstream of the Notch in the generation of somites (Aulehla et al., 2003). Nevertheless, Notch and Wnt oscillations are still observed when β-catenin is constitutively activated in the PSM, indicating that Wnt signalling, like Notch signalling, is not the master oscillator (Aulehla et al., 2008, Dunty et al., 2008).

There are evidences in support of Fgf signalling acting upstream of Notch and Wnt signalling within the mouse segmentation clock. *Fgfr1* mouse mutants or pharmacological inhibition of Fgfr1 cease oscillations in Fgf, Notch and Wnt pathway

components (Wahl et al., 2007). Fgf seems not to be the master oscillator, because loss of Notch oscillations are restored by elevated Wnt signalling even in the absence of Fgf signalling (Aulehla et al., 2008). All together, these studies indicate that in the mouse Notch, Wnt and Fgf signalling pathways oscillate during segmentation and that all of them drive oscillations of others. These studies also suggest that none of these pathways is a unique master oscillator, they rather represent interlinked oscillators that work redundantly or outputs of a yet unidentified master oscillator.

Studies in the zebrafish have lead to a novel interpretation of the role of Notch in the segmentation process. In the zebrafish mutants of the Notch pathway, the first few somites form normally. Jiang et al. (2000) have proposed that the observed delayed disruption of somite formation in the Notch mutants is due to a gradual loss of synchrony between adjacent cells (Lewis, 2008). Experimental evidence, in support of this view, comes from the study of (Horikawa et al., 2006). Thus, at least in the zebrafish, Notch signalling is responsible for synchronising oscillations of neighbouring PSM cells rather than for setting the pace of somite formation. Differently from the zebrafish studies, Ferjentsik et al. (2009) have shown that, in the mouse, blocking all Notch activity prevents cyclic gene expression and somite formation (Ferjentsik et al., 2009). Thus, there might be species-specific differences in the role of Notch signalling during somitogenesis. These differences could be explained by the different degree of complexity of the segmentation clock machinery between the mouse and thezebrafish (e.g. in the mouse, the segmentation clock drives periodic expression of genes of three different signalling pathways: Notch, Fgf and Wnt, while in the zebrafish periodic expression of *Her* genes is dependent on Notch only).

Figure 1.4 Species-specific cyclic genes.
The table shows cyclic genes in the Fgf, Notch and Wnt signalling pathways in different vertebrate species. Only the most representative cyclic genes are reported, the list of genes is based on the micro-array data of (Dequeant et al., 2006),(Krol et al., 2011). Conservation of individual cyclic genes within each pathway and between different species is limited to orthologs of *Her/Her* genes (in red).
*The identification of *Tbx16*, as a cyclic gene associated to the Wnt (and Fgf) signalling pathway suggests that pathways other than Notch oscillate in the zebrafish.
Figure adapted from (Roellig et al., 2011).

1.2.2 The system of opposing gradients

As new somites form periodically in the anterior PSM, they start differentiating into vertebrae, ribs, muscles and dermis. In contrast, the tissue in the posterior PSM remains undifferentiated and unsegmented, being replenished by progenitor cells from the tail bud. A system of opposing gradients is thought to:

- maintain the undifferentiated state of the cells in the posterior PSM
- control differentiation in the anterior PSM (for a review see (Aulehla and Pourquie, 2010)).

The system of gradients also interacts with the segmentation clock, defining the spatial level at which PSM cells respond to the clock and at which they acquire their segmental identity (see a summarising depiction in Figure 1.5). The above-mentioned level is called determination front, and its position moves posteriorly along the anteroposterior body axis as somite formation proceeds (specifically, the front moves by a distance that corresponds to one somite length during one segmentation clock oscillation) (Dequeant and Pourquie, 2008, Gomez et al., 2008).

The system of gradients involves an Fgf/Wnt posterior-to-anterior gradient and a RA anterior-to-posterior gradient. Dubrulle et al. (2004b) were the first to demonstrate how the Fgf protein gradient is established in the mouse and in the chick PSM. This gradient seems to derive from a novel mechanism, based on mRNA decay, whereby active transcription of *Fgf8* mRNA is restricted to the posterior end of the embryo, where progenitor cells reside, and it stops when cells enter the PSM. Degradation of *Fgf8* mRNA generates a gradient of Fgf8 RNA, and, thereby, of Fgf8 protein. In the mouse and in the chick PSM, the Fgf gradient coincides with a graded expression of the intracellular mediators of the Fgf signalling pathway (Dubrulle and Pourquie, 2004b, Delfini et al., 2005). Thus, in the PSM, the *Fgf8* mRNA gradient is first translated in a Fgf8 protein gradient and subsequently transduced by graded activation of downstream effectors of the Fgf signalling pathway.

A graded distribution of the Wnt signalling has also been reported. Aulehla et al. (2003) have shown that *Axin2,* a target gene of the Wnt signalling, is expressed in a posterior-to-anterior gradient in the PSM, indirectly indicating that a gradient of Wnt signalling exists in this embryonic tissue. In a subsequent study, Aulehla et al. (2008) have provided a more direct evidence for the existence of a Wnt signalling gradient in the PSM, as they have observed a posterior-to-anterior protein gradient of β-catenin, the mediator of the canonical Wnt pathway. Therefore, similarly to the Fgf signalling, Wnt signalling acts as a posterior-to-anterior gradient in the vertebrate PSM.

A gradient of RA activity is established in an opposite direction to that of Fgf and Wnt signalling. The spatial distribution of RA along the body axis can be inferred by the expression pattern of one of its synthesing enzymes, *Raldh2* and of one of its degrading enzymes, *Cyp26a1*. *Raldh2* is expressed in the somites and in the anterior PSM, while *Cyp26a1* is expressed in the tail bud. Thus, a source of RA is located at the anterior end of the embryo, while a sink is located in the posterior end (Niederreither et al., 1997, Blentic et al., 2003, Sakai et al., 2001). The activity of RA can be visualised by means of mouse reporter lines. Rossant et al. (1991) have described a RARE-LacZ reporter line which shows that activity of RA is high in the anterior of the embryo and absent in the posterior, consistent with the sites of expression of the RA synthesising and degrading enzymes. These studies provide evidence for the existence of an anterior-to-posterior gradient of RA along the vertebrate body axis.

High levels of Fgf/Wnt signalling in the posterior PSM have been proposed to maintain the undifferentiated state of cells in this region. Indeed, over-expression of Fgf8 by electroporation of prospective chick PSM cells, leads to up-regulation of caudal PSM markers and down-regulation of somite markers (Dubrulle et al., 2001). These observations imply that Fgf signalling is sufficient to maintain the undifferentiated character of PSM cells and to block their differentiation program. Similarly, mouse mutants with elevated levels of *β*-catenin show expansion of various markers of the posterior PSM and inhibition of somite markers, which results in a disrupted somite formation (Aulehla et al., 2008, Dunty et al., 2008). Therefore, similarly to the Fgf signalling, increased Wnt signalling promotes the undifferentiated status of PSM cells.

In contrast, high levels of RA cause cell death of cells in the tail end of the embryo, resulting in a severely truncated body axis (Shum et al., 1999). Interestingly, increased levels of RA by means of ectopic treatments or genetic mutations lead to down-regulation of *Fgf8* and *Wnt3a* and an ectopic source of FGF8 causes down-regulation of *Raldh2*, implying that the gradients antagonise each other (Diez del Corral et al., 2003, Shum et al., 1999). It seems possible that RA-induced axial truncations are caused by loss of expression of genes required for maintenance of the PSM character. Together, these studies indicate that a system of opposing gradients controls the balance between undifferentiated and differentiated status of the PSM cells along the anteroposterior body axis of vertebrate embryos.

Based on the current model, cells in the posterior PSM receive high levels of the Fgf and Wnt signalling that permit oscillations. Once cells are displaced anteriorly, the levels of the signals decrease below a threshold that arrests oscillations and the segmental pattern is determined. Thus, the system of gradients is thought to interact with the segmentation clock to define the position of the determination front, this is the level where PSM cells undergo that dramatic molecular and morphological change that leads to cessation of the oscillations and to formation of the somites. Consistent with the model proposed, both Fgf and Wnt signalling control oscillatory behaviour of cyclic genes, their loss of function blocking oscillations, and their gain of function inducing abnormal oscillations (Aulehla et al., 2003, Niwa et al., 2007, Wahl et al., 2007, Aulehla et al., 2008, Dunty et al., 2008). For example, drug treatment of chick embryos with CKI-7, a Wnt signalling inhibitor, lengthens the period of the oscillations, resulting in the formation of fewer somites (Gibb et al., 2009), while gain of function of *β-catenin* exhibit ectopic stripes of cycling genes in the PSM, (Dunty et al., 2008, Aulehla et al., 2008). Moreover, enhancement or blockade of the Fgf signalling alters the size of the prospective somites (e.g. somite size is reduced when Fgf signalling is enhanced, somite size is increased when Fgf signalling is blocked), and displaces the position of the determination front anteriorly when somite size is decreased, or posteriorly when somite size is increased and presumably changing the velocity of the front (Dubrulle et al., 2001). Alterations of RA levels result in the opposite outcome of that of the Fgf signalling. High levels of RA lead to increased somite size, low levels of RA lead to decreased somite size (Diez del Corral et al., 2003, Moreno and Kintner, 2004). Hence,

the interaction between the gradients and the segmentation clock is crucial to determine where the segmentation clock becomes inactive and where the future somite forms, controlling the spatial distribution of the somites along the body axis (see Figure 1.3).

As cells cross the determination front, expression of *Mesp2* that is expressed in the prospective somite and which encodes a transcription factor involved in the establishment of anteroposterior somite polarity (Saga et al., 1997, Saga and Takeda, 2001) is switched on. Interestingly, *Mesp2* expression is negatively regulated by Fgf and Wnt signalling, and positively regulated by RA consistent with opposite roles of these gradients in regulating differentiation of the PSM (Delfini et al., 2005, Dunty et al., 2008, Aulehla et al., 2008, Moreno and Kintner, 2004).

Figure 1.5 The segmentation clock and the system of opposing gradients.

Schematic of the tail end of a vertebrate embryo (dorsal view). The expression pattern of a cyclic gene is shown in blue, and the expression pattern of *Mesp2* is shown in black. The posterior-to-anterior gradient of Fgf/Wnt is shown red and the anterior-to-posterior gradient of RA is shown in blue. Cyclic gene expression is highly dynamic during few cycles of the segmentation clock and it correlates with the formation of a new pair of somites at the end of the cycle. The segmentation clock is thought to interact with the system of opposing gradients to define the position of the determination front (in orange), where cells aquire their segmental identity and activate *Mesp2* expression (that defines the future somite). The size of the future somite is defined by the distance travelled by the front during one oscillation of the segmentation clock (in green). Figure adapted from (Pourquie, 2011).

1.3 Establishment of the anteroposterior somite polarity

1.3.1 *Mesp2* plays a central role in defining different somite compartments

The PSM can be divided into two different regions, the posterior PSM and the anterior PSM, that correspond to two different cellular states: state 1-the immature state- and state 2-where the PSM cells acquire anteroposterior polarity and become competent to segment-.

The establishment of anteroposterior polarity in the anterior PSM is essential for resegmentation that occurs later on in development. The somites are organised into anterior and posterior compartments. This half-somite identity is conferred before the morphological segment boundary becomes visible. As development proceeds, the posterior compartment of one somite fuses to the anterior compartment of the next somite (the so called resegmentation process). The anterior somitic compartment gives rise to the posterior half of the vertebral body and of the intervertebral disc, while the posterior somitic compartment gives rise to the anterior half of the vertebral body and the pedicle of the neural arch, that are key components of the vertebral unit (for a review see (Saga and Takeda, 2001)).

The state 2 is characterised by the induction of the members of the the Mesp gene family, including *Mesp1* and *Mesp2* in the mouse, which encode transcription factors (Saga et al., 1996),(Saga et al., 1997). Homologous genes have been identified in other vertebrates: *Meso-1* and *Meso-2* in the chick, *Thylacine1* and *Thylacine* 2 in the frog, and *Mespa* and *Mespb* in the zebrafish (Buchberger et al., 1998),(Sparrow et al., 1998),(Sawada et al., 2000). The expression patterns and the functions of these genes appear to be conserved during somitogenesis in all vertebrates.

The expression of *Mesp2* is initially observed in the nascent mesoderm, similarly to that of *Mesp1*. Later in development, *Mesp2* expression domain is found lateral to the node, as a pair of bands in the paraxial mesoderm. During somite formation, the bands of

expression are found in the presumptive somite region. Specifically, *Mesp2* expression appears as a single band occupying one somite length, the posterior half of *Mesp2* expression becomes progressively down-regulated, while the anterior half remains intact and then disappears. The time required for a cycle of *Mesp2* expression matches that of one somite formation (Saga et al., 1996),(Saga et al., 1997),(Takahashi et al., 2000) (Figure 1.6 a).

The *Mesp2* mutants form vertebrae with fused pedicles of the neural arches and fused ribs. The pedicles of the neural arches derive from the posterior somite compartment, implying that this compartment is expanded at the expense of the anterior compartment in the *Mesp2* mutants (i.e. the mutants show a caudalised phenotype). This is confirmed by expression studies of posterior markers, such as *Uncx4.1*, that is expressed in the entire somite of *Mesp2* mutants, while expression of the anterior marker *Tbx18* is absent. Thus, *Mesp2* is required for the correct establishment of the anteroposterior somite polarity, specifically it is required to specify the anterior compartment of the somite (Saga et al., 1997). Gene replacement studies have revealed functional redundancy between *Mesp1* and *Mesp2* in regulation of somitogenesis (Saga, 1998).

An opposite phenotype to that of *Mesp2* has been reported for *Psen1*, a mediator of the Notch signalling pathway. *Psen1* mutants lack pedicles of the neural arches and expression of *Uncx4.*1 is lost in the posterior somite compartment of the mutants, suggestive of a rostralised phenotype (Koizumi et al., 2001). Thus, the mechanisms regulating somite polarity are dependent on *Mesp2* and on the Notch signalling pathway. A Notch ligand, *Dll1*, is also implicated in the establishment of anteroposterior polarity. In WT mouse, *Dll1* expression is restricted to the posterior compartment of the presumptive somite in the anterior PSM, while it is uniformly expressed in the posterior PSM. In *Psen1* mutants, expression of *Dll1* is maintained in the posterior PSM but it is lost in the anterior PSM resulting in a rostralised phenotype. In *Mesp2* mutants, expression of *Dll1* is expanded in the anterior PSM and the resulting vertebrae are caudalised (Takahashi et al., 2000) (Figure 1.6 b). Therefore, expression of *Dll1* in the anterior PSM is essential for determining the rostral and the caudal character of the segments. The expression pattern of *Dll1* in the anterior PSM is established by *Mesp2* through the Notch signalling pathway: expression of *Dll1* is strong in the posterior PSM and it is down-regulated by *Mesp2* in the anterior PSM.

This effect is mediated by the Notch signalling pathway, and also Dll1 induction depends on the Notch signalling (Saga et al., 1997),(Takahashi et al., 2000). Furthermore, there are two Notch signalling pathways that regulate expression of *Dll1* in the anterior PSM: 1) a Psen1 dependent pathway that induces *Dll1* expression; 2) a Psen1 independent pathway that inhibits *Dll1* expression. Mesp2 is supposed to activate the inhibitory pathway and to inactivate the induction pathway. In this respect, *Mesp2* expression is essential to generate the striped pattern of *Dll1* in the anterior PSM. Initially, *Mesp2* expression is found in both the anterior and the posterior compartment of the future somite, suppressing *Dll1* expression via the Psen1 independent Notch pathway. Subsequently, *Mesp2* expression becomes restricted to the anterior compartment of the future somite, where *Dll1* suppression is maintained. In the posterior compartment of the future somite, *Dll1* expression is induced via the Psen1 dependent Notch pathway (Takahashi et al., 2000). Thus, a complicate gene network is established in the anterior PSM where *Mesp2* plays a central role in defining somite polarity (Figure 1.6 c).

In the mouse, two Notch ligands, *Dll1* and *Dll3*, are co-expressed in the PSM. Importantly, feedback loops of *Dll1* and *Mesp2* (i.e. Dll1 induces *Dll1* and *Mesp2*, and Mesp2 suppresses *Dll1*) are essential for establishment of anteroposterior polarity, and *Dll3* is important for localisation of *Dll1* and *Mesp2* expression (Takahashi et al., 2003). Besides Dll1, other factors contribute to up-regulation of *Mesp2* expression in the anterior PSM, including the transcription factor Tbx6 (which is expressed in the entire PSM downstream of the wavefront, its anterior limit being positioned by the previously defined segment) and Ripply2, a target and a negative regulator of *Mesp2* (Yasuhiko et al., 2006),(Morimoto et al., 2007). During each cycle of somite formation, expression of *Mesp2* is induced in the cells that express *Tbx6* and experience a pulse of Notch signalling downstream of the clock in the anterior PSM. Mesp2 is then required for repression of *Tbx6* expression and degradation of Tbx6 protein. Repression of *Tbx6* occurs via the Ripply family of transcription repressors that are activated by Mesp2. Repression of Tbx6 expression within the entire expression domain of *Mesp2* completes the complex feedback loop that shifts the anterior limit of *Tbx6* expression domain by one somite length to the posterior, where a new cycle of somite formation starts (Takahashi et al., 2010),(Oginuma et al., 2008). The *Mesp2* null embryos lack a

segment border, a phenotype common to many segmentation genes, implying that *Mesp2* is also involved in somite boundary formation (Evrard et al., 1998, Bessho et al., 2001, Kusumi et al., 1998). Indeed, genes implicated in somite boundary formation, such as *Lfng*, a modulator of the Notch pathway, and *EphA4,* seem to be regulated by Mesp2 to mediate somite border formation. Noteworthy, *EphA4* appears to be a direct transcriptional target gene of Mesp2 at the anterior boundary of the presumptive somite (Nakajima et al., 2006).

All together, these findings show that *Mesp2* is involved in both somite polarity establishment and somite boundary formation by means of suppression of the Notch signalling pathway (for a review see (Dahmann et al., 2011)), (Figure 1.6 d).

.

Figure 1.6 *Mesp2* and the establishment of somite polarity.
Figure a. Drawing of a time course analysis of the expression pattern of *Mesp2* (gene expression is in blue). Only the posterior part of the embryo is shown (anterior is at the top and posterior is at the bottom), including the PSM, the presumptive somites (S-2, S-1) and the formed somites (S0, S1, S2,S3). Cyclic expression matches to the period of one somite formation. Adapted from (Saga and Takahashi, 2008).
Figure b. Expression of *Dll1* in WT and mutant mice. In WT Dll1 is expressed in region 1 as a uniform pattern, and in region 2 as a striped pattern. *Mesp2* mutants exhibit expanded expression of *Dll1* in region 2, while *Psen1* mutants show loss of the *Dll1* striped pattern. *Mesp2* and *Psen1* have opposite phenotypes in respect to polarity establishment: a caudalised phenotype and a rostralised phenotype, respectively. Adapted from (Saga and Takeda, 2001).
Figure c. Genetic networks and somite polarity establishment. *Dll1* expression is regulated by Mesp2 and Psen1 through two different Notch pathways. Mesp2 suppresses *Dll1* in the entire presumptive somite. When *Mesp2* expression is downregulated in the posterior compartment of the somite, *Dll1* gets induced. Adapted from (Saga and Takeda, 2001).
Figure d. Genetic networks involved in Mesp2 activation and in subsequent events regulated by Mesp2. Adapted from (Saga, 2007).

Remarkably, *Mesp2* has been identified in the ethiology of human spinal disorders (e.g. scoliosis), emphasizing the importance of embryonic segmentation across different vertebrates (Sewell and Kusumi, 2007).

1.4 Vertebral segmentation abnormalities in human

1.4.1 Congenital forms of scoliosis are caused by mutations in segmentation clock genes

In humans, scoliosis is classified as either idiopathic or congenital. Patients with idiopatic scoliosis present an abnormal curvature of the vertebral column, with substantially normal vertebrae. In contrast, patients suffering from congenital scoliosis exhibit various vertebral defects, including: hemivertebrae, vertebral fusions, wedge-shaped vertebrae and vertebral bars (for a review see (Pourquie, 2011)).

The the congenital forms of scoliosis are rare, but their phenotypic patterns are well-characterised. In congenital forms of scoliosis, vertebral abnormalities can occur in association with defects in other anatomical structures, or they can occur as isolated abnormalities. In the latter case, vertebral abnormalities can affect one or two vertebrae; a set of vertebrae confined to a specific region of the spine; vertebrae and ribs at various levels of the spine, as in the case of spondylocostal dysostosis (SCD) and spondylothoracic dysostosis (STD) (Turnpenny et al., 2007, Giampietro et al., 2009).

SCD and STD have been associated with mutations in genes belonging to the segmentation clock machinery, and they represent monogenic autosomal recessive diseases.

SCD generally correlates with abnormal vertebral morphology along the entire spine, its manifestations varying in different mutations. To date, three different forms of SCD have been identified. SCD1 is characterised by rounded vertebral bodies, misaligned and fused ribs (Giampietro et al., 2009). It is caused by mutations of *Dll3,* which encodes one of the Notch ligands. The phenotype observed in patients is reminiscent of that previously characterised in mouse mutants. *Dll3* mouse mutants present defects in somite formation and establishment of somite polarity, accordingly their vertebral column is shortened with fused or incomplete vertebrae (Kusumi et al., 1998).

SCD2 has been associated to a mutation in *Mesp2*, which encodes a transcription factor involved in a complex feedback loop with members of the Notch signalling pathway. In the mouse, *Mesp2* is required for correct subdivision of the somite into anterior and posterior compartments and for proper skeletal organisation (Saga et al., 1997) (and see paragraph 1.3). In contrast to SCD1, where the severity of the defects is similar in all vertebrae, patients with SCD2 exhibit regionalised defects: the thoracic vertebrae are more affected than the lumbar vertebrae (Giampietro et al., 2009).

SCD3 is caused by a mutation of *Lfng*, a target gene of the Notch pathway. In humans, *Lfng* mutation leads to vertebral defects in the cervical region, hemivertebrae and abnormal ribs in the thoracical and lumbar regions, resembling the phenotype described in *Lfng* mouse mutants (Giampietro et al., 2009, Evrard et al., 1998). Notably, *Lfng* mouse mutants, likewise *Dll3* and *Mesp2* mouse mutants, present defects in somite formation and in somite polarity establishment that subsequently results in a disorganised axial skeleton (Evrard et al., 1998, Kusumi et al., 1998, Saga et al., 1997).

Differently from SCD, where ribs abnormalities can occur variably along the thoracic cage, STD is characterised by bilateral fusion of all the ribs. A mutation in *Mesp2* has been identified as the putative cause of some of the STD cases studied so far (Giampietro et al., 2009).

Hence, genetic studies of SCD and STD have revealed that a subset of them is caused by mutations in the genes of the segmentation clock machinery. Strikingly, patients carrying mutations in specific clock genes present spine malformations that resemble those of mouse mutants of the same genes, suggesting that the mechanisms behind the segmentation process are conserved across vertebrates.

In this introduction, I have highlighted some of the cellular and molecular events that underlie the segmentation of the body axis into repetitive units, such as the somites. The studies presented above have widely contributed to the current understanding of somitogenesis, however there are questions that remain to be answered, including what triggers cessation of this embryonic process.

In this thesis, I describe my investigations aimed to understand how the final somite number and the definitive body axis length is controlled in different vertebrate embryos.

In Chapter 3, I investigate some of the molecular mechanisms that might contribute to termination of axial elongation and segmentation, including: permanent loss of genes required for maintenance of axial progenitors; decreased somite formation rate at late segmentation stages.

In Chapter 4, I study whether somite formation is sensitive to gene dosage, by analysing the final number of somites formed in embryos heterozygous for key genes in the axial elongation and segmentation processes.

In Chapter 5, I explore the role of *Greb1*, a gene expressed in the progenitors' area of different vertebrates. I provide evidence that this gene might regulate morphogenetic movements required for proper convergence and extension of the embryonic body axis.

Chapter 2. Materials and Methods

2.1 Chick

2.1.1 Embryos

Fertilised chick eggs were sourced from Henry Stewart & Co and incubated at 37 °C in a humidified incubator. Embryos were staged according to Hamburger and Hamilton, (Hamburger and Hamilton, 1992).

2.1.2 In situ hybridisation

In situ hybridisation was carried out as previously described (Henrique et al., 1995) with some modifications. Formaldehyde fixed, proteinase K treated embryos were pre-hybridised in hybridisation buffer (50% formamide, 5 X SSC pH 4.5, 1 % SDS, 50 μg/ml yeast RNA, 50 μg/ml heparin) at 70 °C for at least 1 hour. Hybridisation with DIG-labelled probes was performed in hybridisation buffer ON at 70 °C. Embryos were then washed in 50% formamide, 2X SSC pH 4.5 at 70 °C and in TBST (0.25 M Tris/HCl pH 7.5, 1.37 M NaCl, 27 mM KCl, 1% Tween) at RT for several hours. Embryos were subsequently incubated in TBST containing 10% heat inactivated goat serum for at least 1 hour, alkaline-phosphatase-conjugated anti-DIG antibody was diluted (Roche, 1:3000) in TBST containing 1% heat inactivated goat serum and incubated at 4 °C ON. After extensive washes in TBST, embryos were transferred into NTMT (100 mM NaCl, 100 mM Tris/HCl pH 9.5, 50 mM MgCl2, 10% Tween) and the colour reaction performed with NBT/BCIP (Roche) at RT until an appropriate level of staining was detectable. For experiments using only one probe, the embryos were washed in PBST and stored in 4% formaldehyde at 4 °C. For double-labelling

experiments, protocol was as described before (Stern, 1998). Both probes were added simultaneously in the hybridisation buffer, the most strongly expressed gene was labelled with DIG and developed second using BCIP, the less strong gene was labelled with FLU (and using alkaline phosphatase conjugated anti-FLU antibody from Roche was used and diluted 1:5000) and developed first with NBT/BCIP. After first colour was developed, embryos were fixed ON, washed in TBST, incubated in TBST containing serum for 1 hour at RT and TBST containing serum and antibody at 4 °C ON. Colour was developed as described above. For photography, embryos were washed in PBST and in increasing concentrations of glycerol: 30%, 50%, 70%, 80% 15 minutes to 1 hour each, depending on embryo size. Then washed in 100% methanol and transferred in PBS for photos. Samples were examined on a Leica MZ16 microscope and photographed using a Leica DC500 digital camera using Leica FireCam software, images were processed using Adobe Photoshop.

2.1.3 Probes synthesis

Probes for *Delta-1* (Henrique et al., 1995), *Fgf-8* (Kawakami et al., 2003), *Spry-2* (Minowada et al., 1999), *Cyp26a1* (Swindell et al., 1999), *Raldh-2* (Swindell et al., 1999), *T* (Knezevic et al., 1997), *Lfng* (Laufer et al., 1997), and *Uncx4.1* (Dale et al., 2003) were as previously described. A second probe for chick *Cyp26a1* was also generated, corresponding to the full-length cDNA sequence. Primers (forward 5'-ATGGGCTTCTCCGCTCTGGTC-3' and reverse 5'-TCAGATTTGGCCGCTGAAAC-3') were designed to target sequence from Ensembl database www.ensembl.org. RT-PCR was performed using the SuperScriptII one step RT-PCR kit (Invitrogen) using 1 µg of chick RNA extracted from HH12 caudal PSM. The RT-PCR product was then cloned into TOPO vector (Invitrogen), sequence verified by restriction analysis and DNA sequencing. For the anti-sense probe, the plasmid was linearised with XhoI and the RNA was made using Sp6 RNA polymerase for 3 hours at 37 °C. Primers for chick *Greb1* probe were as follows: forward 5'-ATCCGCAAGGGGAGTCTTTACC-3' and reverse 5'-GGTGAGGAGGATGAGGAGGTGA-3', cloning and transcription methods

were as described above. The anti-sense probe was generated by linearising the plasmid with SpeI and using T7 RNA polymerase.

2.1.4 *Ex ovo* embryo culture and drug treatments

HH 10-12 chick embryos were cultured in L15 medium supplemented with 15% foetal calf serum and placed on a rolling platform at 37 °C as previously described (Connolly et al., 1995). For pharmacological inhibition of signalling pathways, embryos were cultured in SU5402 for 1.5, 3 and 6 hours (Calbiochem, 10 μM), PD98059 for 6 hours (Calbiochem, 0.5 mM), FGF8 for 6 hours (R&D, 2.5 μg/ml), or the corresponding controls: DMSO (when using SU5402 and PD98059) and PBS (when using FGF8). For inhibition of cell cycle, embryos were cultured in Aphidicolin (Sigma, 150 μM) and Hydroxyurea (Sigma, 20 mM) for 6,12 and 16 hours, or in the corresponding controls: DMSO and water, respectively. For the half-PSM culture, the caudal half of the embryo was bisected down the midline such that each embryo provided two identical explants. Embryos were washed in PBS and fixed.

2.1.5 DiI labelling

DiI crystals (Molecular Probes) were dissolved in ethanol to a final concentration of 1 mg/ml. Small groups of somitic cells were labelled at the same level on both sides of the embryo, by injection using a IM 300 Microinjector (by Narishige). After labelling, the caudal half of the embryo was bisected down the midline and the two PSM halves were cultured *ex-ovo*.

2.1.6 *In ovo* electroporation

Dr. Sheena Pinchin (Developmental Genetics laboratory, LRI), performed the electroporations described here and after. Electroporation conditions were based on those described previously (Momose et al., 1999). DNA plasmids were diluted to 1-2 μg/μl in PBS containing 2% sucrose and mixed with Fast Green to visualise the injection site. For electroporations in the node (HH 4-5), eggs were windowed and the DNA solution was injected between the vitelline membrane and the epiblast. Negative and positive electrodes were placed above and below the embryo, respectively, and five 50 ms pulses of 10 V were applied, using an Intracell Intracept TSS10 pulser equipped with pedal trigger. Eggs were re-incubated until the desired stage and assayed for GFP or RFP expression in the PSM. Only those displaying a normal overt morphology and positive for GFP or RFP were processed for subsequent analysis. For electroporations in the neural tube (HH12) a method based on (Itasaki et al., 1999) was used.

2.1.7 Immunohistochemistry

Embryos were fixed in 4% formaldehyde in PBS 1 hour at 4 °C, and washed in PBS containing 0.5% Triton a few times at RT. Embryos were then incubated in blocking solution (1% BSA, 10% heat inactivated goat serum, 0.5% Triton in PBS) for 2 hours at 4 °C and then in primary antibody diluted in the blocking solution, at 4 °C ON. The primary antibody was washed using PBS containing 0.1% Triton at RT. Secondary antibody was diluted in blocking solution and added for 2 hours at RT. Embryos were washed in PBS 0.1% Triton, incubated in SYTO-13 (1:1000 in PBST, Invitrogen), washed again and transferred in SlowFade Gold Anti-fading reagent (Invitrogen), mounted on slides and imaged using Zeiss LSM510 confocal microscope. Primary antibodies used were as follows: polyclonal anti-phospho-histone H3 (1:100 Millipore), polyclonal anti-caspase 3 activate (1:400, R&D). For secondary detection Alexa-Fluor

546 goat anti-rabbit IgG (1:500, Invitrogen) was used. Scale bars were calculated in LSM510 software. The length of the body axis, PSM and somites were measured in fixed, flat-mounted embryos using a Tonbridge graticule.

2.1.8 Plasmids and morpholinos

For *in ovo* electroporation, the full-length chick *Cyp26a1* cDNA sequence was amplified as described above, and cloned into XhoI/SacI sites of pCAGGs-IRES-nlsGFP expression vector, previously described (Stamataki et al., 2005). The pCIG vector containing full-length *Cyp26a1* cDNA described in (Albazerchi and Stern, 2007) was also used. For RNAi against chick *Cyp26a1,* 22 nucleotides target sequences were chosen using the GenScript design tool at www.genescript.com. Three sequences were cloned into pRFPRNAi plasmid described in (Das et al., 2006): 5'-CCTGCCAAATTCATAGCTTTCA-3'; 5'-CCACCATGATGTTCTGCAGAAA-3' and 5'-GCTGCTAAATGGACCTCCTACA-3'. A morpholinos against chick *Cyp26a1* was also used and was electroporated in conjuction with a carrier DNA as described in (Voiculescu et al., 2008). Sequence of the morpholino was as follows: 5'-ATCCACCATCAGAGCCGTACCTTTT-3'. 250 uM of splicing-blocking morpholino (Gene Tools) and standard control morpholino (5'-CCTCTTACCTCAGTTACAATTTATA-3') and 250 uM/ml carrier plasmid DNA were co-electroporated into HH 4-5 embryos as described above. To evaluate the efficacy of the morpholino against *Cyp26a1*, RT-PCR was performed on caudal PSM of five control-electroporated and five MO-electroporated embryos using the following primers: forward 5'-CATGGGGCTGCCCTTCTTCG-3' and reverse 5'-CTCACCTCCTCTTGGATGACAGG-3'. For the C-terminus tagged version of chick *Cyp26a1*, the full-length cDNA was amplified with the following primers: forward 5'-CCCAAGCTTGCCGCCGCCATGGGCTTCTCCGCTCTGGTC-3' and reverse 5'-GCTCTAGAGGGATTTGGCCGCTGAAACCTATG-3' and cloned into HindIII/XbaI sites of pCDNA6/myc-His vector (Invitrogen).

2.1.9 Cell culture

Dr. Charalampos Rallis (Developmental Genetics laboratory, LRI), isolated chick embryonic fibroblasts (CEF) from 4 HH36 embryos, by passing the embryos through a syringe. The homogenate was then mixed with trypsin and the supernatant was transferred to a new tube. Digestion was stopped by adding completed medium and spinning down. Pellet was resuspended in completed medium and plated, the next day cellular debris were removed and medium changed. CEF were grown at 37 °C under 5% CO2 in completed DMEM (10% foetal calf serum, 1% chick serum, 1% penicillin-streptomycin and 1% glutamine). For transfection, cells were plated into 6-well plate and transfected with 1 μg plasmid DNA per well using Lipofectamine 2000 transfection reagent (Invitrogen) according to manufacturer's guidelines.

2.1.10 Western blotting

Cell lysates from cultured cells were prepared using RIPA (50mM Tris/HCl pH8, 150 mM NaCl, 1% Igepal CA-630, 0.5% sodium deoxycolate, 0.1% SDS, 2mM EDTA). Cells were washed with ice-cold PBS and lysed with RIPA and incubated for 30 minutes at 4 °C at constant agitation. After centrifugation the supernatant was removed and protein concentration was determined using the BCA Protein Assay kit (Pierce). Proteins were separated and transferred using the NuPAGE system (Invitrogen), 4-12% Bis-Tris gels were used. Transfer of protein onto Hybond nitrocellulose membrane (Amersham Biosciences) was checked by Ponceau-S (Amersham Biosciences). Membrane was blocked in 5% milk (Marvel) in TBST for 1 hour at RT. Primary antibody incubation was performed for 3 hours at RT or ON at 4 °C in blocking solution. Following washes in TBST, secondary antibody was applied for 1 hour at RT. Membrane was washed and detection was carried out using the ECL plus western blotting Detection System (GE Healthcare), the membrane was exposed to the high performance chemiluminescence film Hyperfilm ECL (GE Healthcare) which was developed using the JPI Automatic X-ray Film Processor. Primary antibodies used were

as follows: monoclonal γ-tubulin (1:1000, Sigma), polyclonal cyp26a1 (1:500, Abcam), monoclonal c-myc (1:1000, Sigma). Secondary detection was done using: anti-mouse or anti-rabbit IgG HRP-linked antibodies (1:5000, Amersham).

2.1.11 Scanning Electron Microscopy and X-ray micro-computed tomography (micro-CT) Scanning

Dr Anne Weston, from the Electron Microscopy unit at LRI, processed and imaged the embryos for Scanning Electron Microscopy and X-ray micro-CT scanning. HH24 and HH25 embryos were fixed in 2.5% gluteraldehyde plus 4% paraformaldehyde in PBS for 1 hour. Samples were post-fixed in 1% osmium tetroxide in distilled water for a minimum of 1 hour and dehydrated step-wise using 50%, 70%, 80%, 90% and 100% ethanol, 15-20 minutes each. Samples were transferred to 100% acetone and critical point dried using a Polaron CPD. For Scanning Electron Microscopy: samples were mounted on Scanning Electron Microscopy stubs, sputter coated with platinum, using SC7640 sputter coater and viewed in a JEOL FESEM 6700 microscope. For X-ray micro-CT: samples were scanned using a Skyscan 1172 (Skyscan, Kontich, Belgium) set at 40KV and 250μA. The images were reconstructed using the Skyscan NRecon program and analysed using Disect software (Disect systems Ltd).

2.1.12 High Resolution Episcopic Microscopy

Mike Bennett, from the Developmental Biology division at NIMR, processed the embryos for High Resolution Episcopic Microscopy. HH24 and HH25 embryos were processed as described in (Weninger et al., 2006). Samples were fixed in 4% formaldehyde in PBS and dehydrated through 30%, 50%, 70%, 80%, 90%, 100% methanol. Methanol washes were 30-60 minutes each for small samples and 1 day each

for bigger samples. Samples were impregnated in 50% methanol and 50% JB4 (Polyscience) ON, and then in 100% JB4 at 4 °C in the dark at constant agitation for 2 days. JB4 contained: 100 ml JB4 solution A, 6 ml solution B, 1.25 g catalyst, 0.275 g eosin B, 0.055 g acridine orange to stain the samples. Embryos were then embedded under a Leica wild M8 microscope and using moulds filled with JB4. The resin block was incubated in the oven to harden and then mounted on the imaging apparatus as shown in www.embryoimaging.org. The apparatus consists of a rotary microtome (Leica SM 2500) and a modified microscope (Olympus MVX 10) equipped with fluorescence filter sets and a digital video camera (Hamamatsu ORCA-HR). The entire block was sectioned (section thickness was 2 or 4 μm), and one image captured with the GFP filter set, after each section. The resulting digital image series was converted to a volume data set and further processing and analysis was performed using ImageJ. OsiriX was used for the 3D reconstruction.

2.2 Mouse

2.2.1 Embryos

Wild-type *CD1* and *Black6* mouse embryos were obtained from timed mated pregnant females between E8.5 and E14.5 which were sourced from Charles River.

2.2.2 Transgenic lines

Fixed heterozygous and WT E13.5 mouse embryos were obtained as follows:

Cdx2 from Professor Zernicka-Goetz M (Chawengsaksophak et al., 1997), *Fgf3* from Professor Mansour SL (Mansour et al., 1993), *Fgf8* from Dr Basson A (Sun et al., 1999), *Raldh2* from Professor Dolle' P (Niederreither et al., 1999), *Cyp26a1* from Professor Hamada H (Abu-Abed et al., 2001), *POR* from Professor Wolf R (Otto et al., 2003), *Wnt3a* (Takada et al., 1994), *Wnt5a* (Yamaguchi et al., 1999), *β–catenin* (Dunty et al., 2008) and *Mesogenin* (Yoon and Wold, 2000) were obtained from Dr Yamaguchi TP, *Axin2* (Zeng et al., 1997) from Professor Sharpe P, *Bmp4* (Winnier et al., 1995) from Professor Hogan BLM, and the pudgy null line from the Jackson Laboratory www.jax.org and described in (Kusumi et al., 1998).

2.2.3 Genotyping

Yolk sac of mouse embryos of *Wnt3a, Wnt5a, β -catenin, Axin2, Mesogenin* lines were dissolved in 500 µl of the following buffer: 50 mM KCl, 10 mM Tris pH 8.3, 2 mM MgCl2, 0.1 mg/ml gelatin, 0.45% Nonidet P-40, 0.45% tween supplemented with 5 µl of 10 mg/ml proteinase K at 50 °C ON. Proteinase K was inactivated at 94 °C for 10

minutes, 1 μl of DNA was used for PCR reaction with appropriate concentration of primers and *Taq* polymerase (Roche) and Frohman buffer (670 mM Tris/HCl pH 8.8, 67 mM MgCl2, 1.7 mg/ml BSA, 166 mM (NH4) 2SO4) in case of *Wnt3a* and *Mesogenin* or with PCR buffer from Roche in case of *Wnt5a* and *β-catenin.* Primers used were as follows: *Wnt3a* (5'-TGGCTACCCGTGATATTGCTGAA-3', 5'-GTTGTGACGGTTCATGGCAGAG-3', 5'-ACTACAACCCTCCTCACCTGGCC-3'), *Wnt5a* (5'-GACTTCCTGGTGAGGGTGCGTG-3', 5'-GGAGAATGGGCACACAGAATCAAC-3', 5'-GGGAGCCGGTTGGCGCTACCGGTGG-3'), *β-catenin* (5'-AAGGTAGAGTGATGAAAGTTGTT-3' 5'-CACCATGTCCTCTGTCTATTC-3' 5'-TACACTATTGAATCACAGGGACTT-3') *Axin2* (5'-AAGCTGCGTCGGATACTTGAGA-3' 5'-AGTCCATCTTCATTCCGCCTAGC-3' 5'-TGGTAATGCTGCAGTGGCTTG-3'), *Mesogenin* (5'-CCAAGGAGCCTTGTACTGCTGC-3' 5'-GCCACCAGCAGTGTGTAGATAGGGAGGT-3' 5'-GCAAAGCGCCATTCGCCATTC-3'). Ear biopsies of adult mice or yolk sacs of mouse embryos of pudgy line were dissolved in 300 μl of lysis buffer (50 mM Tris/HCl pH 8.0, 5 mM EDTA pH 8.0, 100 mM NaCl, 0.5% SDS) containing 20 mg/ml proteinase K (Roche) at constant agitation at 56 °C ON. The next day, 120 μl of saturated NaCl solution was added, and the solution was mixed and incubated on ice for 20 minutes. Precipitates were eliminated by centrifugation at 13200 rpm for 20 minutes, and supernatant transferred to a new tube. DNA was isolated by adding 600 μl of absolute ethanol and by centrifugation at 13200 rpm for 20 minutes. The pellet was washed in 70% ethanol, dried and dissolved in 300 μl of TE. For genotyping, 1 μl of the DNA solution was used for PCR reaction together with 10 μM of each primer and the *Taq* PCR Master Mix (Qiagen). Primers used were as follows: pudgy (5'-CCCTGCCGCTGCCTGATGG-3' 5'-CCCTGCCGCTGCCTGCCTC-3' 5'-TCCAGCACTTGGGAGATGG-3'). Embryos for other lines (*Cdx2, Fgf3, Fgf8, Raldh2, Cyp26a1, POR, Bmp4*) were genotyped by the original sources.

2.2.4 In situ hybridisation

In situ hybridisation was carried out as previously described (Henrique et al., 1995) with some modifications. Formaldehyde fixed, proteinase K treated embryos were pre-hybridised in hybridisation buffer (50% formamide, 5 X SSC pH 4.5, 1 % SDS, 50 μg/ml yeast RNA, 50 μg/ml heparin) at 70 °C for at least 1 hour. Hybridisation with DIG-labelled probes was performed in hybridisation buffer ON at 70 °C. Embryos were then washed in 50% formamide, 2X SSC pH 4.5 at 70 °C and in TBST (0.25 M Tris/HCl pH 7.5, 1.37 M NaCl, 27 mM KCl, 1% Tween) at RT for several hours. Embryos were subsequently incubated in TBST containing 10% heat inactivated goat serum for at least 1 hour, alkaline-phosphatase-conjugated anti-DIG antibody was diluted (Roche, 1:3000) in TBST containing 1% heat inactivated goat serum and incubated at 4 °C ON. After extensive washes in TBST, embryos were transferred into NTMT (100 mM NaCl, 100 mM Tris/HCl pH 9.5, 50 mM MgCl2, 10% Tween) and the colour reaction performed with NBT/BCIP (Roche) at RT until an appropriate level of staining was detectable. For experiments using only one probe, the embryos were washed in PBST and stored in 4% formaldehyde at 4 °C. For triple-labelling experiments, the three DIG probes were added simultaneously in the hybridisation buffer. For photography, embryos were washed in PBST and in increasing concentrations of glycerol: 30%, 50%, 70%, 80% 15 minutes to 1 hour each, depending on embryo size. Then washed in 100% methanol and transferred in PBS for photos. Samples were examined on a Leica MZ16 microscope and photographed using a Leica DC500 digital camera using Leica FireCam software, images were processed using Adobe Photoshop. For in situ hybridisation on sections, the tissue was dissected out in ice-cold PBS and fixed in 4% PFA ON, processed and embedded in agar, and sectioned at 8-10 μM.

2.2.5 Probes synthesis

Probes for *Uncx4.1* (Mansouri et al., 1997), *MyoD* (Sassoon et al., 1989) and *Tbx18* (Stauber et al., 2009) were as previously described. The *Greb1* probe was generated by Dr Ravindra Prajapati (Developmental Genetics laboratory, LRI) Primers (forward 5'-GCCACGGGGCGTCCGGCCCTTTC-3' and reverse 5'-ACCGCGCTGTGCAGGCGGGGGA-3') were designed to target sequence from Ensembl database www.ensembl.org. PCR was performed using the full-length mouse *Greb1* cDNA sequence cloned into pEF-DEST51 vector as template, the vector was purchased from imaGenes (product name OCACo5052E0918-pEF-DEST51). The PCR product was then cloned into TOPO vector (Invitrogen), sequence verified by restriction analysis and DNA sequencing. For the anti-sense probe, the plasmid was linearised with SpeI and the RNA was made using T7 RNA polymerase for 3 hours at 37 °C.

2.2.6 Scanning Electron Microscopy and X-ray micro-computed tomography (micro-CT) Scanning

Dr Anne Weston, from the Electron Microscopy unit at LRI, processed and imaged the embryos for Scanning Electron Microscopy and X-ray micro-CT scanning. E12.5, E13.5 and E14.5 embryos were fixed in 2.5% gluteraldehyde plus 4% paraformaldehyde in PBS for 1 hour. Samples were post-fixed in osmium tetroxide and dehydrated step-wise to 100% ethanol. Samples were transferred to 100% acetone and critical point dried. For Scanning Electron Microscopy: samples were mounted on Scanning Electron Microscopy stubs, sputter coated with platinum and viewed in a JEOL FESEM 6700 microscope. For X-ray micro-CT: samples were scanned using a Skyscan 1172 (Skyscan, Kontich, Belgium) set at 40KV and 250μA. The images were reconstructed using the Skyscan NRecon program and analysed using Disect software (Disect systems Ltd).

2.2.7 High Resolution Episcopic Microscopy

Mike Bennett, from the Developmental Biology Unit at NIMR, processed the embryos for High resolution Episcopic Microscopy. E12.5, E13.5 and E14.5 embryos were processed as described in (Weninger et al., 2006). Samples were fixed in 4% formaldehyde in PBS and dehydrated through 30%, 50%, 70%, 80%, 90%, 100% methanol. Methanol washes were 30-60 minutes each for small samples and 1 day each for bigger samples. Samples were impregnated in 50% methanol and 50% JB4 (Polyscience) ON, and then in 100% JB4 at 4 °C in the dark at constant agitation for 2 days. JB4 contained: 100 ml JB4 solution A, 6 ml solution B, 1.25 g catalyst, 0.275 g eosin B, 0.055 g acridine orange to stain the samples. Embryos were then embedded under a Leica wild M8 microscope and using moulds filled with JB4. The resin block was incubated in the oven to harden and then mounted on the imaging apparatus as shown in www.embryoimaging.org. The apparatus consists of a rotary microtome (Leica SM 2500) and a modified microscope (Olympus MVX 10) equipped with fluorescence filter sets and a digital video camera (Hamamatsu ORCA-HR). The entire block was sectioned (the section thickness was 5 or 6 μm), and one image captured with the GFP filter set, after each section. The resulting digital image series was converted to a volume data set and further processing and analysis was performed using ImageJ. OsiriX was used for the 3D reconstruction.

2.3 Fish

2.3.1 Embryos

Zebrafish were maintained at 27.5 °C in dechlorinated water on a 14/10 hour light/dark cycle and embryos were collected from spontaneous spawnings. Staging was according to Kimmel et al (Kimmel et al., 1995).

2.3.2 Transgenic lines

p53 heterozygous and homozygous embryos were obtained by crossing *p53* homozygous female to *p53* heterozygous males as described in (Little and Mullins, 2009).The BMP reporter line has been described in (Wu et al., 2011).

2.3.3 In situ hybridisation

Formaldehyde fixed embryos were rinsed in PBST and dehydrated in 50% methanol/PBST for 10 minutes and in 100% methanol for 2-3 times 5 minutes each. Embryos were then rehydrated in 75% methanol/PBST, 50% methanol/PBST, 25% methanol/PBST and PBST for 5 minutes each. Embryos were dechorionated in PBST and rinsed in PBST for 5 times, 5 minutes each. Pre-hybridisation was carried out in hybridisation buffer (50% formamide, 5 X SSC pH 4.5, 1 % SDS, 50 μg/ml yeast RNA, 50 μg/ml heparin) at 65 °C for at least 1 hour. Hybridisation with DIG-labelled probes was performed in hybridisation buffer ON at 65 °C. Embryos were washed as follows: 5 minutes in 50% formamide/2X SSC pH 4.5 at 65 °C; 5 minutes in 2X SSC at 65 °C; 20 minutes in 0.2 X SSC containing 0.1% tween at 65 °C; twice for 20 minutes in 0.1 X SSC containing 0.1% tween at 65 °C and several changes in PBST at RT. Embryos

were subsequently incubated in PBST containing 10% heat inactivated goat serum for at least 1 hour, alkaline-phosphatase-conjugated anti-DIG antibody was diluted (Roche, 1:3000) in PBST containing 1% heat inactivated goat serum and incubated at 4 °C ON. After extensive washes in PBST, embryos were transferred into NTMT (100 mM NaCl, 100 mM Tris/HCl pH 9.5, 50 mM MgCl2, 10% Tween) and the colour reaction performed with NBT/BCIP (Roche) at RT until an appropriate level of staining was detectable. The reaction was stopped by rinsing the embryos several times in deionised water. The embryos were washed in PBST and stored in 4% formaldehyde at 4 °C. For double-labelling experiments with both DIG probes, the probes were added simultaneously in the hybridisation buffer. For double-labelling experiments with DIG and FLU probes, probes were added simultaneously in the hybridisation buffer, the most strongly expressed gene was labelled with DIG and developed second using INT/BCIP (Roche), the less strong gene was labelled with FLU (and using alkaline phosphatase conjugated anti-FLU antibody from Roche was used and diluted 1:5000) and developed first with NBT/BCIP. After first colour was developed, embryos were fixed ON, washed in TBST, incubated in TBST containing serum for 1 hour at RT and TBST containing serum and antibody at 4 °C ON. Colour was developed as described above. For photography, embryos were washed in PBST and in increasing concentrations of glycerol: 30%, 50%, 70%, 80% 15 minutes to 1 hour each, depending on embryo size. Then washed in 100% methanol and transferred in PBS for photos, yolks were removed if needed. Samples were examined on a Leitz Diaplan microscope or on a Leica MZ16 microscope and photographed using a Leica DC500 digital camera using Leica FireCam software, images were processed using Adobe Photoshop. The length of body axis and somites and the width of the notochord and the distance between the segments were measured in fixed, flat-mounted embryos using a Tonbridge graticule.

2.3.4 Probes synthesis

Probes for *Ntl* (Schulte-Merker et al., 1992), *MyoD* (Weinberg et al., 1996), *PapC* (Yamamoto et al., 1998), *Hgg1* (Daggett et al., 2004), *Dlx3* (Akimenko et al., 1994),

Her1 (Takke and Campos-Ortega, 1999), and *RFP* (Wu et al., 2011) were as previously described. *Cb1045* was obtained from the Vertebrate Development lab at LRI, the clone was purchased from I.M.A.G.E. clone, antisense probe was generated by linearising the plasmid with SalI and using T7 RNA polymerase. *MespA, MespB* probes were also obtained from the Vertebrate development lab at LRI, *MespA* and *MespB* plasmids were linearised with NotI and transcribed with T3 RNA polymerase. The probe for zebrafish *Greb1* was generated by Dr Ravindra Prajapati (Developmental Genetics laboratory, LRI). Primers (forward 5'- AAGGAGCCACCCCTCTGCACATTCT -3' and reverse 5'- AATTAACCCTCACTAAAGGGTTAGACGAAACCGCATTCGTCCTC-3' which contains a T3 promoter site) were designed to target sequence from Ensembl database www.ensembl.org. PCR was performed using a clone purchased from Gene Service as a template. For the anti-sense probe, the PCR product was used and the RNA was made using T3 RNA polymerase.

2.3.5 Drug treatments

Embryos at the shield stage were incubated until the 15 somite stage and the 26 somite stage in aquarium water containing Aphidicolin (Sigma, 150 μM) and Hydroxyurea (Sigma, 20 mM), or in aquarium water containing the corresponding control: DMSO. Samples were kept in the dark during the course of the treatment. At the end of the treatment embryos were washed in PBS and fixed.

2.3.6 Immunohistochemistry

Embryos were fixed in 4% formaldehyde in PBS 1 hour at 4 °C, and washed in PBS containing 0.5% Triton a few times at RT. Embryos were then incubated in blocking solution (1% BSA, 10% heat inactivated goat serum, 0.5% Triton in PBS) for 2 hours at 4 °C and then in primary antibody diluted in the blocking solution, at 4 °C ON. The primary antibody was washed using PBS containing 0.1% Triton at RT. Secondary

antibody was diluted in blocking solution and added for 2 hours at RT. Embryos were washed in PBS 0.1% Triton, incubated in SYTO-13 (1:1000 in PBST, Invitrogen), washed again and transferred in SlowFade Gold Anti-fading reagent (Invitrogen). Yolks were removed and embryos mounted on slides and imaged using Zeiss LSM510 confocal microscope. Primary antibodies used were as follows: polyclonal anti-phospho-histone H3 (1:100 Millipore). For secondary detection Alexa-Fluor 546 goat anti-rabbit IgG (1:500, Invitrogen) was used. Scale bars were calculated in LSM510 software. The length of the axis length was measured in fixed, flat-mounted embryos using a Tonbridge graticule.

2.3.7 Plasmids and morpholinos

For mRNA injections, 2 nl of reagents were injected into 1 cell stage embryos. The full-length mouse *Greb1* cDNA sequence cloned into pEF-DEST51 vector was purchased from imaGenes (product name OCACo5052E0918-pEF-DEST51). For morpholino injections, 2 nl of reagents were injected into 1-4 cell stage embryos. Splicing blocking morpholinos (Gene Tools) against zebrafish *Greb1* were as follows: morpholino 1: 5'-AATACTGAAATCACACCTCTCCTCC-3' and morpholino 2: 5'-GGAAGACTGTAAAAGCTCACCCTCA-3'. Mismatch (5'-AATAGTCAAATCAGACCTGTGCTCC-3') and standard control morpholinos (5'-CCTCTTACCTCAGTTACAATTTATA-3') were also used. Sequence of p53 was: 5'-GCGCCATTGCTTTGCAAGAATTG-3'. To evaluate the efficacy of the splice blocking morpholinos against *Greb1*, RT-PCR was performed on five embryos for each conditions used. Primers used were as follows: for morpholino 1 (forward 5'-GCTTGTCTCTGAAGGAGGCTGAGCA -3' and reverse 5'-ATTCTCCCTGTGGATCCATGCCAGT -3') and for morpholino 2 (forward 5'-GGAGTCTGACCGCCAGTGACCAG -3' and reverse 5'-AAGTGCATTACGTCCACATTCATCG -3').

2.3.8 In vitro mRNA synthesis

Plasmids containing the gene of interest were linearized and mRNA was synthesized using the mMessage machine kit (Ambion) according to manufacturer's instructions. In case of the rescue experiment, the following plasmids were used: control plasmid (pTri-Xef, TRIPLEScript plasmid containing xenopus *elongation factor 1 α*); mouse *Greb1* (pEF-DEST51-*Greb1*, expression vector containing full-length mouse). The mouse *Greb1* plasmid was linearised with either BstBI or PmeI restriction enzyme. To optimise the yield of long transcript, 1 μl of GTP was added to the transcription reaction of mouse *Greb1*. 2 μg of each transcription reaction were loaded onto agarose denaturing gel.

2.3.9 In vitro coupled transcription and translation

TNT coupled reticulocyte lysate systems (Promega) was used according to manufacturer's instructions. 1 μg of DEST51 vector containing full length mouse *Greb1* was mixed with required reagents, comprising ^{35}S-methionine in a 25 μl reaction. pCS2+ vector containing *Smad2* (from Dr Antonius Van Boxtel, Developmental Signalling laboratory at LRI) was used as positive control, the negative control was the reaction mixture with no DEST51 vector. 1 μl of each reactions was then used and run on gel. After gel drying, ^{35}S-labelled proteins were visualised by autoradiography using a storage phosphor screen on a Molecular Dynamics STORM 860 PhosphorImager. ImageQuant software was used for gel image analysis.

2.3.10 Bioinformatics

Probir Chakravarty, from the Bioinformatics and Biostatistics service at LRI, performed the analysis. Refseq nucleotide and protein sequences of Human GREB1 were extracted from NCBI's Gene repository (http://www.ncbi.nlm.nih.gov/gene/). For the alignment of GREB1 protein sequences in different organisms, NCBI's UniGene repository

(http://www.ncbi.nlm.nih.gov/UniGene) was used, orthologs of human GREB1 were extracted. GREB1 protein sequences from mouse (accession number: NP_056579), chicken (accession number: XP_419956), frog (accession number: XP_002942230) and zebrafish (accession number: XP_001920606) were used to draw a protein alignment showing areas of amino acids identity. The multiple sequence alignment protein ClustalW (http://www.ebi.ac.uk/Tools/msa/clustalw2/) was used to generate the protein alignment using default parameters. For the functional domains study, the protein sequence of human GREB1 was taken and used to identify the presence of functional domains using INTERPROScan (http://www.ebi.ac.uk/Tools/pfa/iprscan/). INTERPRO is an integrated database of predictive protein signatures used for the automatic annotation of proteins.

2.4 Molecular biology

2.4.1 Polymerase Chain Reaction (PCR)

PCR reactions (Saiki et al., 1988) were carried out in 200 µl thin-walled 8 tube and flat cap strips (Thermo Scientific) using a Peltier (PTC-200, DNA engine) thermal cycler. For cloning of expression constructs *PfuTurbo* (Stratagene) polymerase was used. Reactions were performed in 50 µl with 10 µM of each primer (Sigma-Aldrich), 20 mM dNTPs (Pharmacia Biotech), variable amount of DNA template in 1 X polymerase buffer. The thermal cycling conditions were based on the following settings: 94 °C 3 minutes; 94 °C 30 seconds, 60 °C 30 seconds, 72 °C 1 minute/Kb for 40 cycles; 72 °C 10 minutes; 12 °C forever. The annealing temperature was adjusted to the melting temperatures of the primers and the extension time adjusted to the length of the product. PCR products were confirmed by electrophoresis on agarose gel (Ultra Pure, Invitrogen) with TBE (Tris-Borate, EDTA) running buffer.

2.4.2 Transformation of competent bacteria and ligation

For transformation of DH5α or TOP10 competent bacteria (Invitrogen) with plasmid DNA, a 50 µl aliquot of frozen bacteria was thawed on ice. A variable amount of plasmid DNA was added, and the cells were mixed gently and incubated on ice for 30 minutes. The suspension was heat shocked at 42 °C for 30-45 seconds and kept on ice for 2 minutes. After addition of 250-900 µl of SOC medium, the bacterial suspension was incubated on a shaker for 1 hour at 37 °C. 50 µl of the solution was spread on a Ampicillin (100 µg/µl)/ LB agar plate, and incubated at 37 °C ON, lid side down. Colonies were picked from the plate, placed in 3 ml of LB medium containing Ampicillin and incubated on a shaker ON at 37 °C. Suspensions were centrifuged at

4000 rpm in an Eppendorf floor centrifuge (5810), the medium was discarded and the plasmid DNA was purified using Qiagen mini-prep kit. Site-directed ligation was performed as follows: plasmid and insert DNA were digested using appropriate enzymes and supplied buffers (NEB) for at least 3 hours at 37 °C. Plasmid DNA was phosphorylated with calf intestinal alkaline phosphatase (NEB) at 37 °C for 30 minutes. Both plasmid and insert DNA were purified using QIAquick gel extraction kit (Qiagen) and ligation was performed using T4 DNA ligase (NEB) with a molar ratio of plasmid to insert DNA of 1:3 in a 20 μl reaction. The reaction was incubated at 16 °C ON and 2 μl used for transformation into competent bacteria.

2.4.3 Sequencing

Sequencing reactions were performed in a 20 μl solution containing 8 μl BigDye terminator ready Reaction mix (Applied Biosystem), 200-400 ng of DNA and 3.2 pmol of primer. Primers used were as follows: SP6 5'-CATACGATTTAGGTGACACTATAG-3'; T7 5'-AATACGACTCACTATAG-3'; T3 5'-ATTAACCCTCACTAAAG-3'; M13F 5'-GTAAAACGACGGCCAG-3'; M13R 5'-CAGGAAACAGCTATGAC-3'. Reactions were carried out on a Peltier (PTC-200) thermal cycler using the following conditions: 96 °C 1 minute; 96 °C 10 seconds, 48 °C 5 seconds, 60 °C 4 minutes for 24 cycles; 12 °C forever. Reactions were purified with DyeEx 2.0 Spin kit (Qiagen) and dried in a speed vacuum. Sequencing was performed on an ABI 3730 DNA Analyser (Applied Biosystem) by the CRUK equipment park.

Chapter 3. Mechanisms regulating termination of axial elongation and segmentation

Vertebrate axis elongation and segmentation depend on a population of progenitor cells, located at the tail end of the embryo (Davis and Kirschner, 2000, Kanki and Ho, 1997, Cambray and Wilson, 2007, McGrew et al., 2008) (Tzouanacou et al., 2009). This population contributes to neural, notochordal, presomitic and somitic tissue until the entire embryonic body axis and the correct number of somites is produced. However, the mechanisms by which axial elongation and segmentation terminate are still unknown. My project initially focussed on whether this is due to: 1) loss of expression of genes required for progenitor maintenance; 2) reduction of the rate of somite formation.

First, I examined whether *Delta1*, *Fgf8*, *Spry2*, *Cyp26a1* and *Raldh2* expression patterns change as axial elongation terminates. All these genes are well-known regulators of somite and mesoderm formation, their loss of function leading to somitic defects and axis truncations (Sun et al., 1999, Abu-Abed et al., 2001, Niederreither et al., 1999). Then, I analysed whether the rate of somite formation changes at late embryonic stages. Periodic formation of somites is controlled by a molecular oscillator, the segmentation clock, which has a period of 90 minutes in the chick PSM leading eventually to 50-55 pairs of somites (Palmeirim et al., 1997).

In this chapter, I describe my investigations into the contribution of the two mechanisms cited above to termination of axial elongation and segmentation.

3.1 Results

3.1.1 Gene expression levels, PSM and somite size decline as axial elongation terminates

A possible reason for termination of axial elongation and segmentation is the permanent loss of the expression of genes required for axial progenitor maintenance. I tested this hypothesis by performing in situ hybridisations on chick embryos from HH17 to HH26/28, after elongation has ceased (elongation is thought to cease at ~HH24-HH25). I focussed my study on the tail region, because this is the location where axial progenitors reside. Expression of *Delta1* (Figure 3.1 a, b, c), *Fgf8* (Figure 3.1 f, g) and *Spry2* (Figure 3.1 i, j) progressively declines between HH17 and HH23, until it disappears after HH23. Expression of all the genes tested is undetectable at HH26/28 (Figure 3.1 d, e, h, k). Therefore, loss of gene expression occurs just before axial elongation terminates.

I also observed that the PSM size gradually decreases, as seen in embryos stained for *Delta1* (Figure 3.1 a, b, c). At HH26, only the tip of the tail remains unsegmented (Figure 3.1 d). Also, the somite size changes over time: the posterior somites being increasingly smaller than the more anterior ones, at HH26 (Figure 3.1 h). Thus, exhaustion of the presomitic (the PSM does not get fully exhausted, it disappears at late developmental stages probably because of cell death) and the somitic tissues correlates with a decline in gene expression levels of *Delta1*, *Fgf8* and *Spry2*.

Axial truncations have been described in vertebrate embryos following RA treatment or due to loss of *Cyp26a1*, a RA catabolising enzyme (Abu-Abed et al., 2001, Shum et al., 1999). Interestingly, *Cyp26a1* expression is restricted to the tail region of the embryo and it has been proposed that the enzyme protects the region from deleterious effects of RA (e.g. cell death in the caudal area) (Abu-Abed et al., 2001). In order to test if termination of axial elongation is associated with decrease of *Cyp26a1* expression and increased exposure to RA, I performed in situ hybridisation at different embryonic

stages. The levels of *Cyp26a1* transcripts (Figure 3.2 a-c') decline over time, they are already very low at HH23, and they are not detectable at HH26 (Figure 3.2 c, c'), implying that the expression of *Cyp26a1* declines as axial elongation terminates. Nevertheless, as the *Cyp26a1* in situ hybridisation staining is very weak (especially at HH23), control experiments shall be performed to draw and confirm the conclusions mentioned above. In this regard, one shall analyse expression of *Cyp26a1* by in situ hybridisation using a *Cyp26a1* sense probe to exclude the possibility of a false-positive signal. A blank staining shall be obtained for comparison with that of the *Cyp26a1* anti-sense probe. As an alternative/parallel control experiment, one shall perform physical sectioning of the sample, following in situ hybridisation analysis with the *Cyp26a1* anti-sense probe. This shall confirm the presence and the exact location of the *Cyp26a1* expression domain. As a quantitative and more sensitive approach, the level of *Cyp26a1* transcripts at different developmental stages shall be measured by means of quantitative PCR. The latter analysis shall show a progressive decline of the *Cyp26a1* transcripts, similarly to what observed in the original in situ hybridisation experiment.

Decreased levels of *Cyp26a1* transcripts might correlate with increased retinoid signalling. To this end, I examined the expression of *Raldh2,* a RA synthesising enzyme. At HH18, *Raldh2* is not present at the tail end, but it is found in the proximity of the tail (Figure 3.3 a). Interestingly, *Raldh2* is expressed in the tail at HH23 (and at HH26) (Figure 3.3 b-c') when expression of all the other genes declines.

Together, these data indicate that *Cyp26a1* expression is lost as elongation comes to an end (although control experiments shall be performed to confirm this), and this associates with increasing levels of RA in the tail domain. One could speculate that decline of *Cyp26a1* and the increased levels of *Raldh2* might cause decline of *Delta1*, *Fgf8* and *Spry2*. This would be consistent with reports that show that exposure to RA causes loss of *Fgf8* and *Wnt3a* (Diez del Corral et al., 2003, Shum et al., 1999).

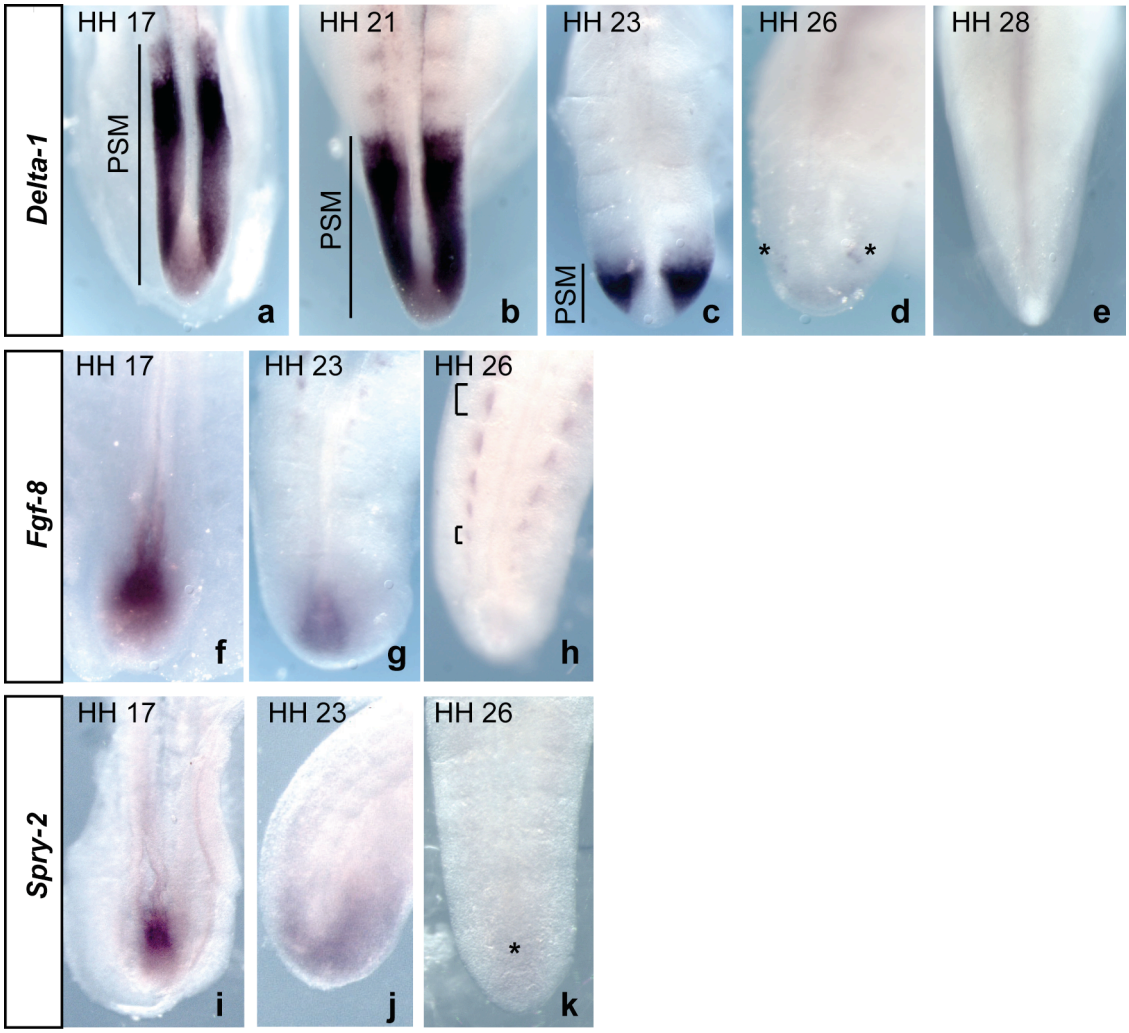

Figure 3.1 Decline of *Delta1*, *Fgf8* and *Spry2* expression as axial elongation terminates.

Dorsal view of chick tails at different embryonic stages stained by in situ hybridisation for *Delta1* (a-e), *Fgf8* (f-h) and *Spry2* (i-k). Typically, 5 embryos for each embryonic stage were subjected to in situ hybridisation. Note decline of *Delta1* expression (a-e, asterisks in d indicate stained scattered cells) and of *Fgf8* expression (f-h) and of *Spry2* expression (i-k, asterisk in k shows very low expression). Vertical lines in a, b and c indicate decrease of PSM size as elongation arrests and bars in h highlight decrease of somite size when comparing older to younger segments.

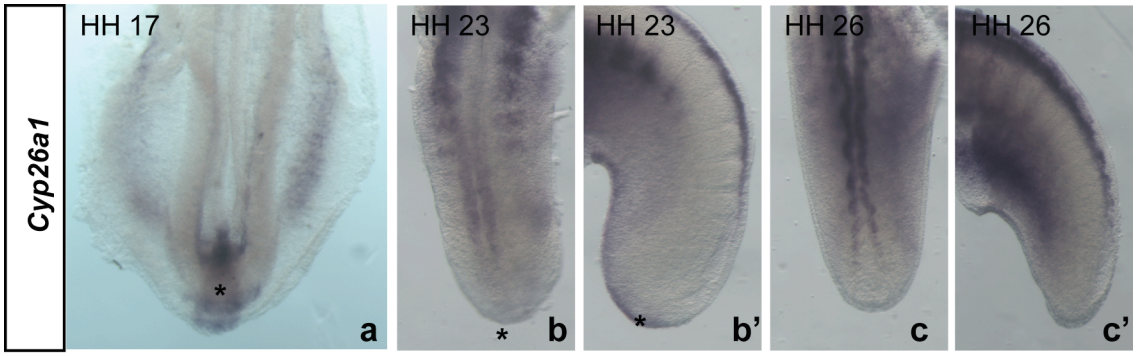

Figure 3.2 Dynamics of *Cyp26a1* expression as axial elongation terminates.

Dorsal (a, b, c) and side (b', c') views of chick tails at the indicated embryonic stage stained by in situ hybridisation for *Cyp26a1*. Typically, 5 embryos for each embryonic stage were subjected to in situ hybridisation. Note decline of *Cyp26a1* expression (a-c', asterisks in a, b and b' indicate expression in the tail which is very low in b').

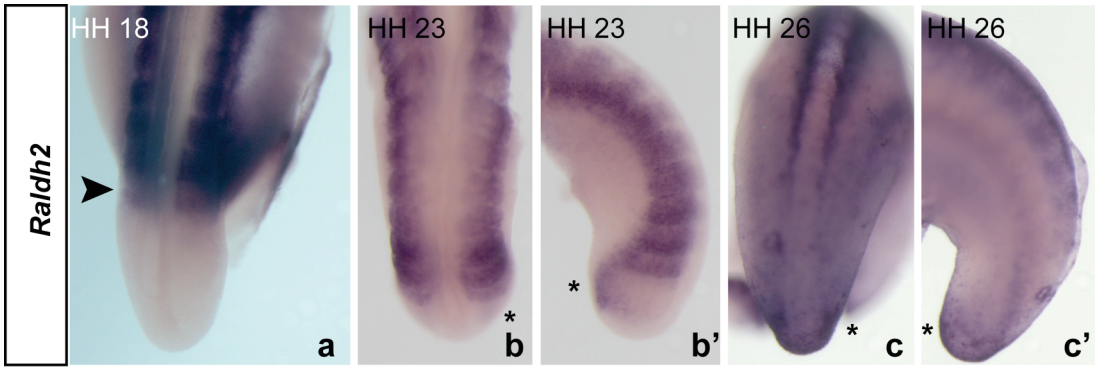

Figure 3.3 Dynamics of *Raldh2* expression as axial elongation terminates.

Dorsal (a, b, c) and side (b', c') views of chick tails at the embryonic stage indicated stained by in situ hybridisation for *Raldh2*. Typically, 5 embryos for each embryonic stage were subjected to in situ hybridisation. Note that expression is in proximity of the tail at HH18 (arrowhead in a) and in the tail at later stages (as indicated by asterisks in b-c').

3.1.2 *Cyp26a1* expression in the progenitor area is regulated by FGF/MAPK signalling

The possibility that retinoid signalling plays an important role in termination of axial elongation raised a number of questions. The first being whether *Cyp26a1* is expressed in the tail region exactly where progenitors reside. To do so, I performed double in situ hybridisation for *Cyp26a1* and *Fgf8*, considered a key marker gene for tail progenitors (Wilson et al., 2009). At HH12/13 both genes are found in a domain coincident with the posterior neural tube and the posterior PSM (Figure 3.4 a, b, c), where *Fgf8* is expressed in a graded fashion that correlates with *Cyp26a1* expression (Figure 3.4 d). The *Cyp26a1* domain is more spatially restricted than that of *Fgf8*. Thus, expression of the two genes is coincident at HH12/13, consistent with *Cyp26a1* playing a role in regulation of progenitor cells. Nevertheless, confocal imaging of the samples processed for fluorescent in situ hybridisation would provide greater resolution and more accurate determination of the degree of gene colocalisation between the two.

To address whether there is an interaction between FGF signalling and *Cyp26a1*, I used a pharmacological approach and cultured HH10/12 whole embryos *ex-ovo* for 6 hours in presence or absence of different drugs, as described in (Connolly et al., 1995). Inhibiting the activity of FGF receptor 1, by using SU5402, results in complete loss of *Cyp26a1* expression (Figure 3.5 c, d n=8/8) and *Spry2* (Figure 3.5 a, b n=8/8), a target gene of FGF signalling. Loss of *Cyp26a1* expression is specific to the tail domain and occurs quickly, within 1.5 (n=12/16) and 3 (n=8/8) hours of culture.

The converse experiment (i.e. stimulation of FGF signalling by addition of FGF8 protein in the culture medium) did not lead to conclusive observations: no expansion of *Spry2*, a FGF signalling target gene (used as a positive control in the experiment), was observed. Thus, FGF8 seems not to be sufficient to induce *Cyp26a1* expression. One could test whether this experiment did not show the expected result because of technical limitations. For example, one could titrate the concentration of FGF8 protein used in the culture medium (by using more than 2.5 μg/ml of FGF8, the amount used in the original experiment) or one could implant beads soaked in FGF8 protein (a localised source of

protein might be more effective than a source of protein dissolved in the culturing medium, as it was done in the original experiment). Previous reports have shown that treatment of embryos with SU5402 and FGF8 protein result in morphological alterations, including changes in somite size (Dubrulle et al., 2001). Nothing similar was observed here, possibly because of the lower drug concentration (10 μM of SU5402 and 2.5 μg/ml of FGF8) and shorter time frame (6 hours).

Several intracellular signalling pathways are activated downstream of the FGF receptors, such as Erk/MAPK, PI3K/Akt and Calcium/PKC (Bottcher and Niehrs, 2005). Previous studies showed that Erk/MAPK is the effector of the FGF gradient in the chick PSM (Delfini et al., 2005). Based on this, I explored whether FGF signalling regulates *Cyp26a1* expression via MAPK, using a chemical inhibitor of the MAPKK, MEK1. I observed that the majority (n=8/10) of the treated embryos show down-regulation of *Cyp26a1* expression (Figure 3.5 k, l). Similarly, *Spry2* expression is down-regulated in treated embryos (n=9/11 Figure 3.5 I, j). Therefore, expression of *Cyp26a1* is regulated by FGF signalling via the MAPK route. It remains possible that regulation of *Cyp26a1* expression occurs via other intracellular effectors such as Akt.

These data suggest that FGF signalling is required for *Cyp26a1* expression in the chick tail region, as previously reported in the frog and in the mouse (Moreno and Kintner, 2004, Wahl et al., 2007). This regulatory interaction is therefore highly conserved among vertebrate embryos.

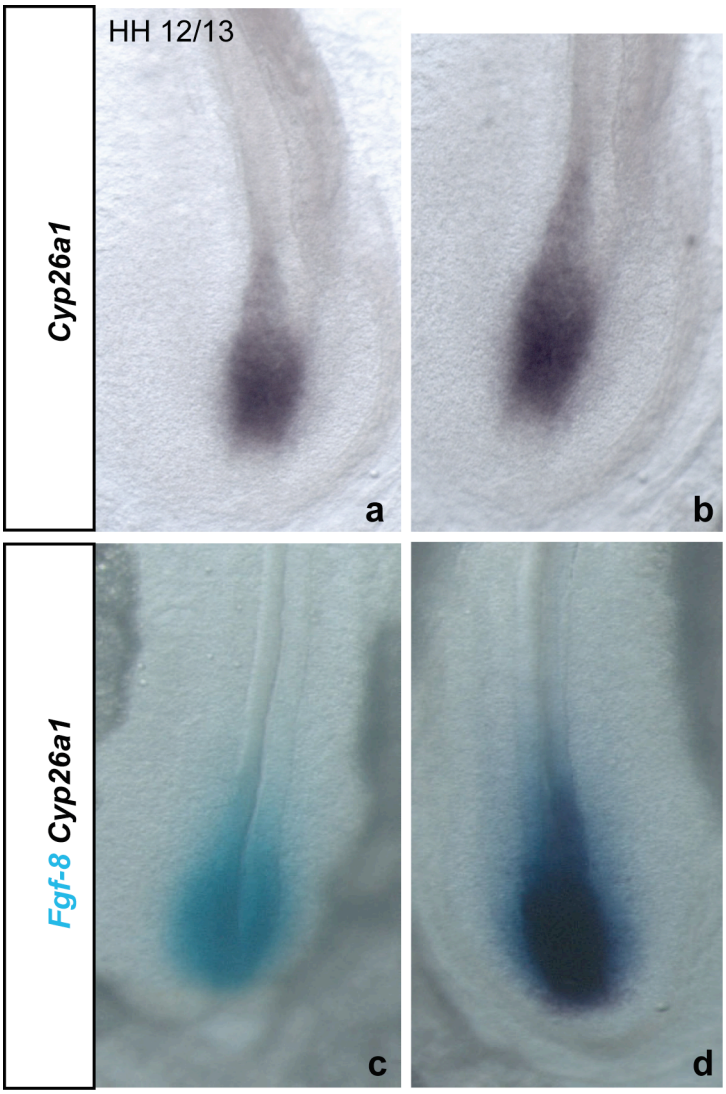

Figure 3.4 *Cyp26a1* expression domain in the progenitor area in comparison to *Fgf8* domain in the same region.

Dorsal view of chick tails at HH12/13 stained by in situ hybridisation for *Cyp26a1* (a,b, b shows a closer view of the expression domain), *Fgf8* (c) and doubled stained for *Cyp26a1* and *Fgf8* (d). A FLU-labelled probe was used for *Cyp26a1* and a DIG-labelled probe for *Fgf8*. The dark blue colour was developed using NBT/BCIP and the light blue colour was developed using BCIP alone. The two genes are expressed in similar domains which correspond to the progenitor region.

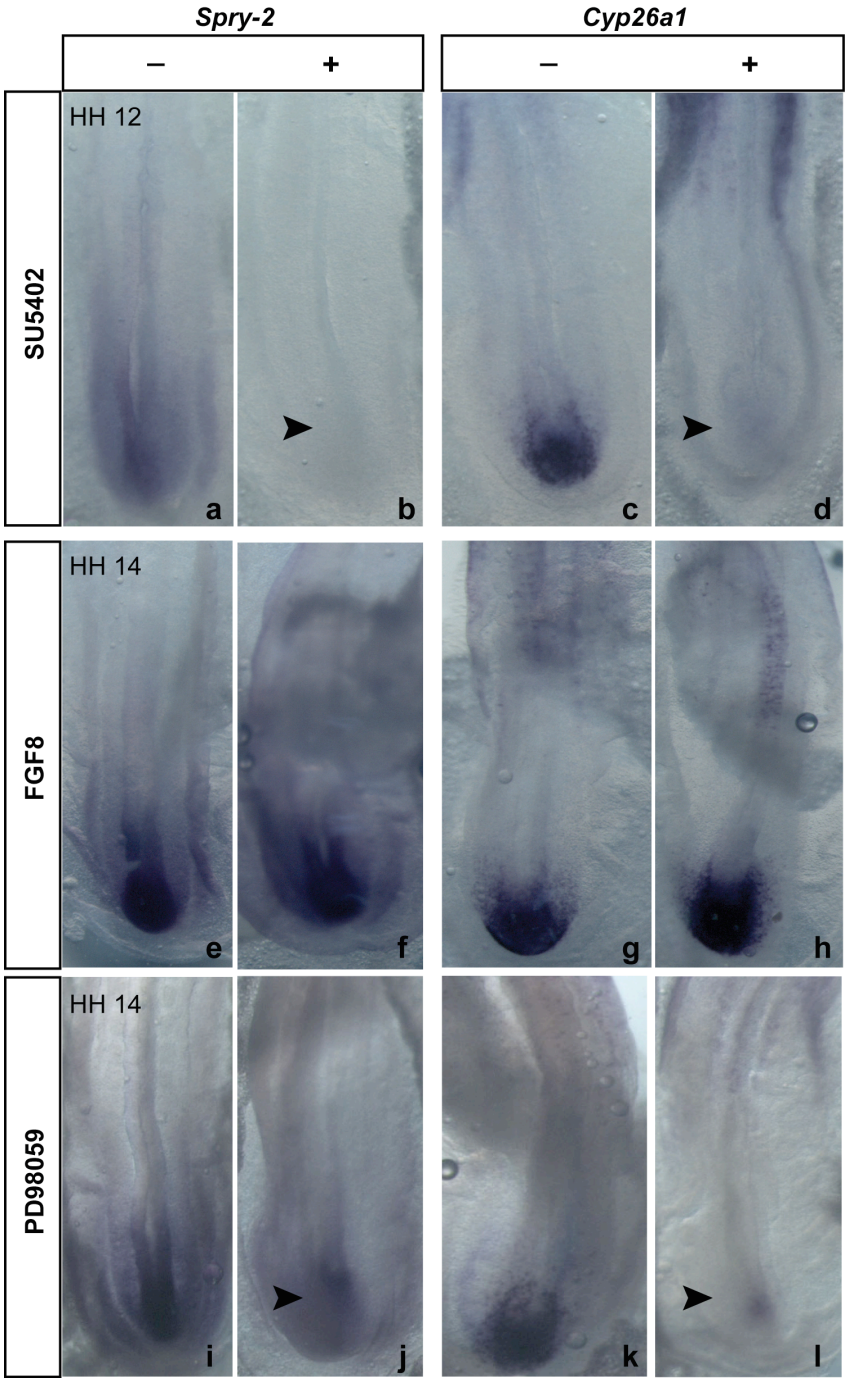

Figure 3.5 Regulation of *Cyp26a1* expression.

Dorsal view of HH12 or HH14 chick tails stained by in situ hybridisation for *Spry2* (a, b, e, f, I, j) and *Cyp26a1* (c, d, g, h, k, l). Note down-regulation of gene expression in treated embryos (b, d, j, l) versus control embryos (a, c, i, k), see arrowheads in b, d, j, l and no expansion of gene expression domains in treated embryos (f, h) versus control embryos (e, g). Embryos were cultured *ex-ovo* in L15 medium supplemented with serum for 6 hours, in presence of DMSO or PBS and 10 μM of SU5402, 2.5 μg/ml of FGF8 or 0.5 mM of PD98059.

3.1.3 Examination of *Cyp26a1* function in chick axial elongation and segmentation

3.1.3.1 Analysis of sufficiency of Cyp26a1 for elongation and segmentation

Cyp26a1 expression is found in a domain similar to that of *Fgf8,* a key marker of axial progenitors, and it is dependent on FGF/MAPK signalling, which controls posterior axial elongation by maintaining PSM cells in an undifferentiated state. To test whether *Cyp26a1* regulates chick axial elongation, a pCIG over-expression vector (expressing only the GFP reporter) or a pCIG-*Cyp26a1* vector (expressing the GFP reporter and the gene of interest) was electroporated into HH4 embryos at the level of the node, which contains presumptive PSM cells. 24 hours after electroporation, HH11 embryos showed GFP contribution in the presomitic region (see schematic in Figure 3.6).

At the molecular level, *Cyp26a1* was ectopically expressed following pCIG-*Cyp26a1* electroporation (n=6/6 Figure 3.6 d), confirming that the over-expression experiment worked. Expression of *Brachyury* (*T),* a caudal PSM marker, was unchanged, implying that over-expression of *Cyp26a1* does not affect the caudal PSM character (n=6/6 Figure 3.7 d).

At the morphological level, HH11 electroporated embryos showed asymmetric somite positioning (Figure 3.6 compare d' to b'). In vertebrates, somite formation is bilaterally symmetric, but it has been reported that RA deprivation causes similar somite asymmetries to those observed in pCIG-*Cyp26a1* electroporated embryos (Vermot and Pourquie, 2005). Thus, it is possible that over-expression of *Cyp26a1*, a RA catabolising enzyme, causes decreased RA levels, resulting in somite asymmetries. As somite positioning depends on the period of the segmentaton clock, asymmetric localisation of the clock genes might result in a change of somite positioning. To explore this hypothesis, *Lfng* expression pattern was analysed in *Cyp26a1* over-expressing embryos and it was found to be asymmetric (n=4/5 Figure 3.8 c-e compare to WT Figure 3.8 a, b). These results are suggestive of a loss of coordination of the

clock oscillations between the two sides of the embryo. Notably, *Lfng* expression seemed to be out of phase, the phase on right side being delayed compared to that on the left side. Thus, *Cyp26a1* might regulate the left-right coordination of the segmentation process by controlling oscillations of the segmentation clock.

Although GFP expression was not recorded, following pCIG-*Cyp26a1* electroporation, one could predict that:

1) fluorescent expression was markedly induced on the right side of the PSM of the embryo, explaining the right-sidedness of the asymmetries;

2) fluorescent expression was equally distributed on the two sides of the embryo, and asymmetries arised because *Cyp26a1* over-expression affected left-right machinery at the node stage (HH4), when pCIG-*Cyp26a1* was electroporated (the node is where initial left-right polarity takes place).

In conclusion, my observations seem to be similar to previous reports showing that blocking RA production from the node stage results in asymmetric *Lfng* pattern around the prospective cervical region (Vermot and Pourquie, 2005).

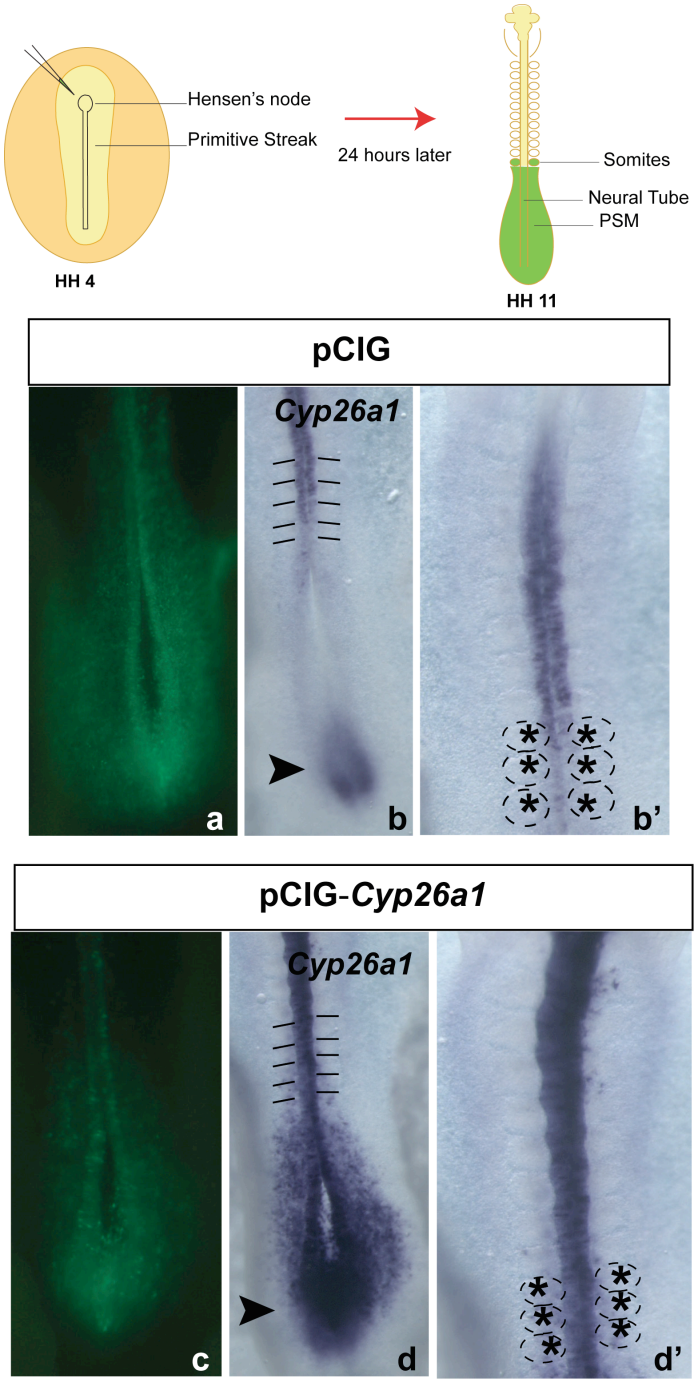

Figure 3.6 Effects of *Cyp26a1* over-expression on somite positioning.

Schematic of *in ovo* electroporation in the node at HH4 and consequent GFP expression in the PSM at HH11. GFP distribution after electroporation of pCIG or pCIG-*Cyp26a1* (a, c). Dorsal view of HH 11 chick tails stained by in situ hybridisation for *Cyp26a1* (b, b', d, d'). Note expansion of *Cyp26a1* expression domain in d and asymmetric somite positioning in d (somite borders are marked with black lines) and at higher magnification in d' (somites are marked by dashed circles).

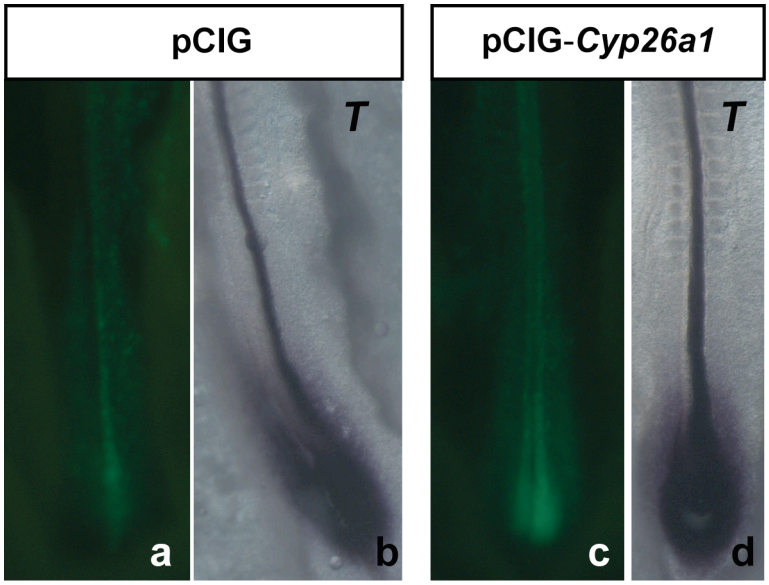

Figure 3.7 Effects of *Cyp26a1* over-expression on gene expression.

Expression of *Brachyury* (*T)* (b) after *in ovo* electroporation of pCIG (GFP expression is shown in a) and expression of *Brachyury* (*T)* (d) after *in ovo* electroporation of pCIG-*Cyp26a1* (GFP expression is shown in c). Expression domain of *Brachyury* (*T*) does not vary between the two experimental conditions.

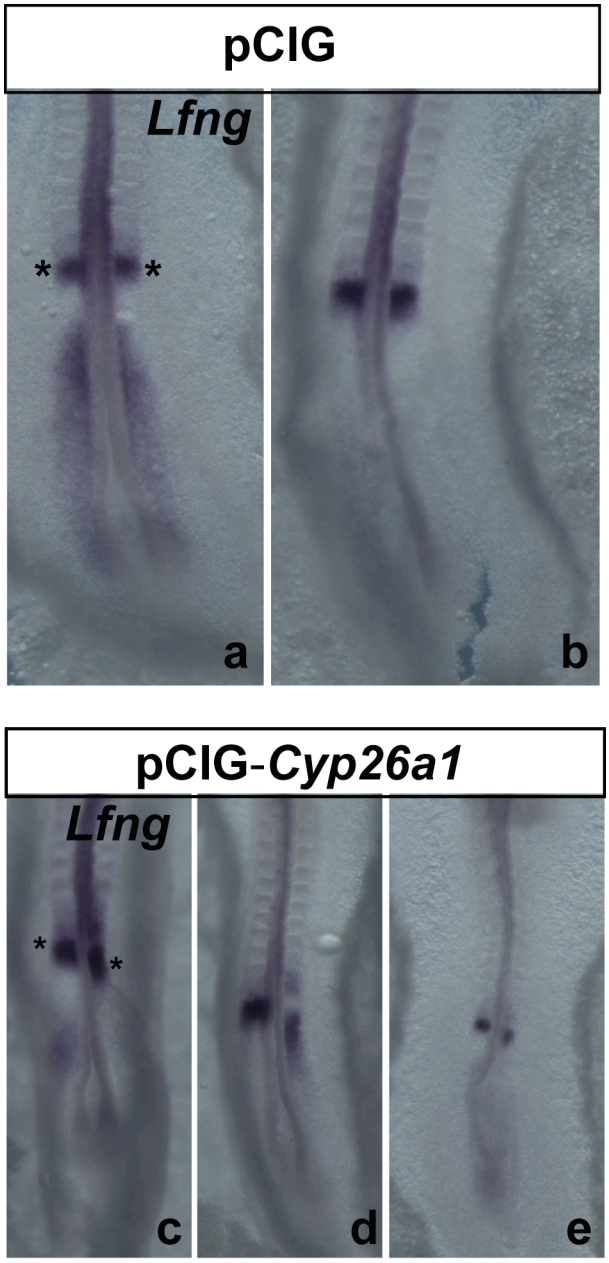

Figure 3.8 Effects of *Cyp26a1* over-expression on *Lfng* expression.

Expression of *Lfng* (a, b) after *in ovo* electroporation of pCIG (different phases of *Lfng* dynamic expression are shown) and expression of *Lfng* (c, d, e) after *in ovo* electroporation of pCIG-*Cyp26a1*. Note asymmetric somite positioning in c (asterisks), d, e when compared to a and b (asterisks).

3.1.3.2 Analysis of requirement of Cyp26a1 for elongation and segmentation

To verify whether *Cyp26a1* is required for chick axial elongation and segmentation, I used shRNAs to down-regulate expression of the protein. I tested the efficacy of three different hairpins *in vitro* and *in vivo*. Primary CEFs (Chick Embryonic Fibroblasts) were co-transfected with a vector expressing full-length *Cyp26a1* and vectors expressing the hairpins. HH12 embryos were co-electroporated in the neural tube with the same combinations of vectors. Western blot analyses of cellular and embryonic protein extracts show that the commercial anti-Cyp26a1 antibody used for the experiments binds multiple targets (Cyp26a1 has been reported to migrate as a band of 56 kDa) (Figure 3.7 a and b). To overcome this problem, I generated a C-terminal tagged version of Cyp26a1. A band at the correct size is present on the gel and it is enhanced when Cyp26a1 is over-expressed, unfortunately none of the hairpins were able to down-regulate Cyp26a1 protein expression levels (Figure 3.7 c). I tested morpholinos as an alternative knock-down strategy, as it has been reported to be preferable to shRNAs for functional studies in chick embryos (Mende et al., 2008).

A morpholino was designed targeting exon2/intron 2 boundary to produce mis-splicing of *Cyp26a1* transcript and protein loss of function. Embryos were electroporated with control and *Cyp26a1* morpholinos and RNA extracted to perform RT-PCR and assay splicing. If the morpholino blocks splicing at the targeted site a possible outcome is excision of exon 2 (another possibility is that the transcript retains the intron). If this is the case, by using primers on exon 1 and exon 3 (see schematic in Figure 3.8 a), a normal transcript gives a product of 813 bp and a mis-spliced transcript of 588 bp. RT-PCR showed no mis-splicing bands in embryos electroporated with *Cyp26a1* (Figure 3.8 b). However, the product at 813 bp was strongly decreased in experimental samples. A possible explanation for this could be nonsense-mediated decay, a cellular quality control mechanism that occurs when a premature termination codon triggers mRNA degradation. If the *Cyp26a1* morpholino causes

either exon skipping or intron retention, the resulting transcripts would contain a premature stop codon, leading to transcript decay. If this explanation were true, amplification of any of the exons of *Cyp26a1* transcript should give the same result (e.g. decrease in strength of the band). However, RT-PCR for exon 1 gave a normal signal (not shown), indicating that *Cyp26a1* morpholino does not cause nonsense-mediated decay.

While I was working on these experiments, new studies reported the importance of retinoid signalling in termination of avian and murine elongation and segmentation (Tenin et al., 2010, Young et al., 2009, Savory et al., 2009). For this reason and because my work on *Cyp26a1* was very preliminary and it would have required more experiments and more time to achieve successful functional studies, I decided to focus on different projects (see results Chapter 4 and 5).

In the next sections, I present my investigations on mechanisms, other than signalling decline, which contribute to termination of axial elongation (e.g. reduction of somite formation rate as elongation ceases).

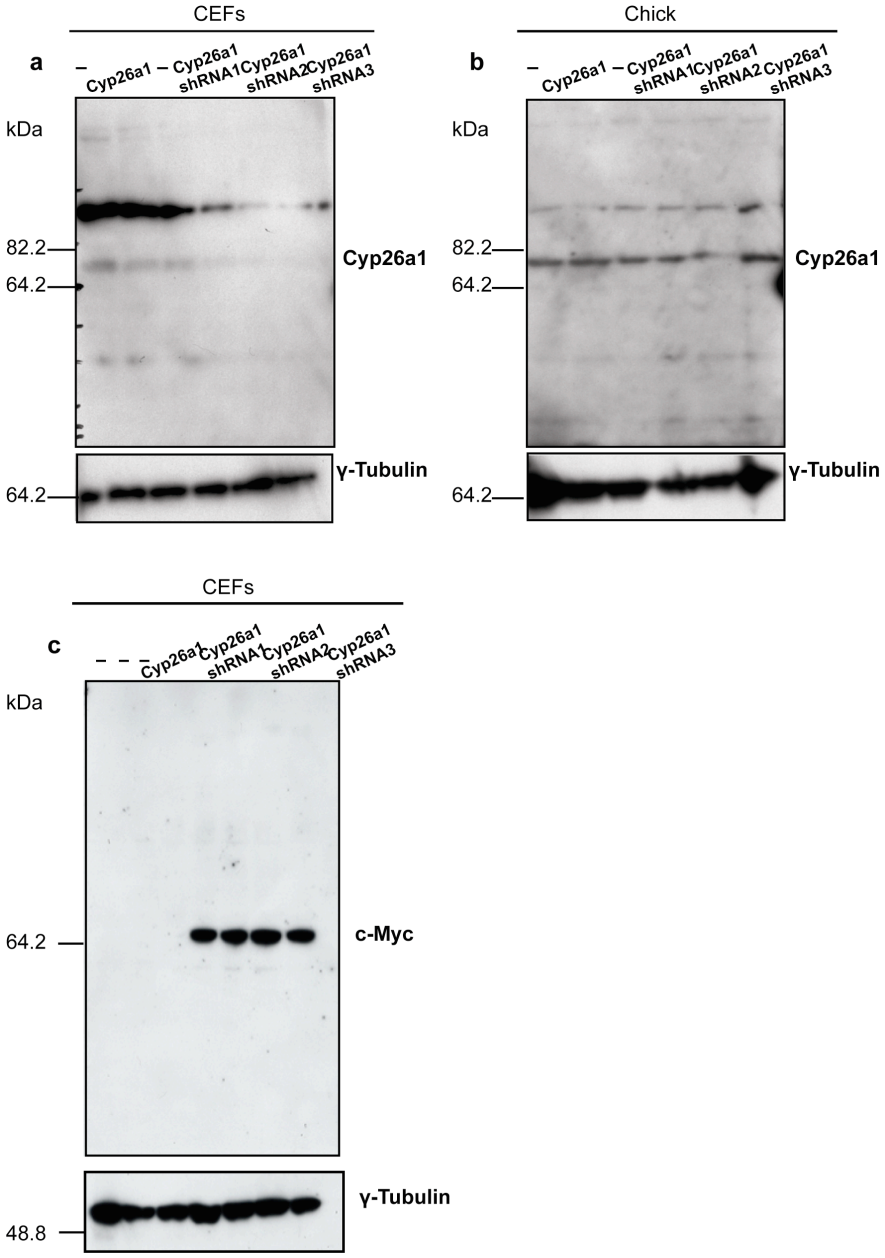

Figure 3.9 Cyp26a1 protein levels in CEFS and chick embryos transfected and electroporated respectively with shRNAs against Cyp26a1.

Figure a and b show Western blot using a commercial Cyp26a1 antibody (presumptive band over 64.2 kDa). Amount of protein loaded in each lane correspond to lysates extracted from ~200 000 cells (a) and 2 embryos (b). In a and b, lysates were from: AING empty vector, AING-*Cyp26a1*, pRFPRNAi empty vector, AING-*Cyp26a1* and pRFPRNAi-shRNA1, ad then as indicated. Figure c shows Western Blot using a c-Myc antibody to recognise a C-terminal tagged form of Cyp26a1 (presumptive band at 64.2 kDa). Lysates were extracted from ~200 000 cells and correspond to: untransfected, pCDNA empty, pRFPRNAi empty, pCDNA-*Cyp26a1* and pRFPRNAi empty, pCDNA-*Cyp26a1* and pRFPRNAi shRNA1, and then as indicated. In a, b, c γ-tubulin is showed as loading control.

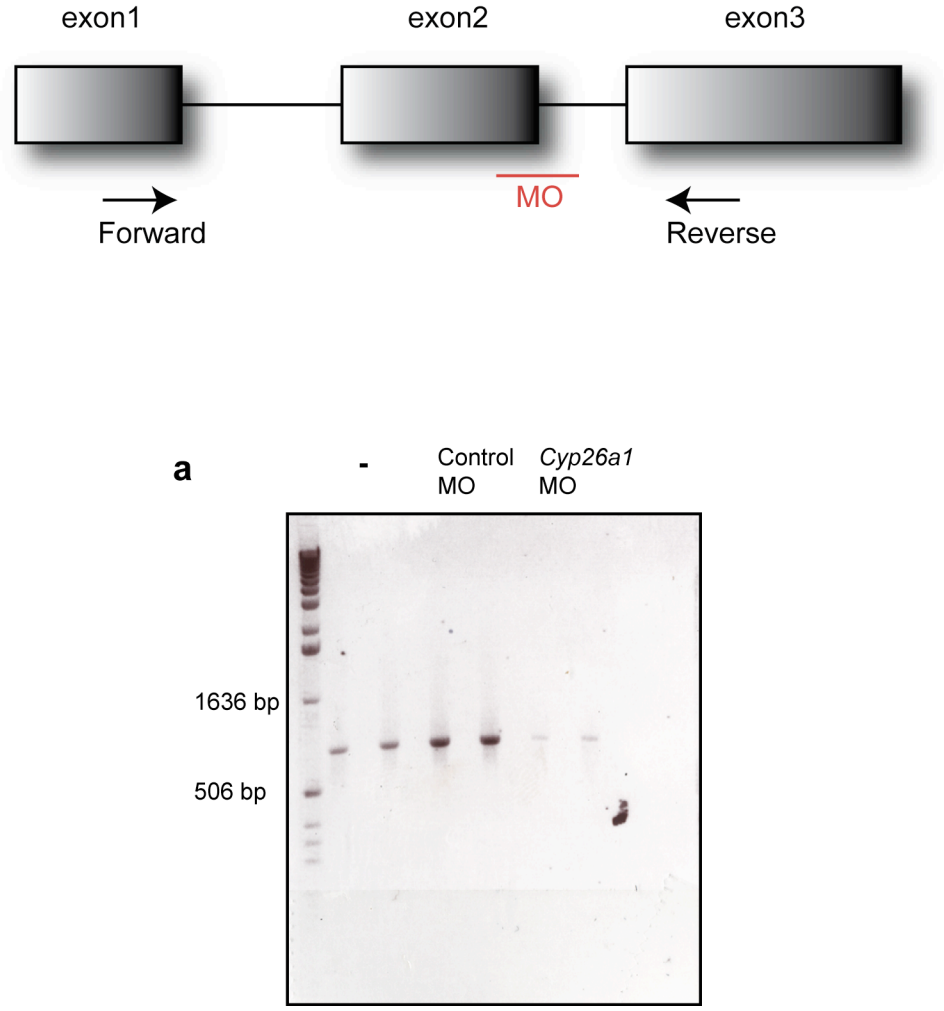

Figure 3.10 Morpholino knock-down of Cyp26a1.

Figure a is schematic of exon/intron structure of *Cyp26a1* gene in the region targeted by the morpholino. Location of primers used for RT-PCR is indicated by arrows and red line shows location of targeting morpholino. In figure b, RT-PCR analysis of *Cyp26a1* splicing, in each conditions RNA comes from 5 HH12 embryos following *in-ovo* electroporation at HH4. Duplicates of each samples were loaded on gel in the following order: not electroporated samples, samples electroporated with control morpholino, samples electroporated with *Cyp26a1* morpholino. No mis-splicing bands are detected on gel, but a decrease in strength of the bands is observed in samples electroporated with *Cyp26a1* morpholino.

3.1.4 Rate of somite formation changes as axial elongation terminates

To test whether termination of axial elongation associates to a change of somite formation rate (e.g. the segmentation clock ticks slower or stops ticking as axial elongation comes to an end), I counted the number of somites formed at late embryonic stages. I made use of Scanning Electron Microscopy (SEM), which images the sample's surface revealing the shape of the segments. As reported by Burke et al. (1995), the chick hindlimb extends from somite 29/30 to somite 34/35 at HH24, thus it can be used as a landmark to count the somites which exist caudally. HH24 embryos have 15.4+/-0.5 somites after the landmark and HH25 embryos have 15.7+/-1 somites (Figure 3.9 a, b), indicating that fewer than one segment forms over this 12 hours period. These observations imply that somitogenesis terminates at HH24, as no more segments form at HH25.

In order to count the total number of somites, including the most cranial segments, I took advantage of micro-computed tomography (micro-CT) scanning that uses X-rays to image internal structures that are not visible in Electron Microscopy imaging. I confirmed that, at HH24, embryos have 48.5+/-0.6 somites and, at HH25, they have 49.8+/-0.4 somites (Figure 3.10 a). These measures correlate well to those obtained by SEM. However, the position of the hindlimb calculated by micro-CT differs from that of other, previous measurements (Burke et al., 1995) (Figure 3.10 b), differences in measured number will be discussed in the next Discussion section. All together, the SEM and micro-CT scanning data suggest that a counting mechanism exists to precisely control the final number of segments (see standard deviation in Figures 3.9 and 3.10).

Interestingly, Tenin et al. (2010) have shown that segmentation clock rate slows down by HH23, the period increasing to 150 minutes rather than 90 minutes as measured at earlier stages. The authors used a large batch of embryos to compare the number of somites formed at different embryonic stages. They also used half-PSM culturing of late embryos (where one half is fixed immediately and the other half is cultured for different time periods) to precisely determine the rate of the segmentation clock when axial elongation terminates. Their data are in agreement with my own work.

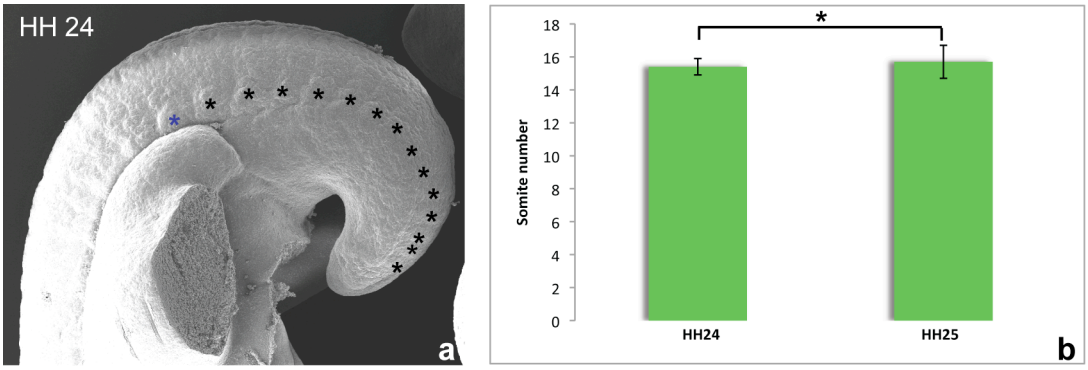

Figure 3.9 Counting the final number of somites by Scanning Electron Microscopy.

Figure a shows scanning electron microscopy of HH24 chick tail, side view. The hindlimb was cut to reveal the somites (marked by asterisks). Somite 34-35 is marked in blue and is used as a landmark. Figure b is analysis of somite number formed after the landmark at different embryonic stages. HH24 embryos (n=11) form 15.4 +/-0.5 somites after the hindlimb, HH25 embryos (n=11) form 15.7+/-1 somites. Error bars represent standard deviation, p-value<0.1 determined using a two-tailed t-test.

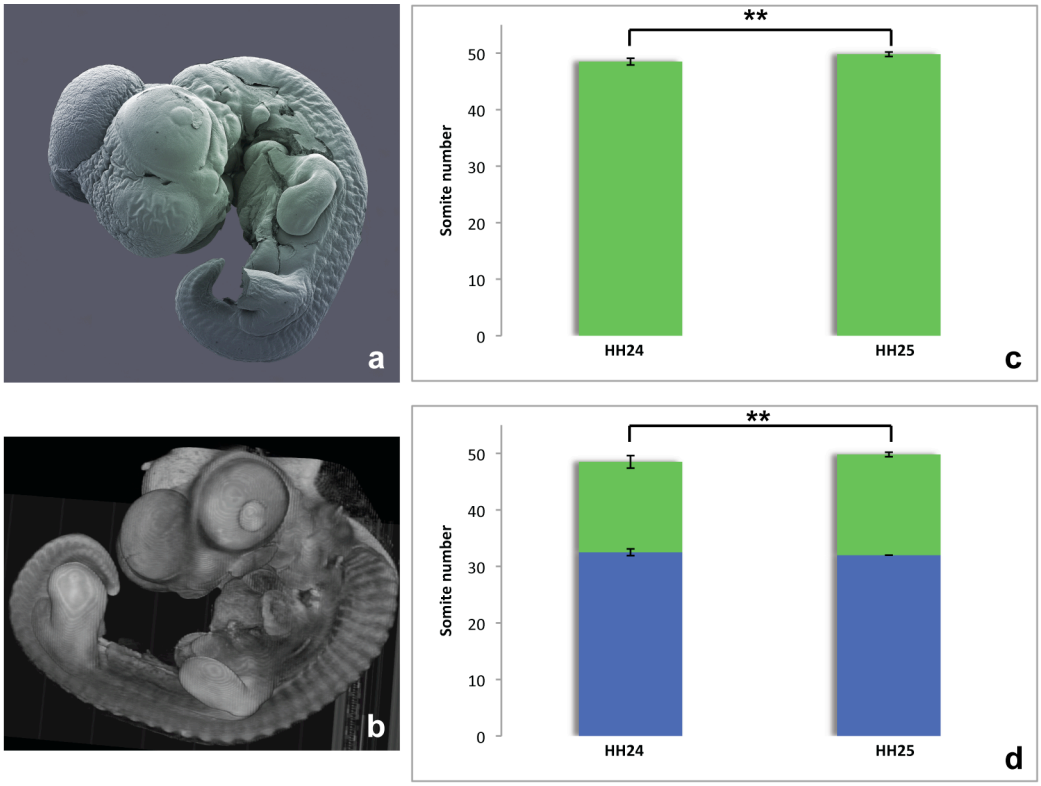

Figure 3.10 Counting the final number of somites by micro-CT scanning.

Figures a and b show chick embryos imaged via Scanning Electron Microscopy and micro-CT scanning respectively. Figure a is a montage. Graphs in c and d represent somite counting by using micro-CT scanning. The total number of somites is counted at different embryonic stages in c, HH24 embryos form 48.5+/-0.6 somites (n=4) and HH25 embryos form 49.8+/-0.4 somites (n=5), p-value<0.05 determined using a two-tailed t-test. In d blue bars represent the number of somites formed until the hindlimb and green bars show the number of somites formed after the hindlimb, HH24 embryos form 32.5+/-0.6 somites before the hindlimb and 16+/-1 after the hindlimb; HH25 embryos form 32 somites before the hindlimb and 17.8+/-0.4 somites after the hindlimb, p-value<0.05 determined using a two-tailed t-test.

3.2 Discussion

3.2.1 Termination of axial elongation associates with decline of signals and reduction of somite formation rate

In this chapter, I have provided evidence that *Delta1*, *Fgf8*, *Spry2* and potentially *Cyp26a1* expression declines when chick axial elongation terminates (Figures 3.1, 3.2), similar to observations in the mouse (Cambray and Wilson, 2007). Therefore, loss of expression of genes required for progenitor maintenance occurs similarly in different vertebrates, suggesting that this is a general mechanism for regulation of axis length.

Decline of gene expression may cause/coincide with depletion of axial progenitors known to contribute to generation of axial structures. Indeed, I observed that the size of the presomitic and the somitic tissues gets reduced as gene expression declines and as axial elongation comes to an end (Figure 3.1), and this is conserved between chick, mouse, fish and snake embryos (Gomez et al., 2008). Interestingly, mutations in *Fgf8* and *Cyp26a1* cause severe axis defects and truncations in the mouse (Sun et al., 1999, Abu-Abed et al., 2001). Thus, these genetic studies represent a link between loss of signals required for axial elongation and segmentation and reduction of tissue size.

Expression of RA synthesising enzyme, *Raldh2,* switches on in the tail region when *Delta1*, *Fgf8*, *Spry2* and *Cyp26a1* decline (Figure 3.3). Previous experiments have shown that exposure to RA causes loss of *Fgf8* and *Wnt3a* (Diez del Corral et al., 2003, Shum et al., 1999). Thus, it is tempting to speculate that down-regulation of genes required for progenitor maintenance, observed at late segmentation stages, could be caused by RA activity (indicated by expression of RA synthesising enzyme) in the tail region. Moreover, Shum et al. (1999) reported that RA treatment causes extensive cell death in the tail and severe truncation of the axis, implying that RA plays a role in termination of axial elongation.

Termination of axial growth could be caused by cell death, in support of this apoptotic foci have been observed in late chick tails and this is consistent with the idea that RA

triggers apoptosis to terminate axis extension (Sanders et al., 1986, Tenin et al., 2010) (Shum et al., 1999).

In a recent study, Tenin et al. (2010) showed that RA activity is present in the chick tail at late stages and it is associated with down-regulation of expression of tail genes such as *Fgf8* and *Wnt3a*, and with reduction of PSM size. These data suggest that tail-derived RA suppresses expression of genes required for progenitor maintenance, leading to consumption of mesodermal tissue and cessation of axis lengthening.

RA is also known to affect expression of Hox genes, which specify development of the anteroposterior axis (Conlon, 1995). Thus, it is possible that RA causes termination of axial elongation by activating posterior Hox genes. Consistent with this idea, Young et al. (2009) have shown that premature expression of *Hoxb13* leads to axis truncation.

A similar phenotype that observed following RA exposure (e.g. axis truncation) has been observed in *Cyp26a1* mouse mutant line (Abu-Abed et al., 2001). *Cyp26a1*, as a RA degrading enzyme, is thought to be in the tail to protect the progenitors from deleterious effects of RA (see Figure 3.11 for summarising schematic).

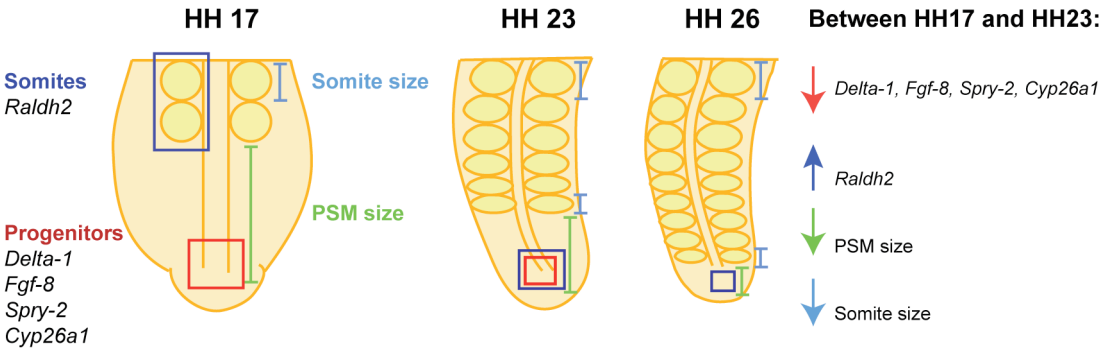

Figure 3.11 Gene expression levels, PSM and somite size decline as axial elongation terminates.

Schematic depiction of changes in genes expression level and in tissue size as tail formation comes to an end. At HH17, genes required for axial progenitor maintenance (*Delta1, Fgf8, Spry2* and *Cyp26a1*) are expressed at the tail end where progenitors reside. RA (see *Raldh2* expression domain), which promotes mesoderm differentiation, is confined to the somites and a region proximal to the tail. Between HH17 and HH23 expression of genes confined to the progenitors region declines, and disappears after HH23. At the same time the *Raldh2* domain approaches the tail end. As gene expression changes over time, PSM and somite size are reduced until somitic tissues is exhausted, when elongation ceases.

Thus, I explored the regulation and function of *Cyp26a1* in the context of segmentation and axial elongation. I found that expression of *Cyp26a1* is downstream of the FGF signalling in the chick PSM (Figure 3.5) as well as in the frog and in the mouse, but not in the fish (Moreno and Kintner, 2004, Wahl et al., 2007, Martin and Kimelman, 2010). FGF and RA signalling have been shown to antagonise each other to repress or promote mesoderm differentiation (Dubrulle et al., 2001, Diez del Corral et al., 2003). It is possible that FGF signalling activates expression of *Cyp26a1*, a RA degrading enzyme, to maintain PSM cells in an undifferentiated state.

However, I have been unable to show that *Cyp26a1* over-expression is sufficient to maintain the PSM in an immature status by inducing caudal gene expression (Figure 3.6). This might be because of technical limitations, such as the gene delivery method of choice (e.g. electroporation in the node). Although electroporation in the node is a popular method for efficient transient transfection of the PSM, expression of the transgene lasts only few days. For this reason, it is difficult to study the effects (in term of molecular and morphological changes) of the gene of interest when elongation ceases. Retroviral infection of the tail region would allow more efficient gene delivery and would allow long-term measurements to be taken (Homburger and Fekete, 1996). As an alternative, a method for stable integration and conditional expression of genes via electroporation which combines extended expression and temporal control of the transgene has been recently established and could be exploited (Sato et al., 2007).

To conclude that *Cyp26a1*, in contrast to *Fgf8* (Dubrulle et al., 2001), is not sufficient to maintain the caudal PSM character, further analysis of presomitic genes, such as *Tbx6* and *Spry2* is required. Moreover, rigorous quantification of morphological parameters (e.g. PSM and somite size) is needed, in the light of the fact that RA deficient quail embryos show increased PSM size and decreased somite size (Diez del Corral et al., 2003).

Although the role of *Cyp26a1* in progenitor maintenance remains to be determined, a previously unreported involvement of *Cyp26a1* in regulation of left-right symmetry might have emerged from the observations described in Figure 3.8. Indeed, pCIG-*Cyp26a1* electroporated embryos exhibit asymmetric somite positioning. A similar phenotype has been described in RA deprivated embryos (Vermot and Pourquie, 2005).

Thus, one could speculate that because *Cyp26a1* encodes a RA catabolising enzyme, over-expression of the gene affects RA levels, resembling a RA deprivation condition and causing a phenotype associated to that condition (Vermot and Pourquie, 2005),(Niederreither et al., 2002). Indeed, in *Cyp26a1* over-expressing embryos, asymmetric somite positioning coincides with asymmetric *Lfng* expression, implying that *Cyp26a1* might regulate left-right symmetry by controlling expression of the segmentation clock machinery.

Completion of somitogenesis could be associated to a change of the segmentation clock rate (e.g. the clock ticks slower or stops ticking as development progresses, leading to the definitive somite number). My results indicate that the last segments form at HH24, implying that completion of somitogenesis occurs at that developmental stage (Figures 3.9, 3.10). My counting measurements slightly differ from previous measurements, possibly because of different criterions used to define the borders of the anatomical landmarks used to count the somites, such as the hindlimbs (Burke et al., 1995).

As no more segments form after HH24, it is possible that oscillations of cyclic genes have ceased at this stage. Indeed, it has been recently shown that that the expression of clock genes is lost at late segmentation stages (Tenin et al., 2010). Moreover, Ferjentsik et al. have reported that absence of cyclic gene expression, due to complete loss of Notch activity, leads to termination of somitogenesis (Ferjentsik et al., 2009).

Tenin et al. have shown that segmentation clock rate slows down by HH23, the period being 150 minutes rather than 90 minutes as for earlier developmental stages (Tenin et al., 2010). Decreased clock rate may result in increased somite size, as more cells can be allocated to each somite (Dubrulle et al., 2001). However, I observed that the youngest somites are increasingly smaller than the older ones (Figure 3.1). This is not because the clock rate increases but presumably because the presomitic tissue gets reduced (e.g. there is not enough tissue left to form somites of the right size) (Gomez et al., 2008).

Generation of mesodermal tissue is regulated (among others) by *Wnt3a* (Takada et al., 1994). Tenin et al. have shown that *Wnt3a* expression is down-regulated at late segmentation stages and they speculated that such down-regulation might be involved in cessation of oscillations observed at late developmental stages (Tenin et al., 2010).

Consistent with this, Wnt signalling is known to regulate Notch signalling in the PSM (Hofmann et al., 2004). Thus, there might be a link between completion of somitogenesis (cessation of oscillations) and termination of axial elongation (tissue exhaustion).

Furthermore, Gibb et al. (2009) have proposed that Wnt signalling plays a major role in setting the clock period, as inhibition of this pathway causes slow down of *Lfng* oscillations and lengthening of segmentation clock period in both in the chick and in the mouse embryos. It is also possible that down-regulation of *Wnt3a* observed at late segmentation stages is caused by increased levels of retinoids, in the tail region. Indeed, it has been reported that RA treatments cause loss of *Wnt3a* expression and axis truncation in mice (Shum et al., 1999).

In addition to the Wnt signalling pathway, FGF might also control periodic somite formation, as shown in zebrafish mutants of *Hes6,* a FGF signalling target gene (Schroter and Oates, 2010). The *Hes6* mutant embryos have been described as "segmentation clock period mutants" because the clock is slowed down, leading to a reduced number of segments. Similarly to the Wnt and FGF signalling pathways, Sonic Hedgehog signalling has been implicated in establishment of proper periodicity of segmentation, suggesting that a complex molecular machinery operates behind the process (Resende et al., 2010).

Based on my experiments and on observations from other studies a summary of the conclusions regarding regulation of termination of axial elongation and segmentation is reported below:

- Axial elongation and segmentation end with a progressive decline of the expression of genes required for axial progenitor maintenance.
- Loss of gene expression might coincide with the depletion of the axial progenitors, which contribute to generation of the axial tissues. Indeed, the unsegmented and newly segmented tissue gets reduced in size as gene expression declines. Consistent with this, genetic studies showed that mutants of the genes required for progenitor maintenance exhibit severe defects to axial structures and axis truncations.

- Decline of the genes required for maintenance of axial progenitors seems to coincide with expression of *Raldh2* in the tail region. Interestingly, previous experiments reported that exposure to RA causes loss of *Fgf8* and *Wnt3a* (two of the genes implicated in maintenance and proliferation of progenitors). Moreover, other studies demonstrated that RA treatment causes extensive cell death in the tail and severe truncation of the axis;
- As development progresses, the rate of somite formation decreases, leading to the definitive somite number. Recent studies have observed that, oscillations cease at late segmentation stage. Cessation of the oscillations might be linked to down-regulation of *Wnt3a* that in turn might be caused by increased retinoid signalling in the tail region. Thus, there might be a link between cessation of oscillations and termination of axial elongation.

In the next chapter, I present my investigations into the role of gene dosage in controlling the definitive somite number. Specifically, I aim to identify mutations that are haploinsufficient for controlling the final somite number in mouse embryos.

Chapter 4. Control of somite number in the mouse embryo

Somites periodically bud off from the presomitic mesoderm (PSM), a derivative of the primitive streak. Periodic somite formation depends on a molecular oscillator, the segmentation clock, which drives expression of cyclic genes in the PSM (Palmeirim et al., 1997). Although somite number is highly variable between vertebrate species, it is accurately controlled in any given species. Mouse embryos form 65 pairs of somites, chick embryos form 50-55 pairs of somites, and zebrafish embryos form 31 pairs of somites. Intersestingly, the clock is extremely accelerated relative to developmental rate in snakes which form around 300 somites (Gomez et al., 2008). Slowing down of the segmentation clock reduces somite number (Schroter and Oates, 2010, Kim et al., 2011).

To date, several homozygous mutations have been shown to cause premature cessation of segmentation leading to axis truncations. These mutations reside in genes of the Fgf, RA, Bmp, Notch and Wnt signalling pathways that regulate various cellular mechanisms of the PSM (Dubrulle and Pourquie, 2004a, Wilson et al., 2009). If termination of axial elongation and segmentation occurs when the concentration of key components of these signalling pathways fall below a threshold, heterozygous embryos would form fewer somites. Conversely, heterozygous embryos for an inhibitor of termination of axial elongation and segmentation would form more somites. However, little is known about the heterozygous counterparts of the mutations cited above.

In this chapter, I present my study aimed at identifying mutations that are haploinsufficient for controlling the definitive somite number in mouse embryo. First, I established a reliable assay to count somites in E13.5 embryos. Second, I examined the final number of somites in heterozygous mutants of genes known to regulate somite formation and axial elongation.

4.1 Results

4.1.1 Establishing a counting assay in mouse embryos

4.1.1.1 Testing somite counting by in situ hybridisation, SEM and X-ray micro-CT

To determine the final number of somites in mouse embryos, I had to establish an assay that permits visualisation and counting of somites at E13.5, when axial elongation has ceased. To do so, I could have counted the segments in adult skeletons, but counting of the most anterior segments would have been difficult as they are incorporated into the skull. Or I could have visualised the somites by staining the somitic compartments with specific markers. I took advantage of the latter approach. *Uncx4.1* is a marker of the posterior compartment of newly formed somites and of the sclerotome of older somites (Figure 4.1 a) (Mansouri et al., 1997). *MyoD* is expressed in somites and muscle myotomes (Figure 4.1 b) (Sassoon et al., 1989). *Tbx18* is expressed in the anterior compartment of prospective and definitive somites and in the sclerotome of epithelialised somites (Figure 4.1 c) (Kraus et al., 2001).

Triple in situ hybridisation for *Uncx4.1*, *MyoD* and *Tbx18* revealed all or nearly all the somites of E10.5 and E12.5 mouse embryos (Figure 4.1 d, e). However, the staining revealed only the most posterior somites of E13.5 embryos preventing quantitation of the final somite number (Figure 4.1 f). The level of the staining did not improve by increasing the incubation time of proteinase K to aid tissue penetration. A possible reason for this is inadequate penetration, because the skin is forming at such embryonic stages.

An alternative way of visualising the somites is by revealing their surface by SEM. In contrast to viewing chick somites when segmentation is finishing (HH24-25 embryos) (see Chapter 3), somites of E13.5 mouse embryos were not visible at any axial levels

except at the tip of the tail (Figure 4.2). This is probably because of different tissue thickness in the different organisms. Thus, SEM could not be used to count the definitive somite number.

X-ray micro-CT images both the surface and the inside of the sample (see Chapter 3), revealing structures that are not visible to SEM. Somites of E13.5 embryos were clearly visible along most of the anteroposterior axis. Nevertheless, the most posterior somites were not detectable (Figure 4.3), possibly because of low imaging resolution. Together, these data indicate that none of the histological (in situ hybridisation) or imaging (SEM, X-ray microCT) techniques tested are appropriate to count the final somite number in mouse embryos.

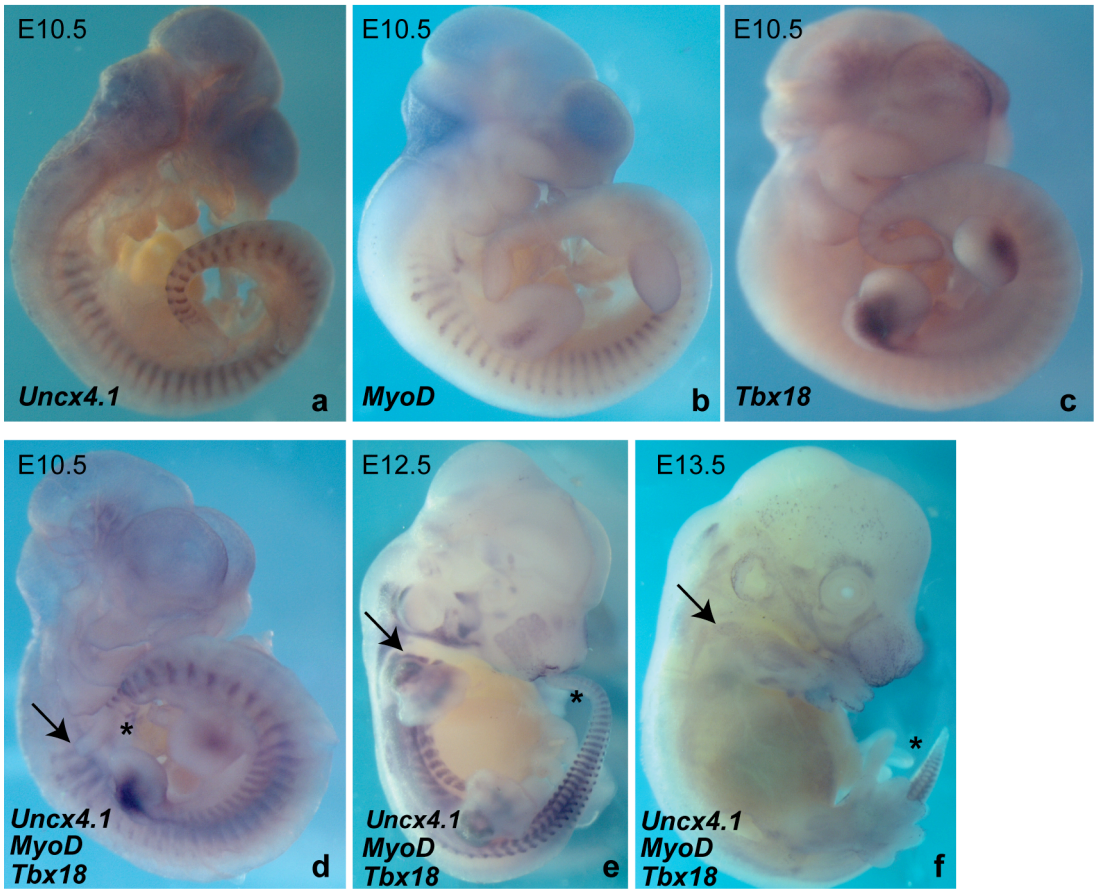

Figure 4.1 Using in situ hybridisation to count the final somite number in mouse embryo.

Figures a-f are side views of mouse embryos at indicated embryonic stages. Embryos were stained by in situ hybridisation for various somite markers: *Uncx4.1* (a), *MyoD* (b) and *Tbx18* (c) or for all these markers combined together (d-f). Arrows point to most anterior somites and asterisks point to most posterior somites. Note that all somites are visible at E10.5 (d) and almost all somites are visible at E12.5 (e). Only the very last somites are visible at E13.5 (f).

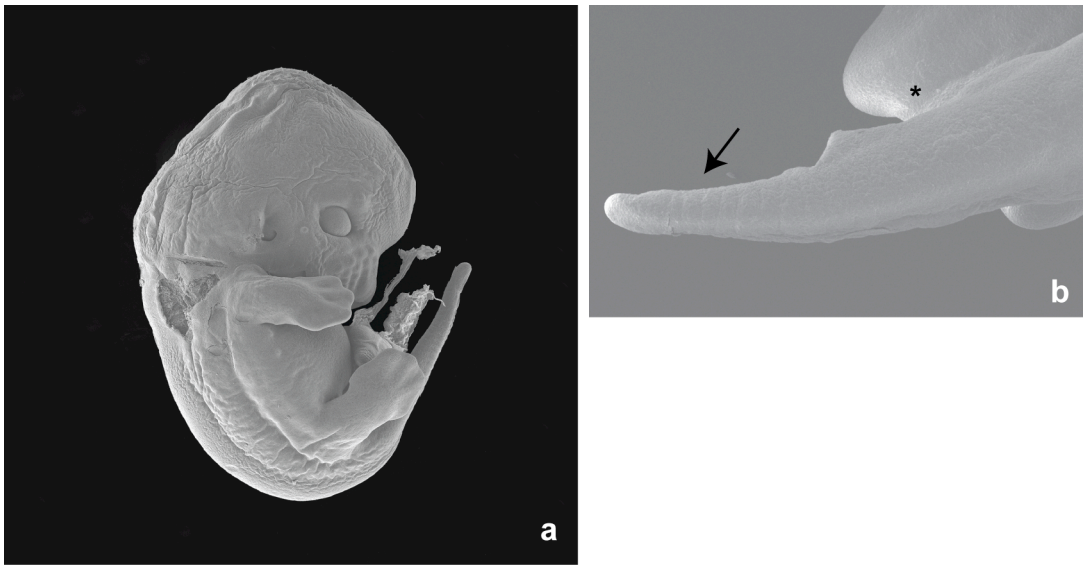

Figure 4.2 Using Scanning Electron Microscopy to count the final somite number in mouse embryo.

Figure a and b show side views of E13.5 mouse embryo and E13.5 mouse embryonic tail imaged via Scanning Electron Microscopy. Figure a is a montage. In figure b the hindlimb is marked by an asterisk. Note that the somites formed after the hindlimb are not visible. Only the very last somites are visible (arrow).

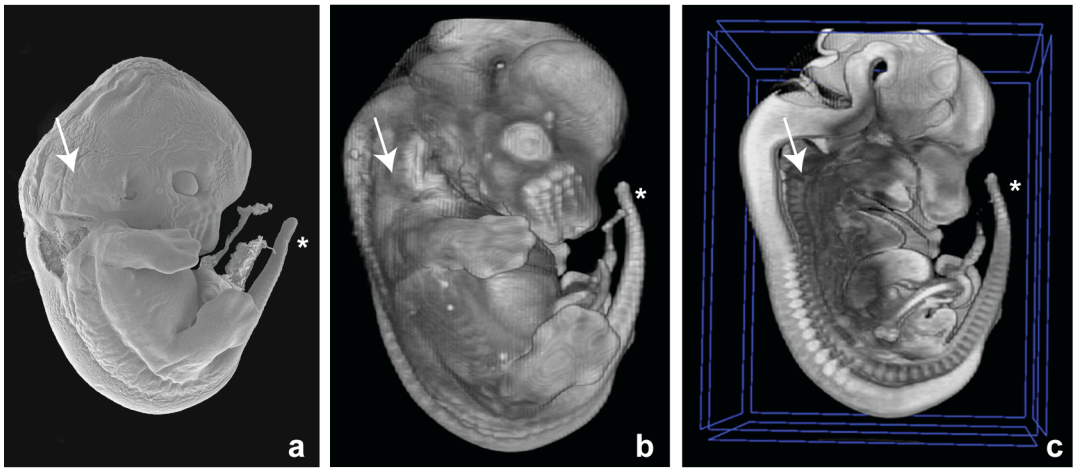

Figure 4.3 Using X-ray micro-Computed Tomography to count the final somite number in mouse embryo.

Figures a, b and c are side views of E13.5 mouse embryos imaged via Scanning Electron Microscopy (a) and X-ray micro-Computed Tomography (b, c). Disect software was used for the 3D rendering and virtual cutting in b and c. Note that the most anterior somites are not visible in the embryo imaged via Scanning Electron Microscopy (arrow in a), differently from the embryo imaged via X-ray micro-Computed Tomography (arrow c). While only the very last somites are visible via Scanning Electron Microscopy (asterisk in a), all posterior somites are clearly visible via X-ray analysis (asterisks in b and c).

4.1.1.2 High Resolution Episcopic Microscopy is the most appropriate technique to count the final somite number

To test a different method of somite counting, I made use of High Resolution Episcopic Microscopy (HREM). HREM involves episcopic imaging of the sample while it is physically sectioned into thin slices, providing a series of highly detailed images. A volume image is subsequently reconstructed by a software program (Osirix) that allows 3D visualisation of the sample (Weninger et al., 2006). Somites were visible along the entire body axis of E13.5 embryos (Movies 1 a, b and Figure 4.4 a-g). In most cases, counting of even the most posterior somites was possible (Figure 4.4 h-n). Therefore, HREM represents the most appropriate technique, to determine the final somite number in mouse embryo.

To confirm that somite formation terminates at E13.5, I analysed somite number at different embryonic stages. E12.5 embryos form 57.7±0.8 somites (n=6), E13.5 embryos form 63.7±1.6 somites (n=8) and E14.5 embryos form 61±1 (n=3). These data show that no more somites form at E14.5 implying that somitogenesis stops at E13.5 leading to 64 somites (Figure 4.4 o). The smaller number recorded at E14.5 reflects the inability to detect caudal somites at this embryonic stage. According to my counts, the posterior border of the hindlimb is at the level of somite 32/33, slightly differing from somite 34/35 as described in (Burke et al., 1995), presumably because of different criterions chosen to define borders of the hindlimb (Figure 4.4 p).

As somite number might vary between WT strains and between WT litters (Tam, 1981), I tested the degree of variability by counting somites in outbred (*CD1*) and inbred (*Black6*) strains, and in different outbred litters. E13.5 *CD1* embryos form 63.7±1.6 (see above) (n=8) and E13.5 *Black6* embryos form 63.7±0.6 (n=3) implying that there is no variation between these strains (there is no statistically significant difference, p-value=0.9) (Figure 4.5 a, b). One *CD1* litter forms 63.7±1.6 somites (see above) (n=8) and a second litter forms 65±1.7 somites (n=3), the difference being not statistically significant (p value=0.3) (Figure 4.5 c, d). When the two *CD1* litters were pooled together, *CD1* embryos form 64.1 ±1.6 somites (n=11), this number is still not

significantly different from that formed by *Black6* embryos, 63.7±0.6 (n=3) (p value=0.5, data not shown). Thus, somite number does not vary between different litters. Taken together, these observations suggest that the final somite number is highly reproducible in WT embryos, without varying between strains or litters.

As a proof of principle for counting somites in mutant embryos, I analysed somite number in E13.5 *Cdx2* heterozygous embryos. These embryos have been shown to exhibit shorter axis and fewer tail vertebrae (Young et al., 2009). HREM analysis revealed that *Cdx2* heterozygous embryos form two fewer tail somites (61.8±1.4) (n=13) than their WT siblings (64±2.1) (n=8) (Figure 4.6). Therefore, HREM can be used for detecting reduction of somite number due to premature cessation of segmentation.

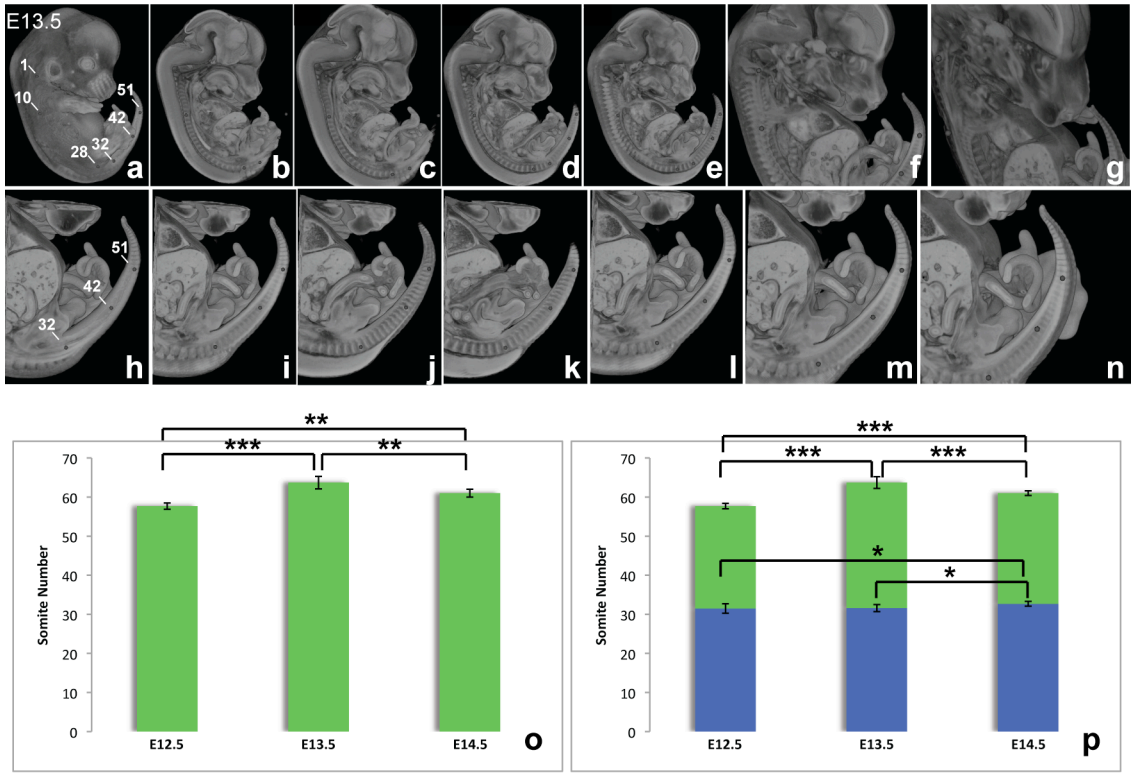

Figure 4.4 Using High Resolution Episcopic Microscopy to count the final somite number in mouse embryo.

Figures a-n are side views of a representative E13.5 mouse embryo (a-g) and its tail (h-n) imaged via High Resolution Episcopic Microscopy. Figures represent different stills of a movie. The software Osirix was used for the 3D rendering. Grey dots in a mark somite 1, 10, 28, 32, 42, 51. Grey dots in b mark somite 32, 42, 51. Figure o is analysis of final somite number in *CD1* WT embryos at E12.5 (n=6) and at E13.5 (n=8) and E14.5 (n=3). Figure p is analysis of somite number before the hindlimb and after the hindlimb. Error bars represent standard deviation, * used for p-value<0.1; ** used for p-value<0.05; *** used for p-value<0.01 determined using a two-tailed t-test. When difference are not statistically significant asterisk is not used.

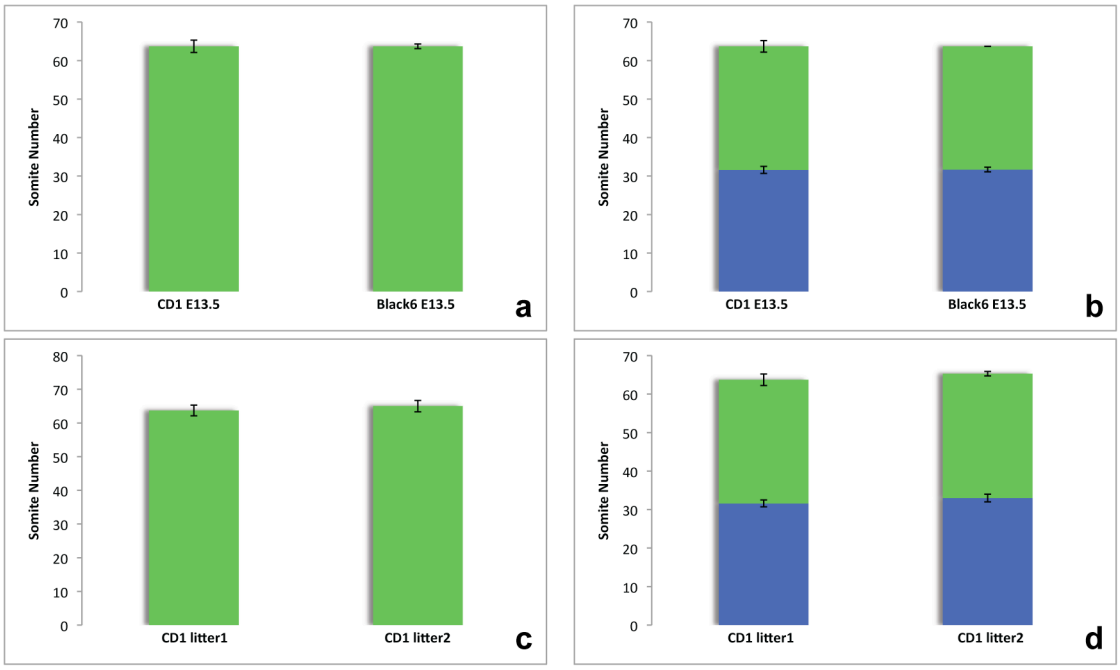

Figure 4.5 Using HREM to count final somite numer in different mouse strains and different mouse litters.

Figures a and b is analysis of final somite number in different mouse strains (*CD1* E13.5, n=8 and *Black6* E13.5, n=3). Figures c and d is analysis of final somite number in different mouse litters (*CD1* E13.5, n=8 litter1 *CD1* E13.5 litter2, n=3). Error bars represent standard deviation. Differences are not statistically significant (a two-tailed t-test was performed and a p-value=0.9 was calculated for the data set of Figure a; a p-value=0.3 was calculated for the data set of Figure b).

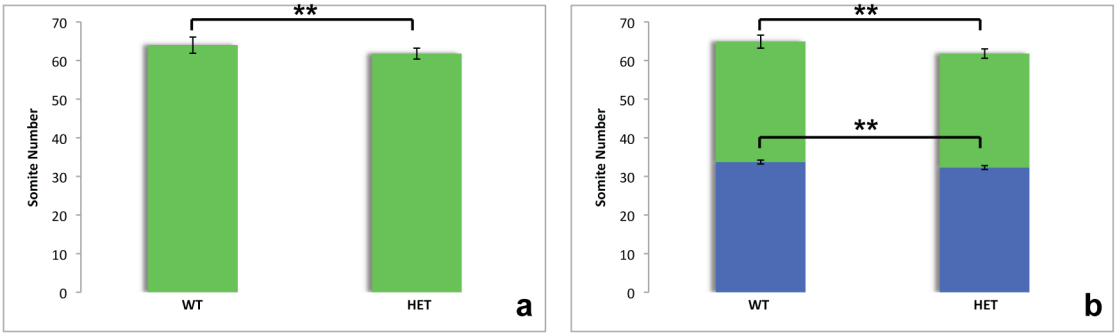

Figure 4.6 Somite number in *Cdx2* mutant embryos.

Figures a is analysis of final somite number in WT embryos (n=8) and in *Cdx2* heterozygous embryos (n=13). Figure b is analysis of somite number before the hindlimb and after the hindlimb. Error bars represent standard deviation. ** is for p-value< 0.05, determined using a two-tailed t-test.

4.1.2 Using High Resolution Episcopic Microscopy to study control of final somite number in mutant embryos

In order to identify mutations that are haplo-insufficient for controlling the final number of somites in mouse embryos, I examined mutant lines of genes known to regulate segmentation and axial elongation (Table 4.1). Candidate genes belong to Fgf, RA, Bmp, Wnt and Notch signalling pathway whose components regulate maintenance, proliferation, differentiation and migration of PSM cells (Dubrulle and Pourquie, 2004a, Wilson et al., 2009). To date, phenotypic characterisation of these lines has been limited to homozygous animals (see Table 4.1), with little details on heterozygous counterparts. To explore whether the control of somite number is sensitive to gene dosage, only heterozygous mutant embryos were analysed.

4.1.2.1 Mutants of the Fgf and RA pathways

Components of the Fgf and RA pathway regulate various cellular mechanisms in the primitive streak and PSM, including somite formation and axial elongation. At gastrulation, Fgf signalling regulates migration of primitive streak cells to form the mesoderm. *Fgfr1* homozygous embryos show accumulation of mesodermal cells in the streak region as they fail to migrate away from the primitive streak (Yamaguchi et al., 1994). A more severe phenotype has been reported for *Fgf8* homozygous embryos which fail to form mesoderm-derived structures, such as the somites, due to impaired cell migration (Sun et al., 1999). Besides regulating migration of gastrulating cells, Fgf signalling controls maintenance of thePSM cells. Various *Fgfs* are expressed in the PSM, and their mutations result in defects of PSM-derived structures. For example, *Fgf3* homozygous embryos exhibit fewer segments and shorter tails (Mansour et al., 1993). PSM cells are maintained in an immature state by high levels of *Fgf8*, its over-expression blocking somite formation (Dubrulle et al., 2001).

This blockade is relieved by RA that promotes differentiation of the PSM cells by activating genes involved in somite formation (Moreno and Kintner, 2004). RA also controls survival of the PSM cells. Excessive levels of RA cause cell death in the posterior PSM leading to axial truncation (Shum et al., 1999). A similar phenotype is observed in homozygous mutants of *Cyp26a1* and of *POR*, which encode for enzymes of RA catabolism (Abu-Abed et al., 2001, Sakai et al., 2001, Otto et al., 2003). Reduced levels of RA also cause axis shortening, observed in mutants of *Raldh2*, a RA synthesising enzyme (Niederreither et al., 1999). Thus, homozygous mutations of components of the Fgf and RA pathway affect cellular mechanisms of the primitive streak and the PSM resulting in defective axial elongation and somite formation, including alterations to the final somite number.

To explore whether heterozygous mutations cause similar defects, I analysed somite number in E13.5 *Fgf3, Fgf8, Cyp26a1, Raldh2* and *POR* heterozygous embryos. As shown in Table 4.2, none of these mutants exhibit significantly different somite number from WT counterparts (see p-values in the table). These observations show that heterozygous mutations of selected genes of the Fgf and RA pathway form the normal number of somites, implying that these mutations are haplosufficient for controlling somite number or that there is a certain degree of functional redundancy.

Gene	Phenotype	Reference
Fgf3	short curly or kinky tail, fewer caudal vertebrae	Mansour SL et al., 1993
Fgf8	lack of mesodermal tissue, e.g. somites	Sun X et al., 1999
Cyp26a1	caudal truncation	Abu-Abed S et al., 2001
Raldh2	shortened axis	Niederreither K et al., 1999
POR	shortened trunk	Otto DME et al., 2003
Bmp4	disorganised posterior structures	Winnier G et al., 1995
Wnt3a	axis truncation	Takada S et al., 1994
Wnt5a	truncation of body extremities, e.g. tail	Yamaguchi TP et al., 1999
β–***catenin***	axis truncation	Aulehla A et al., 2008
Axin2	kinky tail	Zeng L et al., 1997
Mesogenin	enlarged tailbud no somites beyond forelimb	Kusumi K et al., 1998
Dll3	shortened tail	Kusumi K et al., 1998
Hes7	shortened trunk and tail	Bessho Y et al., 2001

Table 4.1 Candidate mutant lines.

Table shows details of gene name, homozygous phenotype and reference for all the mutant lines analysed via HREM. Note that in most cases homozygous phenotype consists in axis truncation/shortening. Sources of mutant embryos are indicated in the Material and Methods chapter.

Gene	Somite Number		Total		p-value
	+/+	+/-	+/+	+/-	
Fgf3	62,65,60	61,64,61, 63,63,64,63	62.3±2.5	62.7±1.2	0.8
Fgf8	65,65,67,64	64,65,66,67	65.2±1.2	65.5±1.3	0.8
Cyp26a1	64,60,59,62	60,59,56,61, 60	61.2±2.2	59.2±1.9	0.2
Raldh2	63,64,61,64	63,60,62,61, 64,62	63±1.4	62±1.4	0.3
POR	62,64,65, 61	59,61	63±1.8	60±1.4	0.1

Table 4.2 Somite number in mutants of the Fgf and RA pathways.

Table shows analysis of final somite number of heterozygous embryos for Fgf and RA pathway components. Somite number of WT siblings is also shown. Standard deviation and p-values are shown. To eliminate observer bias, genotype of each sample was shown to the observer after the analysis.

4.1.2.2 Mutants of the Bmp pathway

Bmp signalling regulates different processes of mesoderm development at different embryonic stages. Winnier et al. (1995) showed that, at gastrulation, *Bmp4* is required for mesoderm formation, most homozygous embryos dying at very early stages. Later, *Bmp4* is presumably required for differentiation of mesoderm of the posterior primitive streak, as mutant embryos that survive beyond gastrulation show truncation of the posterior body. At more advanced embryonic stages, different levels of *Bmp4* control the specification of mesoderm into somitic versus lateral plate mesoderm subtype (Tonegawa and Takahashi, 1998). At the end of gastrulation, inhibition of Bmp signalling by *Noggin*, arrests gastrulation movements in the Ventral Ectodermal Ridge (VER), leading to shortening of the tail (Ohta et al., 2007). VER is the ectoderm derived from the late primitive streak and is located in the ventral part of the embryonic tail. The VER is a site of gastrulation movements and a source of mesodermal cells for the tail. Therefore, Bmp signalling plays an important role in mesoderm development at various embryonic stages, including at late gastrulation when it controls tail elongation.

In order to study whether heterozygous mutation of *Bmp4* affects tail development in terms of the final somite number, I counted somites in E13.5 *Bmp4* heterozygous embryos. No significant change in the somite number was observed between heterozygotes (n=3) and WT embryos (n=4) (see p-value), either because of functional redundancy or because the final somite number is not sensitive to variation of *Bmp4* gene dosage (Table 4.3).

Gene	Somite Number		Total		p-value
	+/+	+/-	+/+	+/-	
Bmp4	**64,64,64,64**	**65,65,63**	**64**	**64.3±1.1**	**0.7**

Table 4.3 Somite number in mutants of the Bmp pathway.

Table shows analysis of final somite number of heterozygous embryos for Bmp pathway components (*Bmp4*). Somite number of WT siblings is also shown. Standard deviation and p-value are shown. To eliminate observer bias, genotype of each sample was shown to the observer after the analysis.

4.1.2.3 Mutants of the Notch pathway

Inactivation of cyclic genes of the Notch pathway often results in poor definition of somite border and altered anteroposterior somite polarity, leading to a disturbed axial skeleton. Moreover, blocking all Notch activity prevents cyclic gene expression and somite formation (Ferjentsik et al., 2009). *Lunatic Fringe* (*Lfng*) and *Hes7* are two Notch target genes. *Lfng* homozygous animals have a shorter skeleton with fusion of vertebrae and ribs; similar defects are found in the *Hes7* mutants where cyclic expression of *Lfng* is lost (Evrard et al., 1998, Bessho et al., 2001). However, 43% of the *Hes7* heterozygous animals present axial problems whereas *Lfng* heterozygotes appear normal, implying that dose of the former gene is important for normal development (Evrard et al., 1998, Bessho et al., 2001). *Dll3*, one of the Notch ligands, is also required for proper skeleton morphology. In *Dll3* homozyogous embryos, abnormal vertebrae and ribs are associated to defective expression of cyclic genes (Kusumi et al., 1998, Dunwoodie et al., 2002).

Therefore, mutations of Notch signalling components and altered cyclic gene expression cause somitic defects implying that cyclic expression is crucial for somite formation.

To analyse whether somite formation is compromised by reduced dosage of Notch genes, I analysed E13.5 embryos (n=3) for heterozygous *Hes7* and *pudgy*, a mutation of *Dll3*. Due to technical reasons (i.e. processing of the *Hes7* samples for HREM microscopy was not successful) data regarding the *Hes7* samples are not shown. Pudgy heterozygous embryos form a similar number of somites to WT embryos (n=3), indicating that somite formation is not sensitive to *Dll3* gene dosage (Table 4.4) (the difference in somite number between WT and heterozygous embryos is not statistically significant, see p-value). Previous studies reported that *pudgy* heterozygotes exhibit a disturbed *Dll3* expression pattern, but it has been shown that this is not sufficient to cause any phenotypic change, consistent with my results (Kusumi et al., 1998).

Gene	Somite Number		Total		p-value
	+/+	+/-	+/+	+/-	
Dll3	65,64,66	67,65,63	65±1	65±2	0.3

Table 4.4 Somite number in mutants of the Notch pathway.

Table shows analysis of final somite number of heterozygous embryos for Notch pathway components (*Dll3*). Somite number of WT siblings is also shown. Standard deviation and p-value are shown. To eliminate observer bias, genotype of each sample was shown to the observer after the analysis.

4.1.2.4 Mutants of the Wnt pathway

Wnt signalling has been proposed to control both the period of the segmentation clock and the rate of the PSM growth. *Wnt3a* is expressed in the primitive streak of young embryos and in the tail bud of older embryos. Consistent with its expression pattern, *Wnt3a* disruption results in absence of posterior somites and in shortening of the tail (Takada et al., 1994). Defective segmentation clock machinery (e.g. non-cyclic *Lfng* expression) and impaired mesoderm formation (e.g. reduced/lost *Brachyury* expression) seem to contribute to these phenotypes (Aulehla et al., 2003, Takada et al., 1994). Conditional loss of function (in the PSM tissue) mutants of *β–catenin*, a component of the canonical Wnt pathway, exhibit defects similar to those of *Wnt3a* mutants. In contrast, *β-catenin* gain of function mutants form a larger PSM than controls, with fewer and smaller somites forming in the anterior PSM. Cyclic gene expression is maintained and ectopic stripes of cycling genes are found in the PSM (Dunty et al., 2008, Aulehla et al., 2008). Thus, *β-catenin* is required and sufficient for regulating segmentation and elongation of the body axis. Deregulation of two target genes of the canonical Wnt pathway, *Axin2* and *Mesogenin*, interferes with expression of components of the Notch pathway causing somitic and axial defects (Aulehla et al., 2003, Yoon and Wold, 2000). Non-canonical Wnt signalling is also involved in the regulation of axis lengthening. *Wnt5a*, is expressed in the primitive streak and later on in the tail bud. Similarly to *Wnt3a* mutants, *Wnt5a* mutants present severe caudal truncations, presumably due to reduced proliferation in the tail region (Yamaguchi et al., 1999). Hence, the Wnt signalling pathway controls both the segmentation and the elongation process.

To explore whether reducing gene dosage for components in the Wnt pathway controls definitive somite number, I analysed *Wnt3a, Wnt5a, β-catenin, Axin2* and *Mesogenin* heterozygous embryos at late segmentation stage. Except for the mutants of the two Wnt signalling target genes, *Axin2* and *Mesogenin* (see p-values), all the mutants analysed present a significantly reduced (see p-value) final somite number. Therefore,

heterozygous mutations of specific genes of the Wnt signalling pathway are haploinsufficient for controlling somite number (Table 4.5).

Gene	Somite Number		Total		p-value
	+/+	+/-	+/+	+/-	
Wnt3a	65,64,64,66, 64	62,64,64,63, 61	64.6±0.9	62.8±1.2	0.04 p<0.05**
Wnt5a	65,65,66	62,62,63,61	65.3±0.6	62±0.8	0.001 p<0.01***
β-*catenin*	65,64,66,64	64,64,63,63	64.7±0.9	63.5±0.6	0.08 p<0.1*
Axin2	64,64,61	62,62,61,61, 63	63±1.7	61.8±0.8	0.3
Mesogenin	66,64,65	64,67,65,62	65±1	64.5±2.1	0.7

Table 4.5 Somite number in mutants of the Wnt pathway.

Table shows analysis of final somite number of heterozygous embryos for Wnt pathway components. Somite number of WT siblings is also shown. Standard devition and p-value are shown. To eliminate observer bias, genotype of each sample was shown to the observer after the analysis.

4.2 Discussion

4.2.1 HREM can be used to count the final somite number in mouse embryos

In this chapter, I describe my search for genes that are haploinsufficient for controlling the definitive somite number. To do so, first I had to establish an assay to count somites in E13.5 mouse embryos. Precise counting is difficult because anterior somites start differentiating into bones, muscles, and dermis whilst posterior ones are still forming. The problem with scoring older embryos/born embryos by means of skeleton preparation is that the most anterior segments are incorporated into the skull. The problem with scoring younger embryos by means of in situ hybridisation is inadequate tissue penetration due to tissue thickness. The latter approach did not allow quantitation of all somites at E13.5 (see Figure 4.1). As an alternative, I took advantage of X-ray micro-CT scanning which is traditionally used to visualise internal hard structures, such as the bones, and which has been employed to analyse mouse vertebrae number in a recent study (Kim et al., 2011). Interestingly, micro-CT analysis revealed even the soft structures, such as the somites, along almost the entire body axis of E13.5. However, it was not possible to count the most posterior, youngest somites, probably due to their small size and the low resolution of the techniques (Figure 4.3).

This counting problem was overcome by using HREM that allowed somite quantitation at E13.5 (Figure 4.4). HREM analysis showed that somite formation terminates at E13.5 when the embryo forms 64 somites. This measurement is similar to previous observations (Tam, 1981). Although a slight inter-litter variability was observed in the embryos from an outbred strain (*CD1*), the final number was reproducible between different strains (*CD1* and *Black6*) and different litters (Figure 4.5).

To test whether HREM can be used to detect altered somite number due to premature termination of somitogenesis, I analysed E13.5 *Cdx2* heterozygous embryos. *Cdx* genes are major regulators of caudal development in different organisms, heterozygous

mutation of murine *Cdx2* resulting in shorter axis and fewer tail vertebrae (Young et al., 2009). Indeed, HREM analysis revealed that *Cdx2* heterozygous embryos form two fewer somites than WTs, confirming that HREM is appropriate to study control of somite number in selected mutants (Figure 4.6).

4.2.2 Somite formation is not sensitive to gene dosage of specific components of the Fgf, RA, Bmp, and Notch signalling pathways

To distinguish between genes that are required and genes whose dose is limiting in determining the definitive somite number, E13.5 heterozygous embryos for genes of the Fgf, RA, Bmp, Notch and Wnt signalling pathways were analysed. None of the Fgf and RA mutations tested showed a significant variation in somite number (Table 4.2). A possible explanation for this, at least for the Fgf mutations, is redundancy of the Fgf ligands. *Fgf3* and *Fgf8* are only two of the four ligands being expressed in the PSM. As an alternative, *Fgfr1* (Fgf receptor 1 which is the only receptor being expressed in the PSM) mutants could be analysed.

Nor was *Bmp4* gene dosage limiting for axial extension. No changes in somite number were recorded in *Bmp4* heterozygous mutants (Table 4.3). However, it remains possible that the dose of other Bmp signalling components is important to control the final somite number. One preferred candidate is *Bmp2* which is expressed in the Ventral Ectodermal Ridge (VER), a region of the tail contributing to posterior development (Goldman et al., 2000). VER removal in mouse embryos results in reduced somite number (Goldman et al., 2000).

HREM analysis of heterozygous embryos for *Dll3*, one of the Notch ligands, failed to reveal any changes in somite number (Table 4.4). Thus, somite formation is not sensitive to gene dosage of *Dll3*. Although Notch plays a crucial role in somitogenesis, controlling the period of somite formation, only few studies have reported that Notch regulates somite number (Ferjentsik et al., 2009). Kim et al. (2011) have reported that *Nrarp*, a regulator of the Notch signalling, controls the definitive number of somites, the analysis being limited to homozygous embryos only. Expression of mouse *Nrarp*

depends on Notch and Wnt activity (Wright et al., 2009), the latter being regulating both segmentation clock rate and PSM growth rate.

Mutations affecting Wnt activity presented a reduced somite number, implying that Wnts might represent limiting factors in determining the correct somite number (Table 4.5).

4.2.3 Dose of Wnt genes might control final somite number in mouse embryo

Wnt signalling has been shown to control posterior development of vertebrates by regulating expression of *Cdx* genes, major players of tail formation, which in turn activate posterior *Hox* genes. *Cdx* and *Hox* signal back to regulate expression of *Wnt*, generating a regulatory network that may play a role in maintaining posterior elongation (Young et al., 2009). In support of this model, over-expression of *Lef1*, a member of the Wnt pathway, rescues tail truncation of *Cdx* mutants (Young et al., 2009). My analysis of *Cdx2* heterozygous embryos shows that *Cdx2* is haploinsufficient for controlling the final somite number. It would be interesting to understand whether *Cdx2* heterozygous embryos form fewer somites because *Cdx2* is a target of a signalling pathway whose dose is limiting for determining the final somite number, such as Wnt, or because *Cdx2* regulates such signalling pathway. Interestingly, the Wnt-Cdx pathways also control posterior development of a number of invertebrates, including insects and spiders, implying that this is an evolutionary conserved mechanism of body formation (Bolognesi et al., 2008, McGregor et al., 2008, Martin and Kimelman, 2009). In addition to *Cdx*, other regulators of tail formation are affected by Wnt signalling: *Spry2* and *Brachyury* (Gibb et al., 2009, Martin and Kimelman, 2008). Therefore, Wnt signalling is upstream of many of the genes known to control axial lengthening. Besides being upstream of genes regulating axis elongation, Wnt signalling also controls expression of genes required for proper axis segmentation (e.g. *Lfng*) (Aulehla et al., 2003, Gibb et al., 2009), strongly supporting a role for Wnt in control of somite number.

It has been reported that homozygous mutants of *Wnt3a, Wnt5a* and *β-catenin* form a severely reduced number of somites/segments in comparison to that of WTs. *Wnt3a* homozygous form only the first 7 to 9 somites (Takada et al., 1994). *Wnt5a* mutants form not more than 4 tail vertebrae, while WTs form ~30 tail vertebrae (Yamaguchi et al., 1999). Embryos homozygous for a conditional-null *β-catenin* in the PSM, form no obvious somites or only few abnormal somites in the anterior end of the axis (Dunty et al., 2008),(Aulehla et al., 2008). My experiments show that heterozygous mutants of Wnt genes form fewer somites than WT embryos. HREM analysis revealed that heterozygous mutants of *Wnt3a, Wnt5a* and *β-catenin* form 2, 3, and 1 or 2 fewer somites than WTs, respectively, suggesting that the final somite number is susceptible to changes in Wnt gene dosage. However, the difference in somite number between heterozygous and WTs does not reflect half the difference reported for *Wnt3a, Wnt5a* and *β-catenin* homozygous in comparison to WTs (future experiments shall investigate whether there is a certain degree of gene dosage compensation from the remaining allele in the heterozygous embryos).

My experiments suggest that Wnt genes might represent limiting factors to define the final somite number. It remains to investigate what is the mechanism behind this. One shall test different hypotheses, including: 1) Wnt controls somite number through regulation of progenitor cells (e.g. Wnt loss of function might affect progenitor maintenance/proliferation affecting axial structures formation); 2) Wnt controls somite number through regulation of the period of somite formation (e.g. Wnt loss of function might result in slow down of the of somite formation resulting in a reducd somite number).

1) Progenitor maintenance/proliferation. To test whether progenitor maintenance is affected in Wnt heterozygous mutants, one shall perform in situ expression analysis or quantitative PCR of markers of progenitor cells, such as *Brachyury*, to assay the presence and the expression level of these genes in comparison to WT counterparts. Previous studies have shown that *Brachyury* expression is completely lost in *Wnt3a* homozygous embryos, supporting the hypothesis that Wnt is required for formation of mesodermal precursors, resulting in truncations of axial structures (Takada et al., 1994). One shall also detect cell proliferation levels by means of cell proliferation markers, e.g.

PHH3 immunostaining. Noteworthy, one possible function of Wnt genes is to control cell proliferation of the streak and the tail cells (as shown for *Wnt5a* mutants) (Yamaguchi et al., 1999).

2) Period of somite formation. Recent findings have shown that blocking Wnt signalling, by means of Wnt signalling inhibitors, lengthens the clock oscillations and that Wnt/β-catenin signalling controls oscillations of cyclic genes (Gibb et al., 2009),(Dunty et al., 2008). One shall explore whether heterozygous embryos of Wnt genes form fewer somites because the period of the clock is extended. To do so, one shall culture PSM halves of heterozygous embryos and compare the period of somite formation in heterozygous halves in comparison to WT halves.

By exploring these possibilities, one shall be able to provide more insights into the potential mechanisms used by Wnt signalling to regulate somite number.

In the next chapter, I present my study of the *Greb1* gene, which our laboratory identified because it is selectively expressed in the tail bud. I use morpholino antisense inhibition in zebrafish embryos to provide evidence that *Greb1* controls axis morphogenesis by regulating movements required for normal convergent extension during gastrulation.

Chapter 5. Role of *Greb1* in axial elongation and segmentation

Axial progenitors contribute to elongation and segmentation of the anteroposterior axis of vertebrate embryos including mouse, chick, fish and frog (Cambray and Wilson, 2007),(Tzouanacou et al., 2009, McGrew et al., 2008),(Kanki and Ho, 1997),(Davis and Kirschner, 2000). These cells are initially located in the primitive streak/organiser and later in a region of the tail bud, called Chordoneural Hinge (CNH) (Cambray and Wilson, 2002). Studies in murine and avian embryos have shown that CNH cells represent a population of long-term axial progenitors, as they contribute to PSM, somites, neural tube and notochord over an extended period of time. In contrast, cells located in other regions of the tail bud are restricted in their differentiation potential (Cambray and Wilson, 2002, Cambray and Wilson, 2007, McGrew et al., 2008). To date, most of the studies have been focussing on defining the location and the potency of axial progenitors, with little understanding of their key marker genes. Functional characterisation of these genes may reveal novel players of vertebrate axial elongation and segmentation.

An array experiment had been performed in the laboratory (Prajapati R et al., manuscript in preparation) with the aim of molecularly characterising the CNH in comparison to surrounding regions. E10.5 mouse embryos were dissected, and fragments of CNH, tail bud mesoderm (TBM) and presomitic Mesoderm (PSM) were isolated and processed for array analysis. *Greb1* (*Growth-regulation-by-estrogen-in-breast-cancer-1* or *Gene-regulated-by-estrogen-in-breast-cancer-1*) was identified as one of the most strongly upregulated genes in the CNH compared to the surrounding PSM. The role of this gene in vertebrate development has not been explored yet.

In this chapter, I present my data on the initial characterisation of the role of *Greb1* in axial elongation and segmentation. As genetic manipulations in zebrafish are well established, I focussed on exploring *Greb1* function in this model organism.

5.1 Results

5.1.1 GREB1 protein sequence is conserved among vertebrates

The predicted transcript of zebrafish *Greb1* encodes a 1802 aminoacid protein, as shown in NCBI database (http://www.ncbi.nlm.nih.gov/guide/). To investigate the degree of evolutionary protein conservation, a multiple sequence alignment was generated using ClustalW (http://www.ebi.ac.uk/Tools/msa/clustalw2/). The percentage identity of zebrafish GREB1 was 61.3% to mouse, 61.8% to chick and 61.1% to frog (*Xenopus*), indicating that the protein is highly conserved among vertebrates (Figure 5.1) and suggesting that it might play an essential role in these organisms. However, no orthologs were identified in other fish species (e.g. in pufferfish: *Tetraodon nigroviridis*, *Takifugu rubripes*; in stickleback: *Gasterosteus aculeatus*; in killifish: *Oryzias latipes medaka*) nor in lower organisms (e.g. in *Drosophila melanogaster*; in *Saccharomyces cerevisiae*). To explore the presence of functional protein domains, an INTERPROScan study of the human GREB1 protein sequence was performed (http://www.ebi.ac.uk/Tools/pfa/iprscan/). The C-terminus of the human GREB1 protein contained a predicted transmembrane domain, which was conserved in zebrafish and in other organisms (Figure 5.1, red box). Thus, GREB1 displays one transmembrane domain whose sequence is similar among vertebrates. However, there are no data in the protein database or in the literature to confirm the functional importance of this domain.

Figure 5.1 GREB1 protein alignment.

Protein sequence comparison of zebrafish GREB1 (accession number: XP_001920606) and orthologues in the mouse (accession number: NP_056579), in the chick (accession number: XP_419956) and in the frog (accession number: XP_002942230). Protein sequences were obtained from NCBI database and the alignment was generated in ClustalW. * indicates identical amino acids, : indicate conserved amino acids, . indicates similar amino acids. Percentage identity of zebrafish GREB1 is 61.3% to mouse, 61.8% to chick and 61.1 % to frog. Red box marks putative transmembrane domain. Presence of the domain was identified by INTERPROScan analysis of GREB1 human sequence.

5.1.2 *Greb1* is expressed in the caudal region of different vertebrates

Greb1 appears to be greatly enriched in the mouse CNH. Evolutionary conservation of the expression site of the gene might imply that it is functionally important at that site. In order to understand whether *Greb1* expression pattern is conserved, a comparative gene expression pattern analysis was performed in those model organisms where axial elongation depends on CNH progenitors (in particular in mouse, chick and zebrafish).

5.1.2.1 Expression of mouse Greb1

To determine if *Greb1* is expressed during mouse axial elongation, I performed in situ hybridisation on E10.5 embryos focussing my attention on the caudal area of the embryo where the CNH is located. *Greb1* was detected in the tail bud, in two domains: a dorsal domain and a ventral domain posterior to the neural tube resembling the CNH (Figures 5.2 b, b' and 5.3). To determine more sites of *Greb1* expression, I analysed gene expression at various embryonic stages. At E8.5, *Greb1* expression was observed in a region surrounding the primitive streak (Figures 5.2 a, a'), suggestive of the CLE, which is known to contain progenitors of the neural tube and somites and which is the precursor of the CNH (see Introduction) (Wilson et al., 2009). At E12.5 and E13.5 *Greb1* was found to be expressed in the tail region (Figures 5.2 c, c'), and at E13.5 when axial elongation ceases levels of gene expression were very low (Figures 5.2 d, d'). Together, these data show that mouse *Greb1* expression is restricted to the tail region, and in a location similar to the CNH at E10.5, confirming the results obtained in the array experiment and suggesting a role for *Greb1* in regulation of CNH cells.

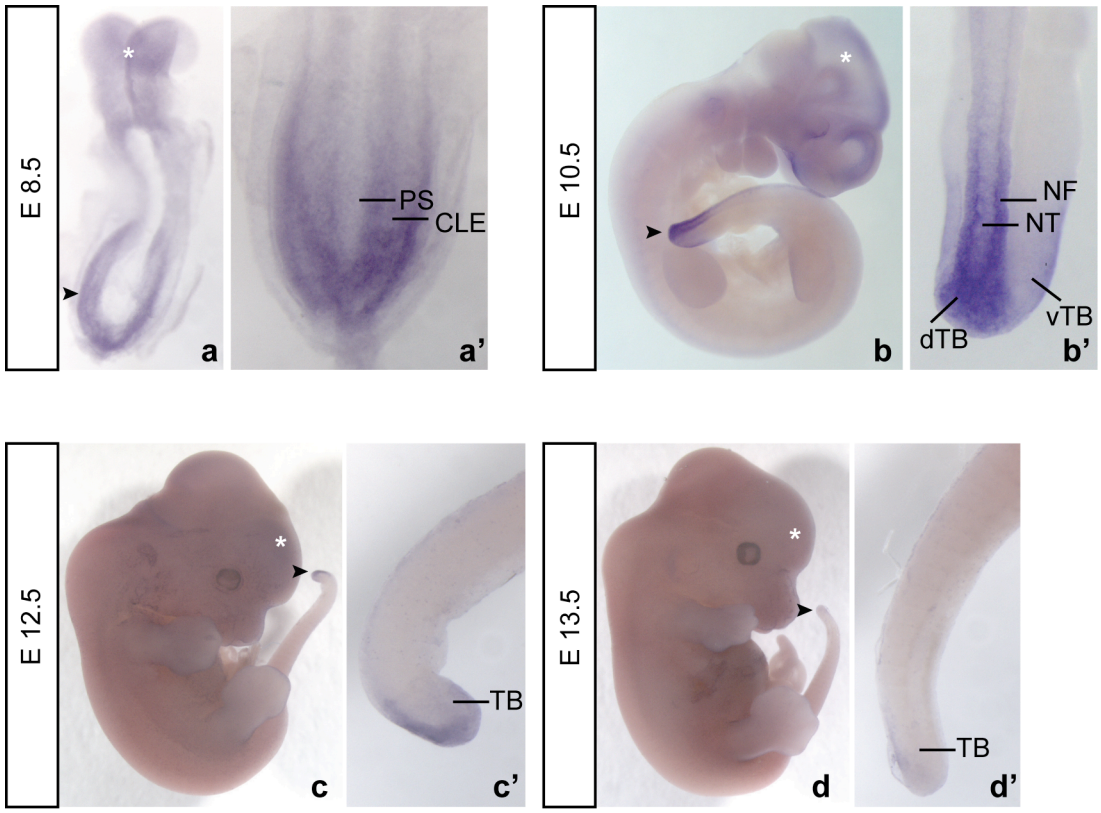

Figure 5.2 Expression of mouse *Greb1*.

Mouse embryos (a, b, c, d) and mouse tails (a', b', c', d') at the stages indicated, stained by in situ hybridisation for *Greb1*. a, a', b' show dorsal views and b, c, c', d, d' show side views. Typically, 5 embryos for each embryonic stage were subjected to in situ hybridisation. Note that *Greb1* expression is found in the tail region at all stages analysed (arrowheads). Expression is also found in the head (asterisk). PS Primitive Streak; CLE Caudal Lateral Epiblast; NT Neural Tube; NF Neural Folds, dTB dorsal Tail Bud; vTB ventral Tail Bud; TB Tail Bud.

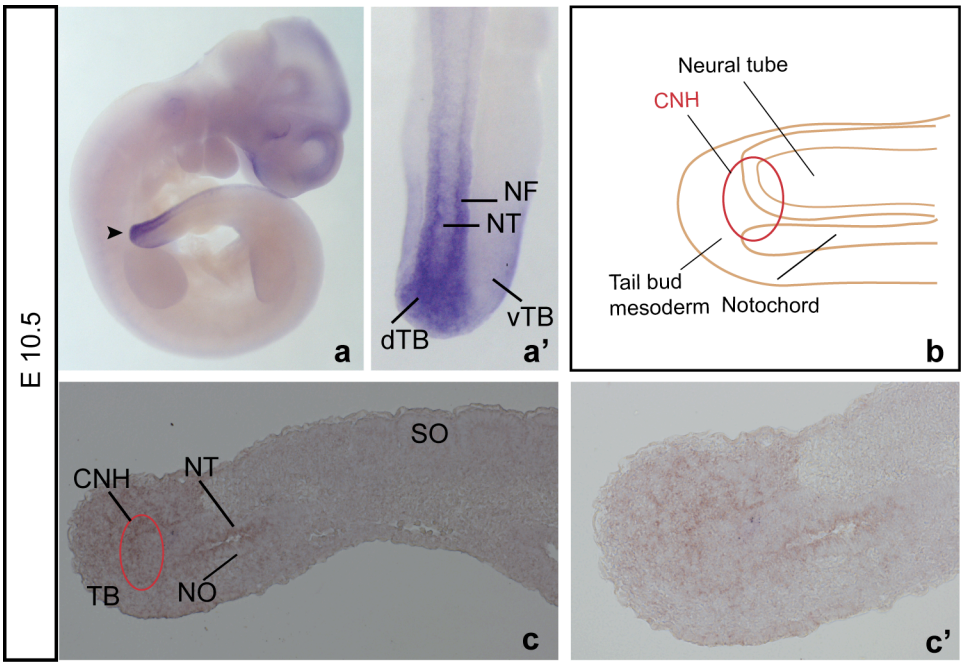

Figure 5.3 Expression of *Greb1* in the mouse tail.

Greb1 in situ hybridisation staining on a whole-mount mouse embryo and sagittal sections (a, a', c, c') at the stage indicated. Figure b is a graphic depiction of a mouse tail (sagittal view), showing the location of the CNH.
Note that *Greb1* expression is found in the tail region (whole-mount) and in a location resembling the CNH (section). NT Neural Tube; NF Neural Folds, dTB dorsal Tail Bud; vTB ventral Tail Bud; TB Tail Bud; CNH Chordoneural Hinge; NO Notochord; SO Somite.

5.1.2.2 *Expression of chick* Greb1

During early chick development, *Greb1* expression was detected at low levels around the node, in the primitive streak and at higher levels in a region similar to the CLE (Figure 5.4 a, b, c). At HH13, the gene was expressed in the caudal neural tube and in the area surrounding the caudal neural tube (Figure 5.4 d, d'). At stage HH17, *Greb1* expression was in the tail bud (Figure 5.4 e, e'), in a domain comparable to the CNH. A similar expression pattern persisted at HH18, HH23 and HH26 (Figures 5.4 f-h), being restricted to the tip of the tail at the last stage (Figure 5.4 h). Therefore, chick *Greb1* expression is found in the tail throughout development as observed for the mouse orthologue.

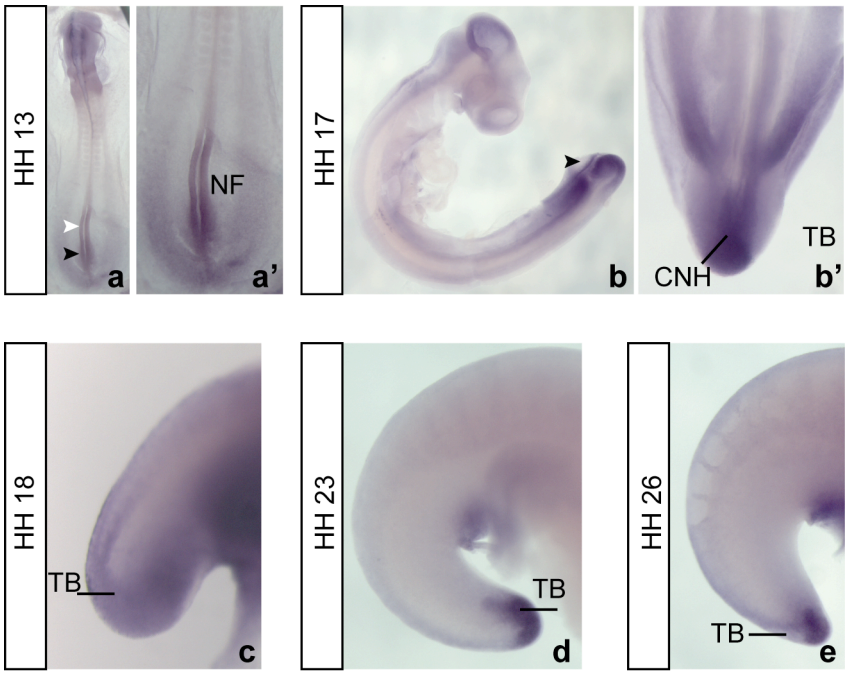

Figure 5.4 Expression of chick *Greb1*.

Chick embryos (a, b, c, d, e) and chick tails (d', e', f, g, h) at different embryonic stages stained by in situ hybridisation for *Greb1*. a, b, c, d, d', e' show dorsal views and e, f, g, h show side views. Typically, 5 embryos for each embryonic stage were subjected to in situ hybridisation. *Greb1* expression is found in the tail region as indicated in a-a' (arrowheads in a point to posterior neural tube and posterior PSM), b-b', c, d, e. NF Neural Folds, CNH Chordoneural Hinge; TB Tail Bud.

5.1.2.3 *Expression of zebrafish* Greb1

During gastrulation, zebrafish *Greb1* was found ubiquitously expressed in the embryo and enriched at the dorsal and ventral margins (Figure 5.5 a). At the 6 somites stage, gene expression was restricted to the caudal region of the embryo (Figure 5.5 b). At the 18 somites stage, *Greb1* was expressed in a broad tail domain, which includes the predicted area of the CNH (Figures 5.5 c, c'). At the 26 somites stage, gene expression was in the ventral and dorsal regions of the tail (Figures 5.5 d-d'). These findings mirror those for mouse and chick *Greb1*.

In summary, at early developmental stages, *Greb1* is expressed within the regions of the embryo where cells ingress during gastrulation (primitive streak in mouse and chick, dorsal and ventral margins in zebrafish) (Wilson and Beddington, 1996, Hatada and Stern, 1994, Kimmel et al., 1990). Later, *Greb1* expression is confined to a domain resembling the CNH, with respect to the location, in all the organisms studied. As elongation terminates, *Greb1* expression disappears from the caudal domain (in mouse) or gets restricted to the tip of the tail (in chick and zebrafish). These data suggest that the *Greb1* may play a role in regulation of gastrulation movements during early development and in regulation of CNH progenitors later in development.

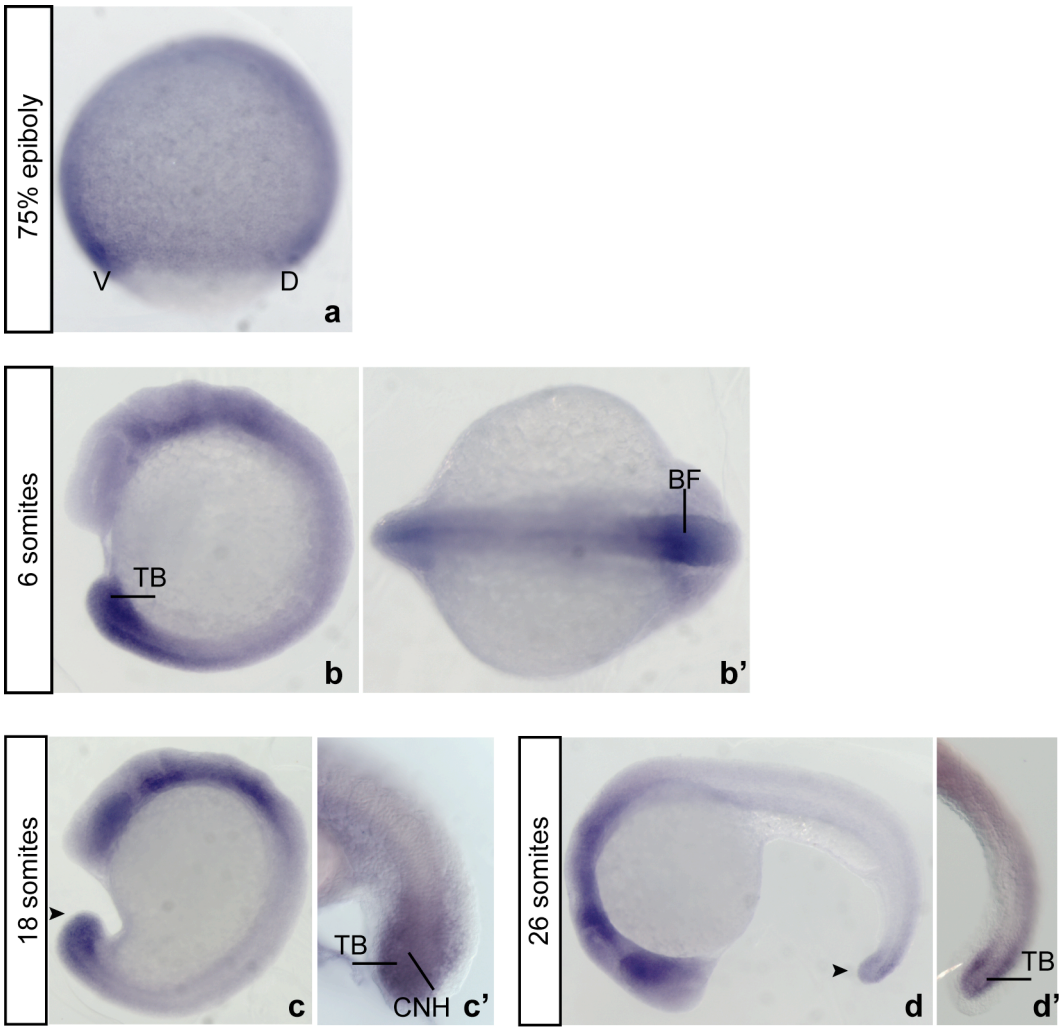

Figure 5.5 Expression of zebrafish *Greb1*.

Zebrafish embryos (a, b, b', c, d) and zebrafish tails (c', d') at different embryonic stages stained by in situ hybridisation for *Greb1*. a, b, c, c', d, d', e' show side views and a' is animal view (dorsal margin on the right) and b' is top view, showing the head region. Typically, 15 embryos for each embryonic stage were subjected to in situ hybridisation. *Greb1* expression is found in the tail region as shown in b, c, d and as shown in c' and d'. At early stages, *Greb1* expression is ubiquitous, but upregulated in the margins, (a). V Ventral margin; D Dorsal margin; TB Tail Bud; BF Brain Folds; CNH Chordoneural Hinge.

5.1.3 GREB1 is required for proper axial elongation and segmentation

Progenitor cells located at the tail end of the embryo contribute to axial elongation and segmentation until the entire body axis is laid down (Cambray and Wilson, 2007),(Tzouanacou et al., 2009, McGrew et al., 2008),(Kanki and Ho, 1997),(Davis and Kirschner, 2000). Given that zebrafish *Greb1* expression is found in the tail region where axial progenitors should reside (see Figure 5.5), I asked whether GREB1 regulates elongation and segmentation of the body axis. To address this, I blocked GREB1 function, by injecting splicing-blocking morpholinos in the zebrafish (Nasevicius and Ekker, 2000). Two types of morpholinos were designed, one targeting the exon 2/intron 2 boundary (Figure 5.6) and the other targeting the exon 16/intron 16 boundary (Figure 5.7). If morpholinos block splicing at the targeted sites, a possible outcome is excision of exon 2 (in case of the first morpholino) and excision of exon 16 (in case of the second morpholino) (Figures 5.6 and 5.7).

To determine the efficacy of the two morpholinos in altering the splicing of *Greb1* transcript, I performed RT-PCR across the region intended for splicing modification. RT-PCR amplified a 571 bp product corresponding to the normal transcript and a 466 bp product corresponding to the mis-spliced product in case of the first morpholino (Figure 5.6 b); in case of the second morpholino, a 899 bp product (normal transcript) and a 762 bp product (mis-spliced transcript) was detectable (Figure 5.7 b). Although normal transcripts were not completely abrogated, my data indicate that both morpholinos block splicing of *Greb1* transcript by excising exon 2 and exon 16, respectively. However, sequencing of the resulting RT-PCR products shall be performed. This experiment shall confirm the form of the mis-spliced products and it shall predict the form of the protein generated. Because *Greb1* consists of 31 exons, morpholino-induced excision of exon 2 or of exon 16 shall result in a truncated protein. Based on the current knowledge regarding the functional domains of the GREB1 protein, it is difficult to predict whether the truncated protein is functional.

Morpholinos blocked splicing even at the lowest doses tested (e.g. 2 ng in case of the first morpholino and 4 ng in case of the second morpholino, Figures 5.6 b, 5.7 b). Mis-

splicing was not observed with standard control morpholino and with *Greb1* mismatch morpholino, which were used to rule out off-target effects (Figures 5.6 b, 5.7 b).

In the RT-PCR experiments, the non-spliced endogenous products (in case of both morpholino 1 and morpholino 2) are amplified even when high doses of the splicing-blocking morpholinos are used. To quantify the residual amount of non–spliced product still present after morpholino injections, a quantitative PCR shall be performed.

It remains to determine whether GREB1 protein function is blocked, as a consequence of an altered splicing mechanism caused by morpholino injection. This aspect could provide the basis for future experiments, including the generation of a GREB1 antibody.

To study the requirement of GREB1 for axial elongation and segmentation, I injected splicing-blocking morpholino into 1-4 cell stage embryos and examined axis length and somite morphology at the developmental stage when axis elongation normally ceases. For both morpholinos, affected embryos at around 24 hpf (n=11) were more curved and shorter (by 23%) than controls (n=12) (Figure 5.8 c). Moreover, staining for *MyoD,* which marks the posterior half of the formed somites, revealed loss of integrity of somite boundaries (n=18/21) (Figures 5.8 a, arrow in b) (Weinberg et al., 1996). The typical chevron shape of the somites was lost. *MyoD* expression was stronger in experimental embryos versus controls (Figure 5.8 b), suggesting that mis-splicing of *Greb1* somehow affects *MyoD* expression. These findings imply that GREB1 is required for proper zebrafish axial elongation and somite morphology. It is not known whether the period of the segmentation clock is affected, as it was not possible to count the somites due to their irregular morphology.

Morphant embryos also had smaller head when compared to controls (arrowhead in Figure 5.8 b). This observation correlates well with the known sites of *Greb1* expression.

To verify the minimum dose of morpholino necessary for mis-splicing of *Greb1*, I injected different doses of antisense oligonucleotides in the range of 0.1-8 ng in the embryo and scored the frequency of the phenotype at these various doses. 1 ng of the first morpholino caused axial and somitic defects in 42% of embryos (n=36); and 1 ng of the second morpholino caused defects in 26% of embryos (n=46), indicating that this dose is enough to interphere with GREB1 function in some embryos. Injecting 4 ng of

morpholino was more efficient at disrupting elongation. 57% of embryos were affected with the first morpholino (n=107) and 57% with the second morpholino (n=110) Therefore, I used 4 ng of the second morpholino for all the following experiments. Knock-down technologies such as morpholino antisense oligonucleotides and shRNAs have been shown to activate the p53 pathway and cell death as an off-targeting effect (Robu et al., 2007, Mende et al., 2008). To exclude the possibility that observed shortening of the axis upon GREB1 knock-down is a consequence of morpholino induced-cell death, I simultaneously knocked-down GREB1 and p53 by means of morpholino co-injection or morpholino injection in p53 deficient background (Little and Mullins, 2009). The phenotypic frequency for embryos co-injected with *Greb1* and *p53* morpholinos was at least as great (92% n=37) as for embryos injected with *Greb1* morpholino alone. These data indicate that the phenotype of *Greb1* morpholino is not due to p53-activated cell death.

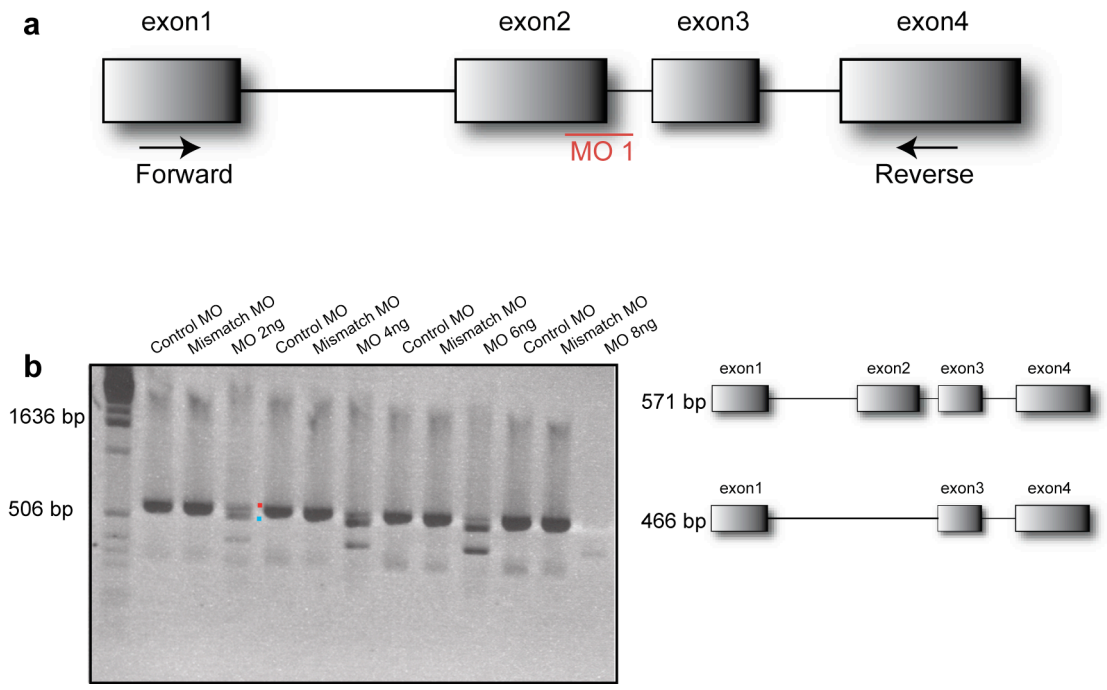

Figure 5.6 Morpholino knock-down of zebrafish GREB1.

a) A schematic of exon/intron structure of *Greb1* gene in the region targeted by the first morpholino. Location of primers used for RT-PCR is indicated by arrows and the red line shows location of the targeting morpholino. b) RT-PCR analysis of *Greb1* splicing. In each condition, RNA comes from 5 24 hours old embryos following morpholino injection at the 1-4 cells stage. Order of samples as indicated: standard control morpholino, mismatch morpholino and *Greb1* morpholino. Increasing doses (2-8 ng) of various morpholinos have been tested. WT and mis-splicing PCR products are detected at 571 (red dot) and 466 bp (blue dot), respectively.

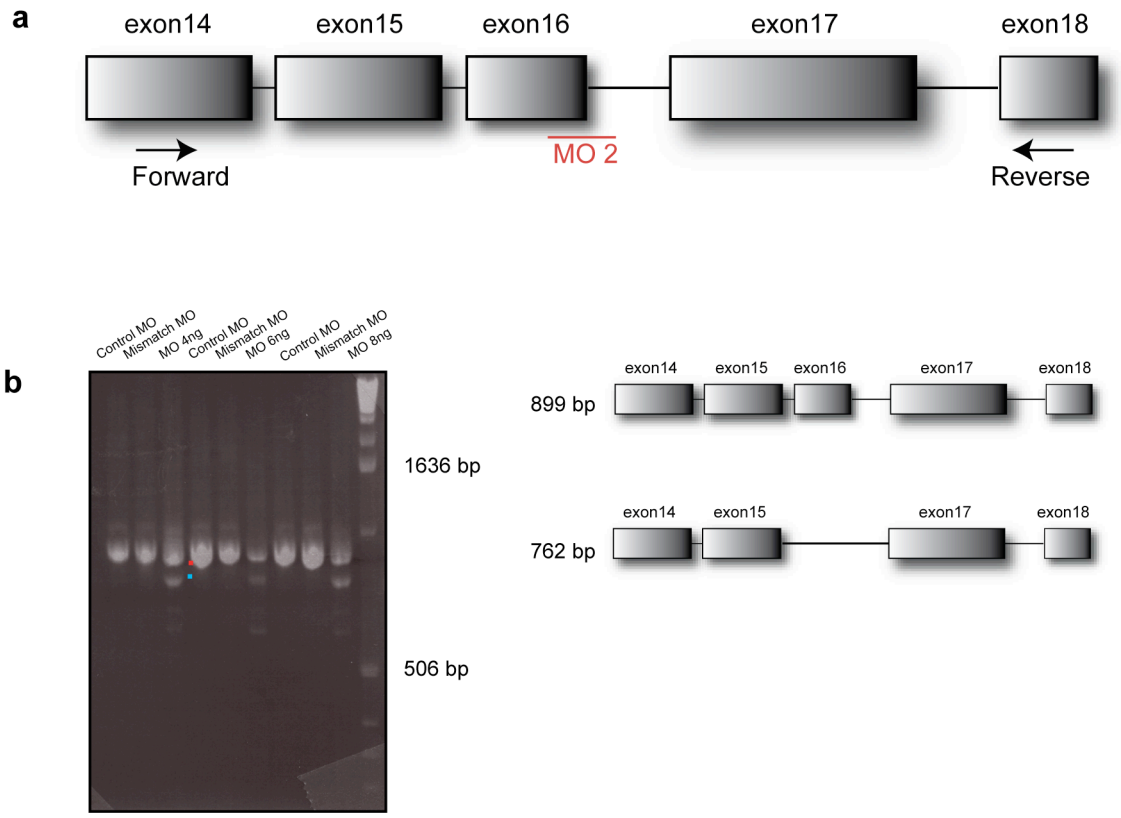

Figure 5.7 Morpholino knock-down of zebrafish GREB1.

c) A schematic of exon/intron structure of *Greb1* gene in the region targeted by the second morpholino. Location of primers used for RT-PCR is indicated by arrows and the red line shows the location of targeting morpholino. d) RT-PCR analysis of *Greb1* splicing. In each condition, RNA comes from 5 24 hours old embryos following morpholino injection at the 1-4 cells stage. Order of samples as indicated: standard control morpholino, mismatch morpholino and *Greb1* morpholino. Increasing doses (4-8 ng) of various morpholinos have been tested. WT and mis-splicing PCR products are detected on gel at 899 (red dot) and 762 bp (blue dot), respectively.

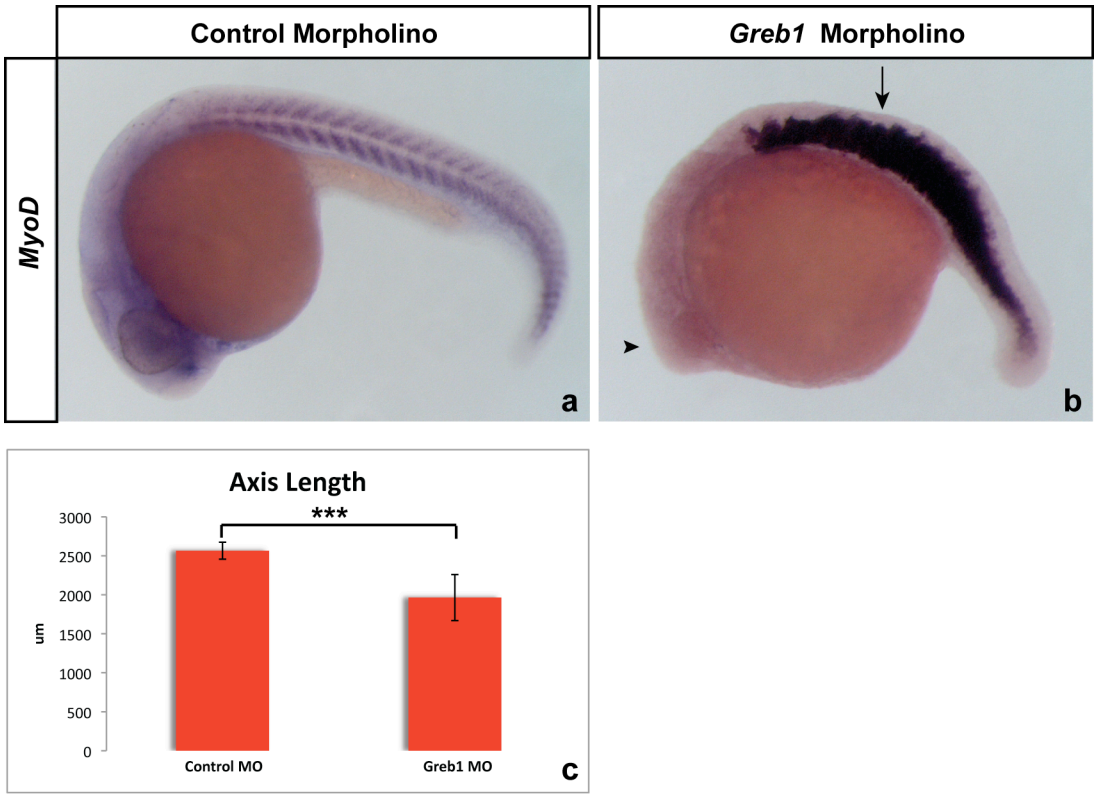

Figure 5.8 Effects of *Greb1* morpholino on zebrafish axial elongation and segmentation.

Figures a and b are side views of zebrafish embryos at termination of axial elongation. Embryos were stained by in situ hybridisation for *MyoD*. Typically, 15 embryos or more for each experimental condition were subjected to in situ hybridisation. Embryos were injected with a standard control morpholino (a) and a *Greb1* splicing blocking morpholino (b). Note variation in head size (arrowhead) and somite shape (arrow) in experimental embryos versus controls. Body axis is more curved and shorter in embryos injected with *Greb1* morpholino, as represented in the graph in c. Error bars represent standard deviation, p-value<0.01 determined using a two-tailed t-test.

Getting the same phenotype with two independent *Greb1* morpholinos argues strongly that the phenotype is not due to off-target effects. To test this further, I performed a rescue experiment by expressing a wild-type, morpholino-resistant *Greb1* RNA, specifically the mouse *Greb1* RNA. Co-injection of the RNA and the morpholino is expected to result in reversion of the phenotype, if the morpholino effect is specific to the target.

The mouse *Greb1* RNA was *in vitro* synthesised. However, *in vitro* transcription of large transcripts such as *Greb1* (5.985 Kb) often results in low yield of transcription. To overcome this problem, the ratio of cap analogue to GTP used in the transcription reaction was adjusted resulting in higher yield of transcription (Figure 5.9) but presumably in decreased capped transcripts. Because of the difficulty in synthesising an intact full-length *Greb1* transcript, co-injection of mouse *Greb1* RNA and the morpholino did not rescue the phenotype (co-injected embryos presented axial and somitic defects similar to those observed in embryos injected with morpholino alone).

In support of this, *in vitro* transcribed mouse *Greb1* mRNA resulted in ineffective translation of mouse GREB1 protein, as seen on an autoradiogram after an *in vitro* coupled transcription translation reaction (Figure 5.10). To avoid problems caused by inefficient *in vitro* synthesis of large transcripts, synthesis of shorter transcripts could be performed. For example, one could use the C-terminus sequence (see Figure 5.1) of GREB1 as an alternative to rescue the phenotype, as the C-terminus has been predicted to contain the functional domain of the protein.

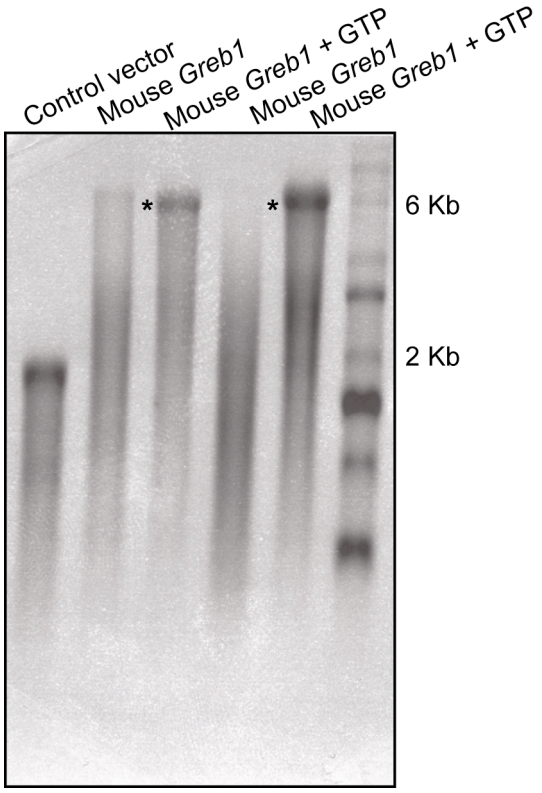

Figure 5.9 Rescue of the phenotype.

Agarose gel analysis of *in vitro* transcription reactions. 2 μg of each reaction were loaded onto denaturing gel. Loading order was as follows: control vector (pTri-Xef, TRIPLEScript plasmid containing *Xenopus elongation factor 1* α); mouse *Greb1* (pEF-DEST51-*Greb1*, expression vector containing full-length mouse *Greb1* and linearised with BstBI); mouse *Greb1* +GTP (1 μl of GTP was added to the transcription reaction to optimise yield of long transcript); mouse *Greb1* (pEF-DEST51-*Greb1*, expression vector containing full-length mouse *Greb1* and linearised with PmeI); mouse *Greb1* +GTP (1 μl of GTP was added to the transcription reaction to optimise yield of long transcript). Control reaction resulted in a product of the expected size (1.85 Kb), only reactions supplemented with GTP gave products of expected size (5.985 Kb), as indicated by asterisks, and were used for subsequent injections into zebrafish embryos.

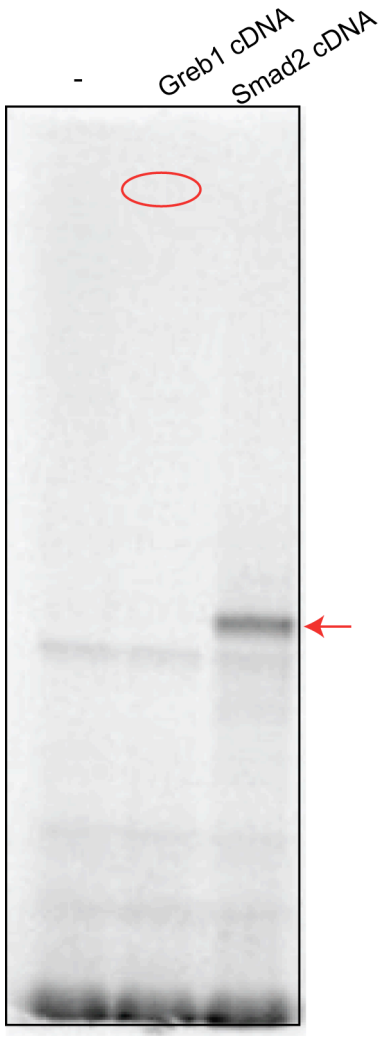

Figure 5.10 Rescue of the phenotype.

Autoradiogram of *in vitro* coupled transcription translation reactions. Protein were labelled using ^{35}S-methionine and visualised by autoradiography. 1 µl of each reaction was loaded onto Bis-Tris gel. Loading order was as follows: - negative control reaction (reaction in absence of cDNA); *Greb1* cDNA (reaction in presence of pEF-DEST51-*Greb1* containing full-length mouse *Greb1*); *Smad2* cDNA (reaction in presence of pCS2+-*Smad2* containing full-length *Smad2* and used as positive control). A band of the correct size was detected for Smad2 (at 52.5 kDa) as indicated by the arrow, no band was detected for GREB1 at expected size (at 216.9 kDa) as highlighted by the circle. Unexpected bands (sign of unbound radioactive aminoacids) were visualised on gel but this happened even in absence of cDNA.

5.1.4 Loss of GREB1 and progenitor contribution to axial tissues

Axial progenitors located in the CNH contribute to various axial tissues (e.g. neural, notochordal and somitic) (Davis and Kirschner, 2000, Kanki and Ho, 1997, Cambray and Wilson, 2007, McGrew et al., 2008). Given that *Greb1* is expressed in the progenitor area (Figure 5.5), I asked whether GREB1 was required for progenitors to contribute to axial tissues. To do so, I performed in situ hybridisation for *Ntl* and *MyoD*, markers of notochordal and somitic tissue, respectively. At both the 15 somite stage and at 24 hpf, morphant embryos did not exhibit major changes in *Ntl* expression in respect to the axial mesoderm domain (n=20/34 and n=6/8, respectively, n being the number of embryo that did not show any phenotype), although a slight reduction of caudal *Ntl* expression was observed at the latter time point (Figure 5.11 a-d'). Therefore, GREB1 is not required for progenitors to contribute to notochordal tissue. *Ntl* staining revealed defects in notochord morphology upon knock-down of GREB1 i.e. the notochord of morphant embryos was more undulated and wider than that of controls (Figure 5.11 c-d').

Morphant embryos stained for *MyoD* did not show any changes at either the 15 somite stage or at 24 hpf, when compared to controls. Thus, GREB1 is not required for progenitors to contribute to somitic tissue.

However, up-regulation of *MyoD* was observed at 24 hpf (as already indicated in Figure 5.8). Furthermore, in situ staining showed that somites of morphant embryos were more laterally expanded and thinner at the 15 somite stage (n=18/38) (Figure 5.12 a-b'), and that integrity of somite borders was lost at 24 hpf, consistent with the hypothesis that GREB1 is required for proper somite morphology (n=7/15) (Figure 5.12 c-d').

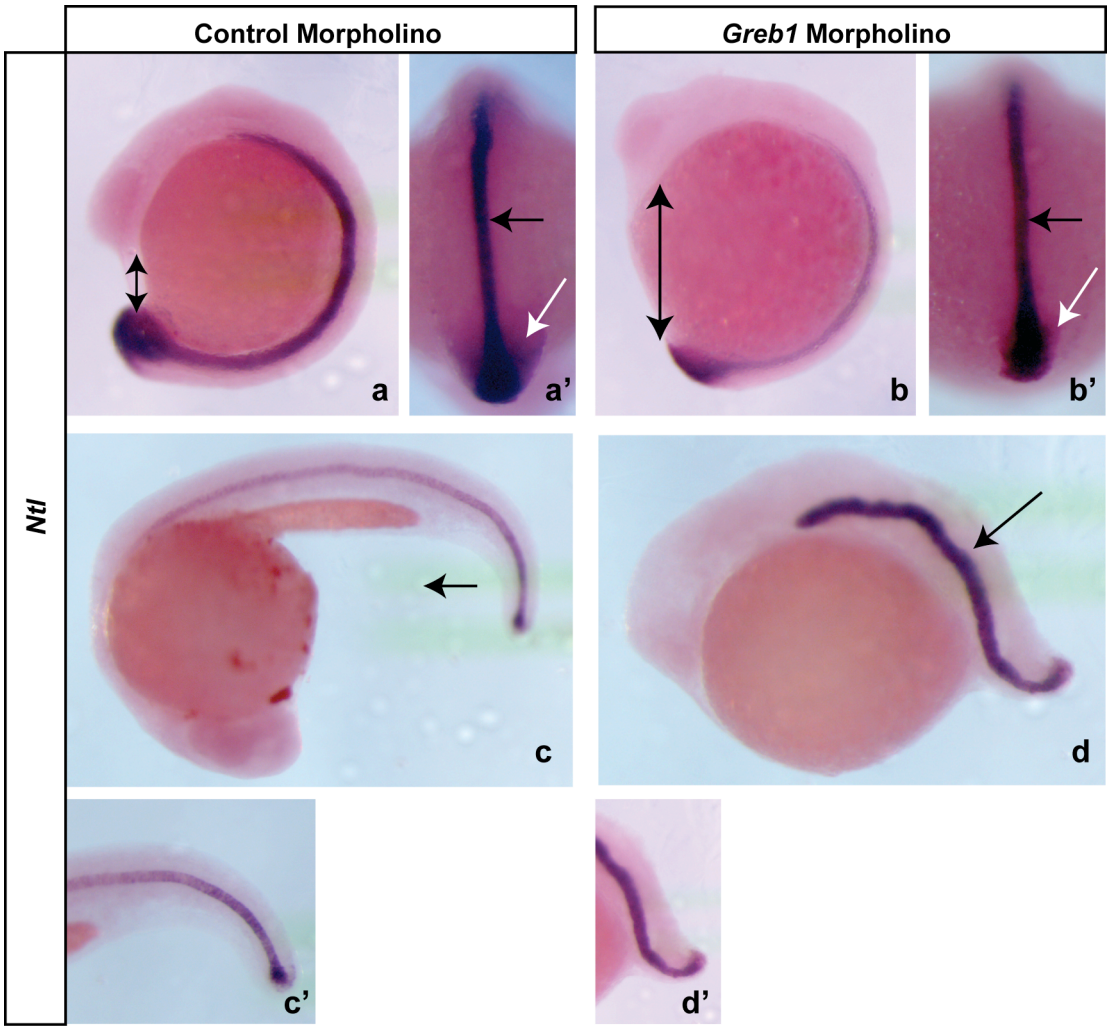

Figure 5.11 Effects of GREB1 knock-down on its ability to contribute to axial tissues (notochord).

Figures a, b, c, d are side views of zebrafish embryos at 15 somite stage (a, b) and at 24 hpf (c, d). Figures a', b', c', d' are dorsal and side views of zebrafish tails at 15 somite stage (a', b') and at 24 hpf (c', d'). Embryos were stained by in situ hybridisation for *Ntl* to mark the notochord. Typically, 15 embryos for each conditions were subjected to in situ hybridisation. Levels of *Ntl* gene expression were similar in controls and morphant embryos at all stages analysed, except for a reduction in *Ntl* expression in the caudal mesoderm domain of 15 somite stage embryos (white arrows in a' and b'), *Ntl* expression in the axial mesoderm domain does not change (black arrows in a' and b'). Staining for *Ntl* reveals defects in notochord morphology (in morphant embryos notochord is undulated, wider and shorter than control embryos), arrow in d. Also note the change in body axis proportions of morphant embryos, arrowheads in a and b.

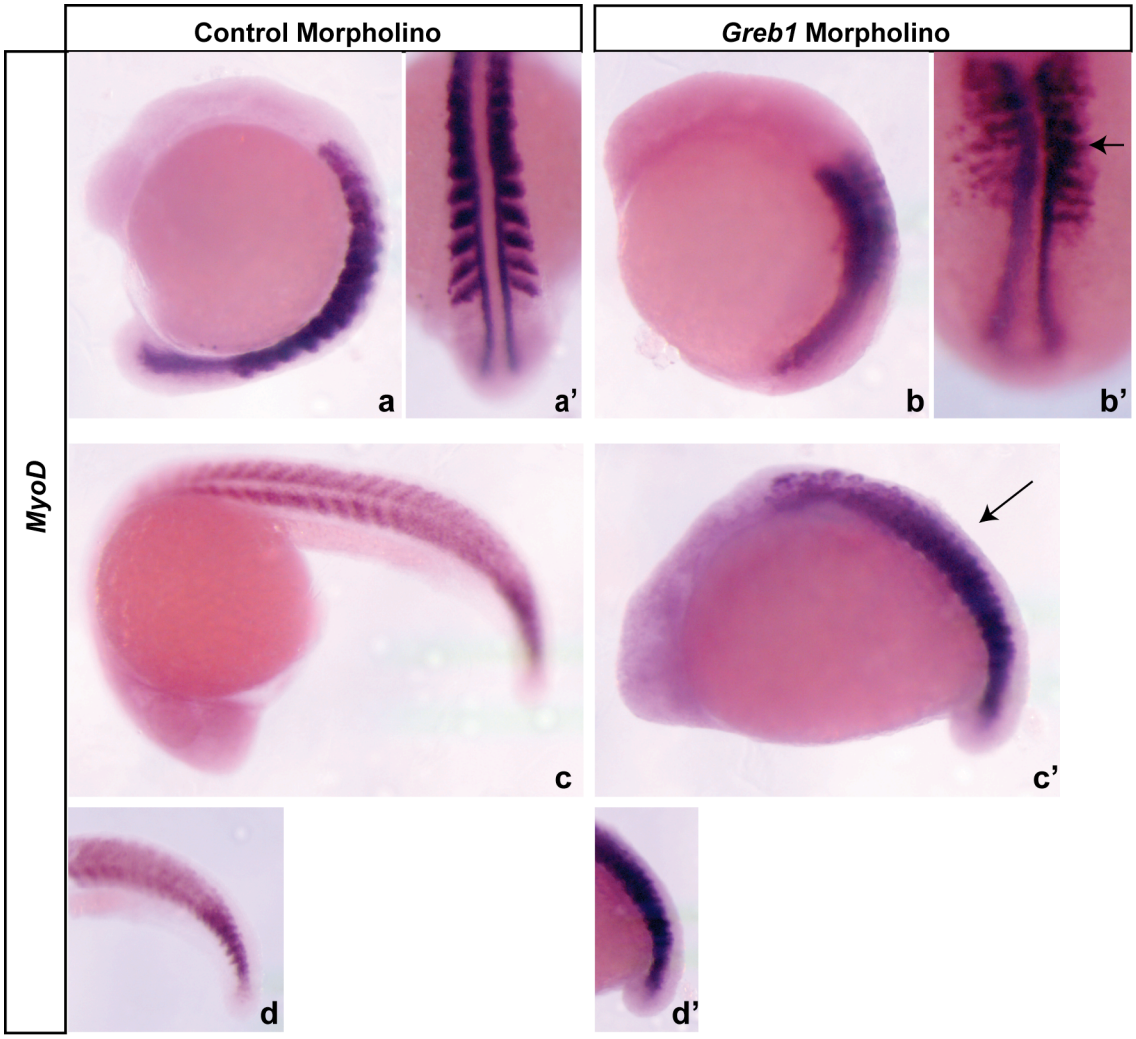

Figure 5.12 Effects of GREB1 knock-down on its ability to contribute to axial tissues (somites).

Figures a, b, c, d are side views of zebrafish embryos at 15 somite stage (a, b) and at 24 hpf (c, d). Figures a', b', c', d' are dorsal and side views of zebrafish tails at 15 somite stage (a', b') and at 24 hpf (c', d'). Embryos were stained by in situ hybridisation for *MyoD* to mark the notochord. Typically, 15 embryos for each conditions were subjected to in situ hybridisation. Levels of *MyoD* gene expression are similar in controls and morphant embryos at 15 somite stage, levels of *MyoD* gene expression seem up-regulated in morphant embryos at 24 hpf. Staining for *MyoD* reveals defects in somite morphology (in morphant embryos somites are thinner and mis-positioned at 15 somite stage, and somites look compacted at 24 hpf), arrows in b' and d. Also note change in body axis proportions of morphant embryos, in b and d.

5.1.5 Loss of GREB1 does not affect somite polarity or cyclic gene expression

Given that *Greb1* morphant embryos show loss of somite border integrity (Figure 5.12), I explored whether this is due to defective somite polarity. It has been shown that somite border formation depends on establishment of somite polarity into anterior and posterior compartments (Durbin et al., 2000). I performed in situ hybridisation at the 15 somite stage for *MespA, MespB* and *PapC*, all markers of the anterior somite compartment (Sawada et al., 2000, Yamamoto et al., 1998). *MespA* and *MespB* were segmentally expressed in three stripes in the anterior PSM of control embryos (n=21 for both genes) and a similar expression pattern was observed in the morphant embryos (n=14/14 for *MespA* and n=10/10 for *MespB*) (Figure 5.13 a-d). However, stripes of *MespA* and *MespB* expression were thinner, in height, in the *Greb1* embryos. Similarly, *PapC,* which is expressed in four bands, marking the newest, forming somite, and immature somites was not different between control (n=22) and morphant embryos (n=11/11), except that, like *MespA* and *MespB*, the bands were finer in the morphant embryos (Figure 5.13 e, f). At the 15 somite stage, the expression pattern of *MyoD,* which is a marker for posterior somite compartment, was not disturbed (Figure 5.12). Therefore, GREB1 is not required for establishment of somite polarity.

Alternatively, somitic defects of *Greb1* embryos could result from a defective segmentation clock. To explore this possibility, I analysed cyclic expression of *Her1* (Takke and Campos-Ortega, 1999). Both control (n=19) and morphant (n=16) embryos exhibited dynamic expression pattern in the posterior PSM, suggestive of a functioning segmentation clock machinery (Figure 5.14). Thus, GREB1 is not required for cyclic gene expression. Together, these observations show that loss of somite border integrity in *Greb1* morphant embryos is not due to defective somite polarity or defective clock machinery.

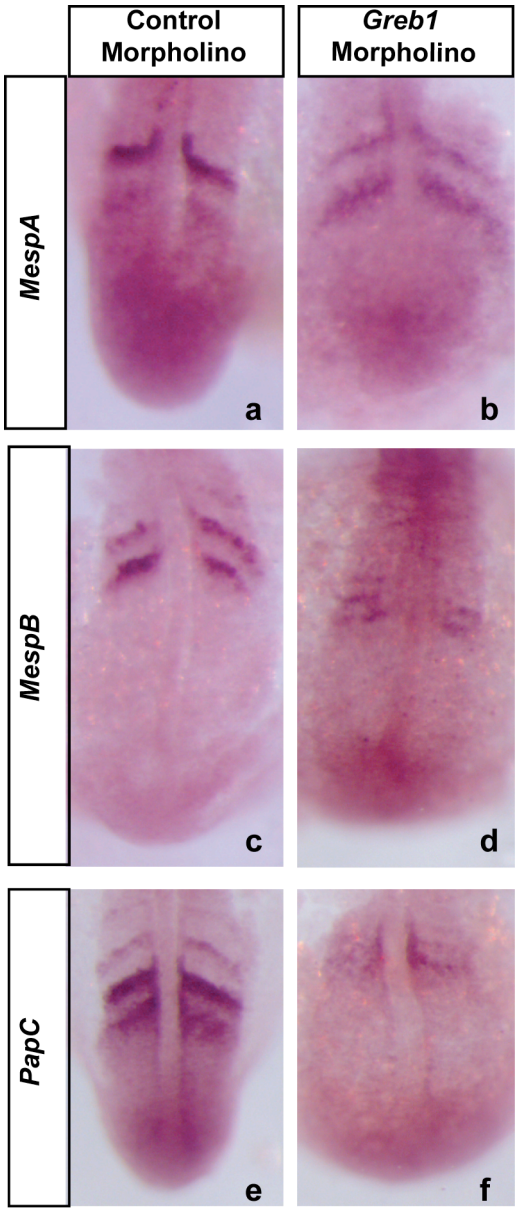

Figure 5.13 No effects of GREB1 knock-down on somite polarity.

Figures a-f are dorsal views of zebrafish embryos at 15 somite stage stained by in situ hybridisation for *MespA, MespB and PapC* to mark anterior and posterior somite compartments. Typically, 15 embryos for more or each conditions were subjected to in situ hybridisation. Expression pattern of all genes analysed is similar in morphant and control embryos. Somite morphology is disturbed in morphant embryos (e.g. somites are laterally expanded and thinner).

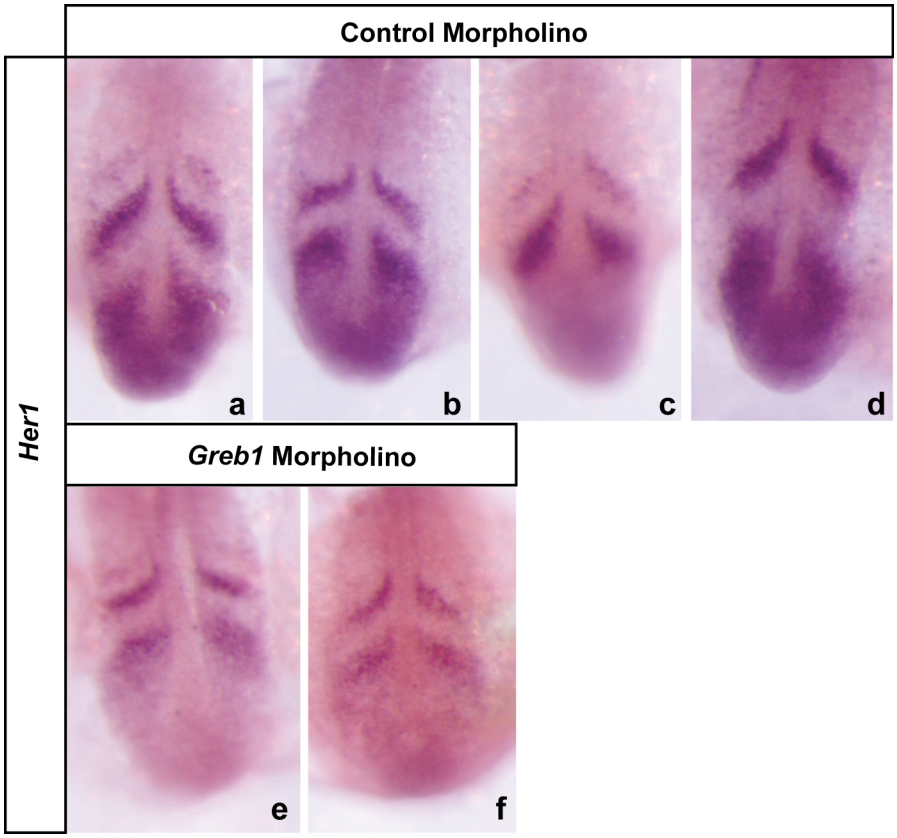

Figure 5.14 No effects of GREB1 knock-down on expression of a cyclic gene.

Figures a-f are dorsal views of zebrafish embryos at 15 somite stage stained by in situ hybridisation for *Her1* whose expression is cyclic in the PSM (see figures a-d). Typically, 15 embryos or more for each conditions were subjected to in situ hybridisation. Cyclic expression of *Her1* is maintained in *Greb1* morphant embryos (e, f). Note that the PSM is wider in morphant embryos when compared to controls.

5.1.6 Loss of GREB1 causes defects in convergent extension movements

The irregular somite morphology (e.g. thinner somites: Figures 5.13 and 5.14) and the shortened body axis (Figure 5.8) observed in *Greb1* morphant embryos are suggestive of a disruption in convergent extension movements during gastrulation (Keller, 2002). In vertebrates, convergent extension movements are required for proper narrowing and elongation of the body axis, which is achieved by cell intercalation (Myers et al., 2002b). Indeed, *Greb1* is expressed within the region of the embryo were gastrulation movements occur (Figure 5.5).

To test if GREB1 is required for convergent extension movements, I analysed somite morphology in morphant embryos at early stages by performing in situ hybridisation for *PapC* and *MyoD* which mark the somites. At the 2 and 10 somite stage, morphant embryos showed more laterally expanded (n=19/43) and thinner somites (n=22/37) than controls (Figure 5.15), consistent with the altered somite shape observed in older embryos (Figures 5.13 and 5.14). Morphant embryos also exhibited a wider notochord and a rounder body (n=19/43) (Figure 5.15, b and d). Defective narrowing of the body of *Greb1* morphant embryos (e.g. broadened somites and notochord) has been previously reported for *trilobite* and *knypek* convergent extension mutants (Topczewski et al., 2001, Park and Moon, 2002, Jessen et al., 2002). These data suggest that GREB1 might be required for gastrulation movements.

Morphometric analysis revealed significant changes of notochord and somite size (Figure 5.16).

Notably, abnormal notochord size recovers over time (compare graphs in b and d, relative to notochord width at the 2 and at the 10 somite stage, respectively). If abnormality of the notochord is caused by defective convergent extension movements, one can speculate that the recover occurs because gastrulation movements are only temporarily delayed (but they still take place).

On the contrary, the somite size does not recover over time. Because the notochord plays an important role in patterning of the the somites, it is possible that the defective

somite size is a consequence of an impaired notochord development. If this is true, one expects that the somite size recovers when notochord does so, but the somite size does not recover. A possibility is that the change in somitic features has been irreversibly caused. Convergent extension mutants display a shortened anteroposterior axis (Topczewski et al., 2001, Park and Moon, 2002, Jessen et al., 2002, Carreira-Barbosa et al., 2003, Weiser et al., 2007). To investigate whether this is the case for *Greb1* morphant embryos, I analysed two axial structures, the notochord and the neural plate by in situ staining for *Ntl* and *Dlx3* (Schulte-Merker et al., 1992, Akimenko et al., 1994). Tail bud stage morphant embryos presented a shorter and undulated notochord (n=8/20) (Figure 5.17 b) (as already observed in Figure 5.11) that is wider than that of controls (Figure 5.17 b').

The shape of the neural plate seemed similar to that of controls, in terms of size and length (n=11/12) (Figure 5.17 d, e). Thus, anteroposterior lengthening of the body axis is slightly affected in *Greb1* tail bud embryos.

Expression domain of *Hgg1*, a marker of the prechordal mesoderm got reduced in treated embryos (n=11/12) (Figure 5.17 d, e) (Daggett et al., 2004), implying that migration of prechordal mesoderm is impaired, further supporting the idea that GREB1 is required for proper convergent extension movements. Together, these data confirm that irregular somite morphology and shortened body axis observed in *Greb1* morphant embryos are due to impaired convergent extension movements during gastrulation.

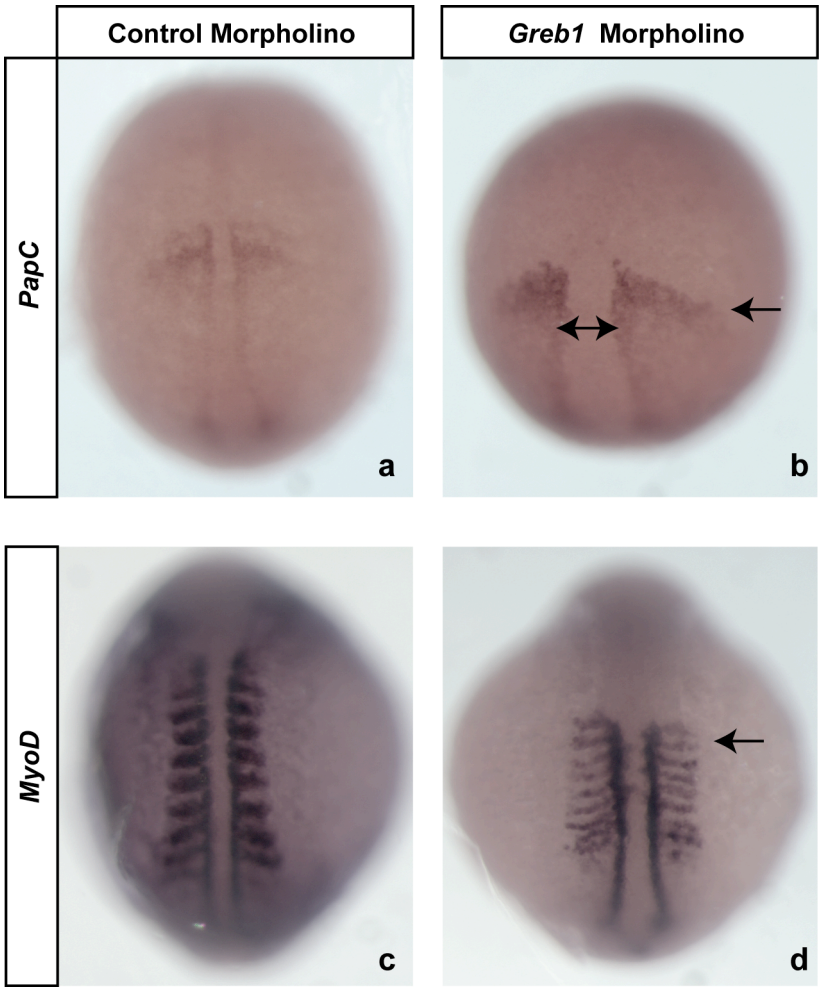

Figure 5.15 Effects of GREB1 knock-down on convergent extension.

Dorsal views of zebrafish embryos at 2 and 10 somites stage, embryos were stained by in situ hybridisation for *PapC* and *MyoD*, respectively. Tipically, 15 embryos or more for each experimental condition were subjected to in situ hybridisation. Embryos were injected with a standard control morpholino (a, c) and a *Greb1* splicing blocking morpholino (b, d). Note the variation in notochord size (arrowhead) and somite length (arrow) in experimental embryos (b) versus controls (a), and the change in distance between somites as indicated by arrow in d.

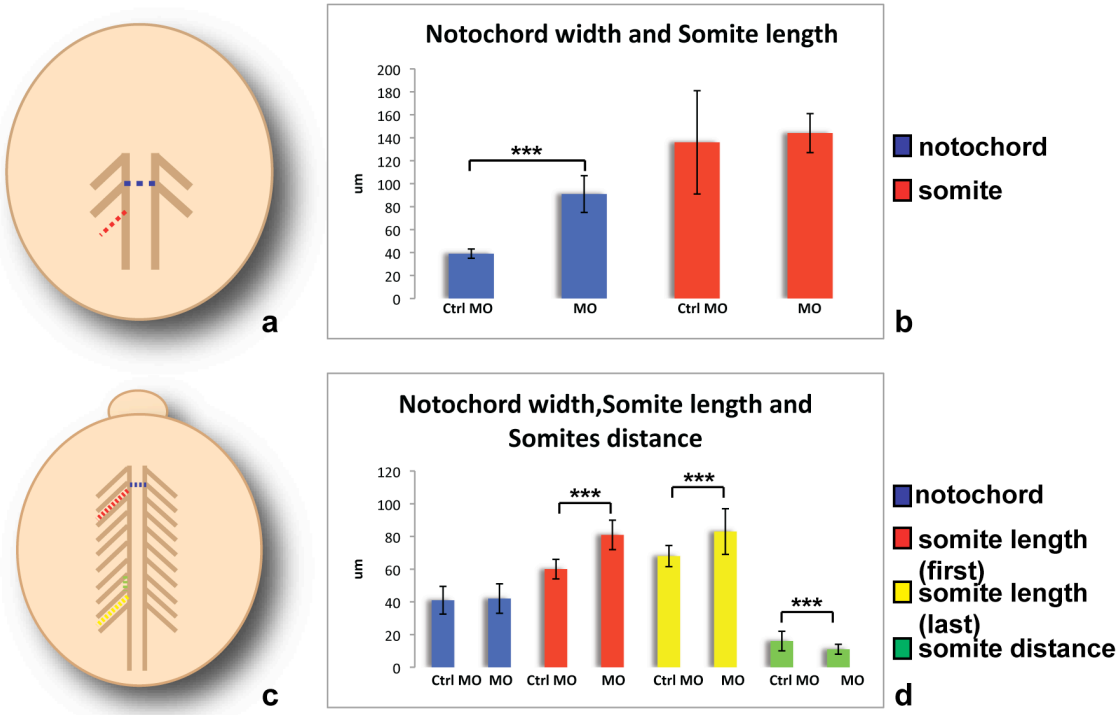

Figure 5.16 Effects of GREB1 knock-down on embryo morphology.

Figure a is a depiction of a 2 somite stage control embryo, to show how measurements were taken. Dotted lines represent notochord width (blue) and somite length (red). Figure b is an analysis of notochord width and somite length in control and morphant embryos. Approximately 10 embryos were measured for each conditions. Error bars represent standard deviation, variation in notochord width between controls and morphant embryos is statistically significant (p-value<0.01 determined using a two-tailed t-test). Variation in somite size is not statistically significant. Figure c is depiction of 10 somite stage embryo, dotted lines represent notochord width (blue), length of first somite (red), length of last somite (yellow), and distance between somites (green). Figure d is analysis of notochord width, somite length and somite distance in control and morphant embryos. Approximately 10 embryos were measured for each conditions. Error bars represent standard deviation. Variation in notochord size is not statistically significant. Variation in somite size and somite distance is statistically significant (p-value<0.01 determined using a two-tailed t-test).

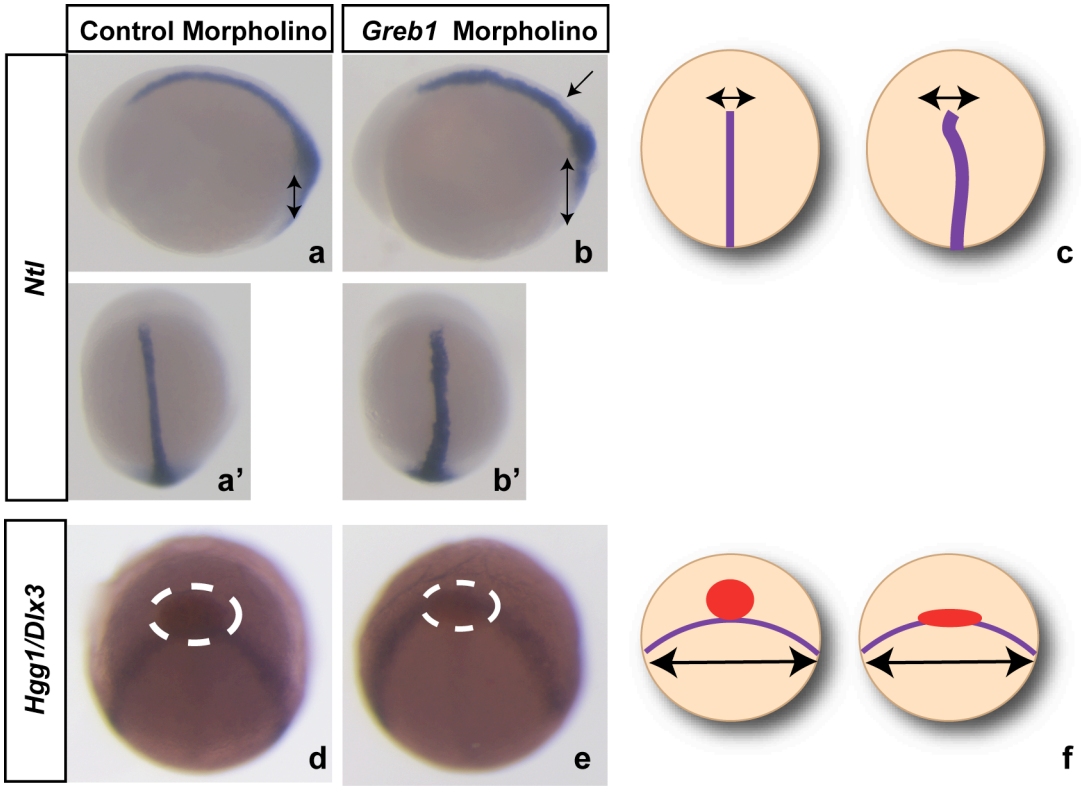

Figure 5.17 Effects of GREB1 knock-down on convergent extension.

Figures a and b are side views of bud stage embryos stained for *Ntl* to mark the notochord. Approximately 10-20 embryos were stained for each probe. Note the undulation of the notochord (arrow in b) and the slightly reduced notochord length (arrowheads in b) in morphant embryos. Figures a' and b' are different orientations of bud stage embryos to show defective morphology and length of the notochord. Notochord appears wider in morphant embryos (b'). Figure c is depiction of notochord length, size and morphology in control and morphant embryos. Figures d and e show bud stage embryos stained for *Dlx3* to mark the anterior edge of the neural plate (blue) and Hgg1 to mark the prechordal mesoderm (red). Approximately 10-20 embryos were stained for combination of two probes. For double-labelling the most strongly expressed gene was labelled with DIG (*Hgg1*) and developed second using INT/BCIP (red colour), the less strong gene (*Dlx3*) was labelled with FLU and developed first with NBT/BCIP (blue colour). There is no difference in neural plate width between control and morphant embryos. There is difference in prechordal mesoderm size between controls and morphant embryos. Figure f is graphic depiction of figures d and e.

5.1.7 Loss of GREB1 causes defects in convergent extension without affecting Bmp activity

At early gastrulation, a ventral to dorsal gradient of Bmp activity defines cell fate, and also influences convergent extension movements (Myers et al., 2002b, Myers et al., 2002a). In convergent extension mutants (including *trilobite* and *knypek*), cell movements are impaired but dorsoventral cell fate remains unaffected (Heisenberg et al., 2000, Topczewski et al., 2001, Jessen et al., 2002, Kilian et al., 2003). To investigate whether this is also the case for *Greb1* morphant embryos, I took advantage of a Bmp reporter line where expression of *mRFP* is driven by Bmp responsive elements (Wu et al., 2011). *Greb1* morpholino was injected into embryos containing the Bmp reporter, and Bmp activity was detected by in situ hybridisation for *mRFP*. At the 75-85% epiboly stage *mRFP* expression pattern was unchanged in morphant embryos (n=24/24) when compared to controls (n=21).

At the 10-15 somite stage, *mRFP* gene expression pattern was similar between morphants (n=14/14) and controls (n=26) (Figure 5.18). However, quantitative PCR analysis would be desirable to confirm that *mRFP* gene expression levels are not changed when comparing 10-15 somite stage controls to morphant embryos at the same developmental stage.

If confirmed, these results would suggest that Bmp activity is normal in the *Greb1* morphant embryos, implying that dorsoventral cell fates remain unaffected and that the *Greb1* phenotype might be explained in terms of impaired cell movements, once this hypothesis will be confirmed by further experiments (see Discussion section in this chapter) .

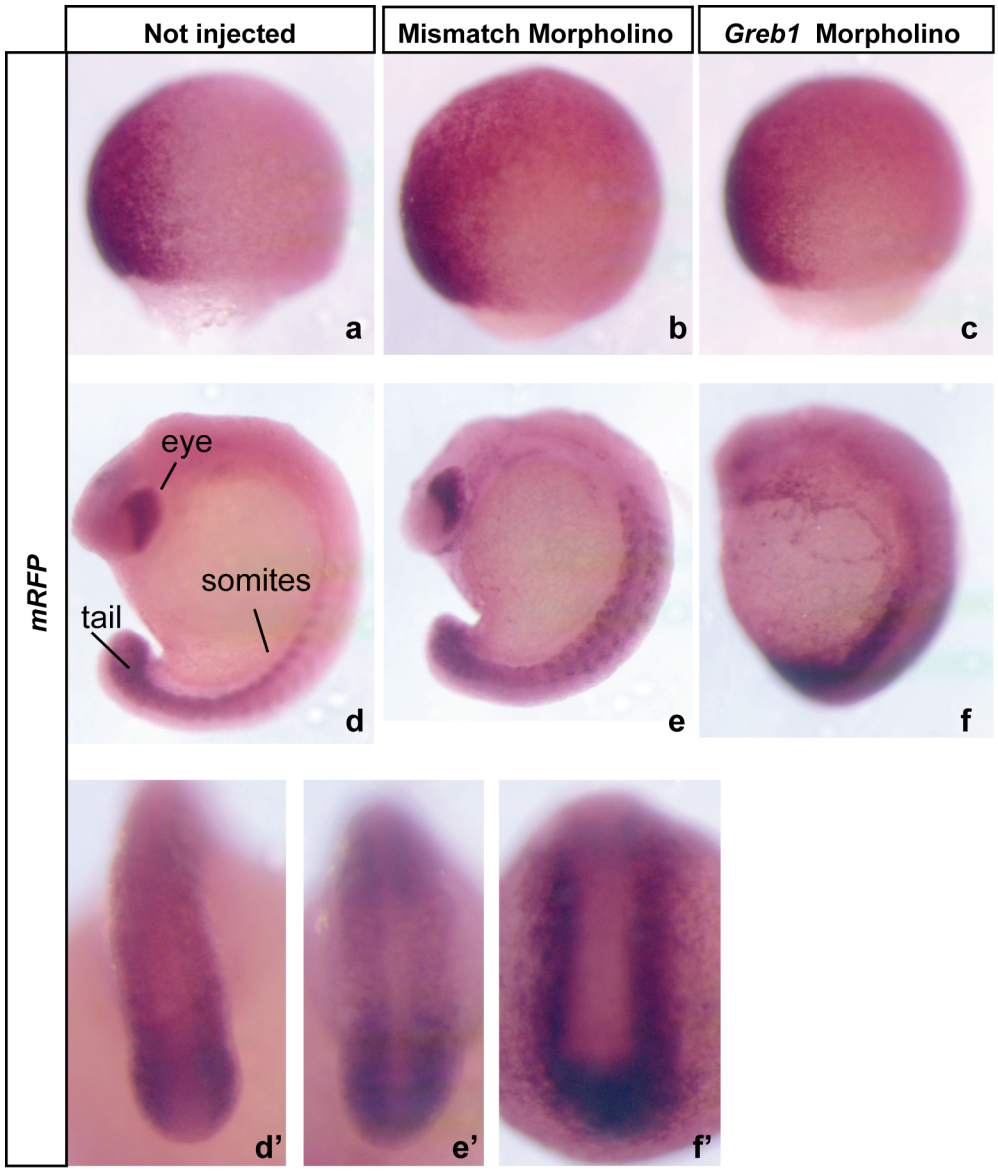

Figure 5.18 Effects of GREB1 knock-down on Bmp activity.

Figures a, b, c are side views of 75-85% epiboly zebrafish embryos stained by in situ hybridisation for *mRFP*. Dorsal margin is on the right. Approximately, 15 embryos for each conditions were processed for in situ hybridisation. *mRFP* expression remains unchanged in morphant embryos versus controls (b, c). Figures d, e, f are side views of 10-15 somite stage embryos. Approximately, 15 embryos for each conditions were subjected to in situ hybridisation. mRFP expression does not change in morphant embryos in comparison to controls. Size of expression domains (eye, somites, tail) changes but note that body axis proportions of morphant embryos differ from controls as well (e, f). Figures d'-f' show higher magnification of the tail region of embryos in figures d-f.

5.1.8 Discussion

5.1.8.1 GREB1: a novel player in vertebrate axial elongation and segmentation?

Our data indicate that *Greb1* is one of the most upregulated genes in the mouse CNH compared to the surrounding regions (e.g. the PSM) (Prajapati R et al., manuscript in preparation). In contrast to the PSM, the CNH contains progenitor cells that subsequently differentiate into PSM, somites, neural tube and notochord contributing to the elongation of the body axis (Cambray and Wilson, 2007, McGrew et al., 2008, Kanki and Ho, 1997, Davis and Kirschner, 2000) . Therefore, *Greb1* might be a putative marker of progenitor cells. In this chapter, I have provided evidence that *Greb1* is expressed in a region of the murine tail that resembles the CNH, confirming the data from a previous array experiment performed in the laboratory. The expression pattern of mouse *Greb1* was similar in the chick and in the zebrafish, suggesting that the gene is expressed in the progenitor cells of different vertebrate embryos.

The function of GREB1 was studied in the zebrafish as it represents a convenient model for genetic manipulations. Morpholino oligonucleotides were injected into zebrafish embryos to cause mis-splicing of *Greb1* and to impair GREB1 protein function. Injected embryos exhibited a shortened axis and severe somitic defects (i.e. the somites lose their typical chevron shape) suggestive of impaired mesodermal differentiation. An attempt to rescue the phenotype by co-injecting the morpholino and the full-length mRNA of mouse *Greb1* failed, because of technical limitations. However, multiple controls confirmed that the morphant phenotype was not due to toxicity of the knock-down agent, or to off-target effects (that was checked by injection of a mismatch morpholino) or to non-specific effects (that was checked by co-injection with a p53 morpholino). Furthermore, the same phenotype (e.g. shortened axis and defective somites) was observed using two different non-overlapping morpholinos.

Shortening of the body axis has been reported for *Ntl* deficient embryos (Amacher et al., 2002). *Ntl* is known to be required both in axial (e.g. notochord) and caudal (e.g. tail

bud) mesoderm, where it plays a major role in progenitor maintenance (Martin and Kimelman, 2010). It is possible that reduction of axis length observed in the *Greb1* morphant embryos is due to a reduction of *Ntl* gene expression. However, no major differences were observed between control and treated embryos, arguing against this possibility. Martin et al. (2008) have shown that maintenance of progenitors depends on an autoregulatory positive feedback loop between *Ntl* and canonical Wnt signalling. It remains to be tested whether this loop acts upstream of *Greb1* to regulate progenitor cells and axis length (future experiments shall analyse *Greb1* expression in *Ntl* and *Wnt* mutant embryos or in embryos treated with inhibitors of the Wnt signalling pathway).

The *Greb1* morphant embryos show additional phenotypes (e.g. severe somitic defects that correlated with up-regulation of *MyoD* expression), suggestive of impaired somite differentiation, and resembling those embryos where Hedgehog signalling pathway is aberrantly activated. *MyoD* is strongly induced in *Ptc1; Ptc2* double mutants (Ptcs are both receptors and negative regulators of the Shh signalling pathway), indicating that somites give rise to slow but not to fast muscle fibres (Koudijs et al., 2008). In the *Greb1* embryos, the typical chevron shape of the somites was lost, and, again, this has been previously observed in mutants of the Hedgehog signalling (van Eeden et al., 1996). Xu et al (2006) have identified *Greb1* as a Hedgehog signalling target gene in a genome-wide expression profiling experiment performed in the zebrafish. Thus, it remains possible that the somitic defects observed in the *Greb1* morphant embryos are due to altered Hedgehog signalling, providing the basis for future experiments. If *Greb1* is a Hedgehog signalling target gene, one expects that *Greb1* morphants exhibit an opposite phenotype to that of *Ptc1; Ptc2* double mutants, differently from what described in this chapter. However, it is possible that: 1) *Greb1* is a negative regulator of the Hedgehog signalling; 2) the protein derived from the morpholino-induced mis-splicing is a dominant active form of GREB1 protein. Both possibilities would explain the similarity between *Greb1* morphants and double mutants of *Ptc1; Ptc2,* well-known negative regulators of the Shh signalling pathway. To investigate whether Shh signalling is induced or repressed following *Greb1* morpholino injection, one could analyse the expression of dorsoventral markers in the neural tube, which are typical read-out of the Shh activity.

Markers of somite polarity and components of the segmentation clock machinery were not affected in *Greb1* embryos. Together, these results suggest that GREB1 knock-down results in defective somite differentiation (e.g. into muscle fibres), but not in defective somite formation (e.g. formation of somite borders linked to clock function, and formation of anterior and posterior somite compartments linked to polarity establishment). Further analysis of more genes required for somite formation and maturation (e.g. more clock genes, components of the FGF/RA pathways, and *Tbx24* which is required for somite maturation) would be required to confirm this (Dequeant and Pourquie, 2008, Nikaido et al., 2002).

Axial progenitors located in the CNH contribute to PSM, somites, neural tube and notochord (Cambray and Wilson, 2002). It remains to be determined whether GREB1 knock-down affects the progenitor ability to contribute to neural tissue. An analysis of the expression of neural markers (e.g. *Neurogenin*) would help answer this question (Blader et al., 1997).

5.1.8.2 Convergent extension is required for proper axial elongation and segmentation

At early developmental stages, *Greb1* expression was found at the site of gastrulation movements in various vertebrates. In the zebrafish, *Greb1* is expressed in the dorsal and ventral margin where convergent extension movements take place, contributing to mediolateral narrowing and anteroposterior elongation of the embryo (Myers et al., 2002b).

I have provided evidence that *Greb1* might be required for convergent extension movements. At the 2 and 10 somite stage, *Greb1* embryos remained rounded and showed thinner and laterally expanded somites similar to phenotypes caused by convergence defects. This phenotype persisted in older embryos, as revealed by staining for somite polarity and for segmentation clock markers at the 15 somite stage. At the tailbud stage, morphant embryos exhibited a slightly shorter notochord than normal and additionally, the notochord was undulated, suggestive of impaired extension. In support

of this, at 24 hpf, morphant embryos were shorter than controls. Similar observations have been reported for two convergent extension mutants: *trilobite* which encodes a mutant transmembrane protein required for Planar Cell Polarity/non-canonical Wnt signalling and which regulates cell movements at gastrulation; *knypek* which encodes a member of the glypican family and mediates convergent extension by potentiating Wnt11 signalling (Topczewski et al., 2001, Park and Moon, 2002, Jessen et al., 2002).

In addition to broadened somites and a shortened axis, *trilobite* and *knypek* mutants present a wider neural plate and a flattened prechordal mesoderm (Topczewski et al., 2001, Jessen et al., 2002). The size of the neural plate did not change in *Greb1* morphant embryos as revealed by in situ staining for *Dlx3*, but the prechordal mesoderm, as marked by expression *Hgg1*, was clearly affected in treated embryos. These data suggest that convergent extension of mesodermal but not ectodermal tissue is impaired in *Greb1* embryos.

It is possible that similarly to the phenotype observed in *knypek* and *trilobite*, *Greb1* phenotype can be explained in terms of defective gastrulation movements rather than altered cell fates (Heisenberg et al., 2000, Topczewski et al., 2001, Jessen et al., 2002, Kilian et al., 2003). *Greb1* morphant embryos did not show severe alterations in Bmp activity (although qPCR analysis would be desirable to quantify the mRFP expression levels between morphants and controls), which is normally required to specify dorsoventral fate. Taken together, these findings suggest that *Greb1* might be required during gastrulation for convergent extension movements, with its loss affecting both the narrowing and elongation of the embryonic axial structures, such as the somites and the notochord.

Greb1 morphant embryos displayed impaired axial structures even at late embryonic stages, suggesting that such defects are a consequence of earlier defects in convergent extension movements. If *Greb1* indeed acts in the same pathway as *trilobite* and *knypek*, then the following would be true: 1) *trilobite* embryos present shortened axis and irregular somites at late embryonic stages in a way similar to *Greb1* embryos (Jessen et al., 2002); 2) both *knypek* and *Greb1* embryos maintain dynamic expression of cyclic genes (Aerne and Ish-Horowicz, 2004); 3) *knypek;trilobite* double mutants exhibit normal anteroposterior somite polarity as for *Greb1* embryos (Henry et al., 2000); 4)

specification of slow muscle fibres is affected in *knypek;trilobite* double mutants as hypothesised for *Greb1* embryos (Yin and Solnica-Krezel, 2007). It remains to be tested whether *Greb1* genetically interacts with convergent extension genes (e.g. by means of morpholino co-injection), and whether it modulates components of the convergent extension pathway at the protein level, as shown for *Prickle1*, a gene implicated in regulation of convergent extension movements (e.g. by looking at intracellular localisation of core components of the pathway following *Greb1* morpholino injection) (Carreira-Barbosa et al., 2003).

Given that *Greb1* is expressed around the CNH (where axial progenitors reside) and that is required for convergent extension movements, my results possibly provide a link between progenitor contribution to axial elongation and cell movements in the tail. Studies in other organisms support this possibility. In mouse, mutations of genes expressed in the progenitor area, such as *Fgf8* and *Brachyury*, result in axial truncations as a consequence of failed gastrulation movements. Furthermore, recent studies from Savory at al. (2011) have shown that *Cdx* genes, well known regulators of caudal development, interact with components of the Planar Cell Polarity pathway to regulate cell movements, a double mutation of *Cdx1;Cdx2* resulting in typical convergent extension defects (e.g. laterally expanded somites)

.

5.1.8.3 GREB1: the unsolved questions

Greb1 morphant embryos exhibit a broader and shorter axis, suggesting defective convergent extension movements at gastrulation (Keller, 2002). This is further supported by morphometric and gene expression studies that reflect changes in tissue size and embryonic axis proportions (e.g. broadening of the somites and the notochord, and shortening of the anterorposterior axis). However, convergent extension movements have not been directly assayed in the *Greb1* morphants. Future experiments shall focus on the latter aspect. One shall visualise cell movements within the affected tissues, by labelling clusters of cells at the gastrulation stage and at the site of convergent extension, by means of fluorescent dye injection into the embryo. By comparison with control embryos, impairements or delays of cell movements shall be detected in the

morphants (Myers et al., 2002a). Alternatively, one shall take advantage of a photoconvertible construct and inject it into the early embryo. A better control of the labelled area, in terms of number of cells labelled and spatial and temporal coordinates of the labelling shall be achieved (Mara et al., 2007). For this purpose, a nls-Kaede construct has been developed and tested in the lab. Time-lapse movies of the photoconverted cells shall be taken, and precise measurements of the distance travelled by the cells shall be recorded, providing a highly detailed assay of cell movements/migration within the tissue of the *Greb1* morphant embryos.

Convergent extension is driven by cell intercalation, and the cells taking part to convergent extension movements become elongated and oriented mediolaterally (Keller, 2002). Using in vivo confocal microscopy of the photoconverted cells, one shall explore and measure whether defective cell shaping and orientation are the basis for the potentially impaired cell movements in the *Greb1* morphants.

It also remains to determine whether *Greb1* genetically interacts with members of the convergent extension pathway. To answer to this question, interaction studies shall be performed by means of morpholino co-injection (i.e. co-injection of the *Greb1* morpholino and of the morpholino of the genes of the convergent extension pathway) or by means of *Greb1* morpholino injection into a mutated background (several mutants of the genes of the convergent extension pathway have been thoroughly described) (Topczewski et al., 2001),(Sepich et al., 2000), (Heisenberg et al., 2000), (Kilian et al., 2003). If *Greb1* interacts with any of the genes of the pathway, co-injection or injection into a mutated background shall result in an enhancement of the convergent extension phenotype for comparison with single morpholino injection or the mutant alone. Severity of the phenotype shall be expressed in terms of morphometric analyses or gene expression studies, to detect changes in tissue size and embryonic axis proportions.

One shall also attempt to explore whether *Greb1* modulates the convergent extension pathway at the protein level, by regulating the intracellular localisation of components of the pathway, including Dsh. In cells taking part to gastrulation movements, Dsh is localised at the cell membrane in response to Fz7 (Wallingford et al., 2000). By taking advantage of a Dsh-GFP construct, and by co-injecting a Fz-7 construct and the *Greb1* morpholino, potential changes in Dsh localisation shall be analysed (e.g

inhibition/alteration of Dsh localisation), providing further insights into the functional importance of *Greb1* within the convergent extension pathway (Carreira-Barbosa et al., 2003).

Ultimately, it seems possible that because *Greb1* is expressed at the gastrulation site at early developmental stages and around the progenitor area at later stages, it plays different roles at different times and places: 1) an early gastrulation role in the margins (i.e. in the convergent extension movements), and a progenitor role in the tail (i.e. in the regulation of axis lengthening). Future experiments shall confirm this hypothesis by separating the two different functions and by circumventing the early gastrulation phenotype, by knocking-down GREB1 at later stages. For example, one shall take advantage of light-activatable morpholinos, that have been recently developed, to allow temporal control of gene expression (Tomasini et al., 2009). By using conditionally active morpholinos, one shall understand whether the late phenotypic changes in the axial structures of *Greb1* morphants are due to impaired progenitor function or whether they represent a consequence of the early gastrulation phenotype.

Chapter 6. Discussion

In this thesis, I have described my investigations into the mechanisms controlling termination of axial elongation and segmentation. My PhD project began with an interest on the generality of the molecular events characterising late avian segmentation stages. In Chapter 3, I showed that termination of axial elongation is associated with progressive decline of signals required for maintenance of axial progenitors, a pool of cells located at the tail end of the embryo which contributes to axial tissues (PSM, somites, neural tube and notochord) as elongation of the body axis proceeds (see Introduction). Because similar observations have been reported for murine embryos (Cambray and Wilson, 2007), these results suggest that a conserved mechanism regulates vertebrate axis length. As signals decline, axial tissues get reduced, implying that depletion of progenitors is imminent. Analogous reduction of tissue size has been described in mouse, fish and snake embryos indicating that the same events concur in termination of axial elongation of different vertebrates (Gomez et al., 2008). Mutations of genes required for axial progenitor maintenance cause severe axial defects, including premature termination of elongation and segmentation (Dubrulle and Pourquie, 2004a, Wilson et al., 2009). Thus, genetic evidence provides a causative link between loss of signals and tissue exhaustion.

It is not known whether signals required for progenitor maintenance are sufficient to maintain unlimited elongation and segmentation of the axis. This question could provide the basis for future experiments. To date, prolonged axial elongation has been observed in mouse mutants of *Hoxb13*, only. The phenotype of these mutants has been associated with over-proliferation in the tissues derived from the tail bud (Economides et al., 2003). One shall combine over-expression of genes known to promote proliferation, maintenance and survival of axial progenitors, such as *Wnt3a, Fgf8* and *Cyp26a1,* by means of viral infection of the late tail region or by means of electroporation using a method for conditional gene expression in chick embryos (Homburger and Fekete, 1996, Sato et al., 2007). If these genes are sufficient to maintain axial growth/elongation, at the morphological level one shall expect to observe increased axis length and formation of supernumerary somites, and downregulation of

RA levels at the molecular level. Recently, Young et al. (2009) have shown that *Hoxb13* is somehow interconnected with *Cyp26a1* and components of the Wnt signalling pathway to regulate tail development, supporting the idea that *Cyp26a1* and *Wnt3a* are good candidates for promoting axis extension.

Periodic somite formation is driven by a molecular oscillator, the segmentation clock (see Introduction). It is possible that a change of the period of the segmentation clock contributes to completion of somitogenesis (e.g. slow down of the clock contributes to completion of somitogenesis, as previous studies have shown that preventing cycli gene expression results in premature completion of somitogenesis) (Ferjentsik et al., 2009). My results (see Chapter 3) suggest that oscillations cease at late avian somitogenesis stages. In support of my study, studies from others have reported that expression of clock genes is lost as somite formation terminates, and that slow down of the segmentation clock reduces somite number (Tenin et al., 2010, Gibb et al., 2009, Schroter and Oates, 2010, Kim et al., 2011).

In Chapter 4, I explored whether the definitive somite number is sensitive to gene dosage by counting somites in mouse embryos that are heterozygous for mutations in genes known to regulate somite formation and axial elongation. Among the heterozygous mutations tested, those of Wnt genes reduce somite number. Thus, it is possible that Wnt gene activity is limiting in determining the final somite number. Previous studies have shown that *β-catenin* gain of function mutants form an enlarged PSM, with cyclic gene expression being maintained as ectopic stripes, supporting the idea that Wnt signalling sustains PSM lengthening (Dunty et al., 2008, Aulehla et al., 2008). It remains to determine whether excessive Wnt signalling prolongs somite formation, leading to supernumerary somites. Heterozygous mutation of *Axin2*, which encodes an inhibitor of the Wnt signalling, does not cause increased somite number, presumably because of redundancy with *Axin1* (Chia and Costantini, 2005). Nevertheless, it would be of interest to analyse somite number in mutants of other antagonists of the Wnt signalling pathway.

I provide evidence that somite number is reduced in mouse mutants of *Wnt5a*, a component of the non-canonical Wnt pathway. This observation contradicts previous studies showing that zebrafish mutants of the non-canonical Wnt pathway form normal

number of somites (Solnica-Krezel et al., 1996). It is possible that this discrepancy reflects differences between the two organisms. In support of my results, Goldman et al. (2000) have reported that mouse *Wnt5a* is expressed in the Ventral Ectodermal Ridge (VER), a region of the tail which contributes to mesoderm formation, and that removal of such region results in reduced somite number. In the mouse (*Wnt5a* homozygous embryos) and in the zebrafish (*Wnt5/*pipetail mutants), *Wnt5a/Wnt5* mutant embryos exhibit shortened body axis, similarly to other mutants of the non-canonical Wnt pathway. This pathway is known to regulate gastrulation movements required for normal convergent extension of the embryonic body axis. Thus, it is possible that *Wnt5a* loss of function causes defective cell movements required for extension of the body axis, and that defective cell movements are responsible for axis shortening (Kilian et al., 2003) (see Introduction).

As discussed in Chapter 5, convergent extension movements contribute to proper axial elongation and somite morphology. Particularly, I show that *Greb1*, a gene expressed at the gastrulation site and later in the progenitor area of various vertebrate embryos, might be required for proper convergent extension in zebrafish. *Greb1* loss of function causes axis shortening and somite mis-shaping. Although my results suggest that *Greb1* regulates movements at gastrulation, similar to components of the non-canonical Wnt pathway, it is not known whether *Greb1* is part of the pathway. To elucidate this, genetic interaction studies shall be performed by means of morpholino co-injection, or morpholino injections into mutant embryos of the convergent extension pathway.

Somitic defects observed in *Greb1* morphant embryos do not result from impaired segmentation clock machinery or somite polarity establishment as judged by in situ hybridisation for cyclic genes, such as *Her1*, and for genes expressed in the anterior and posterior somite compartments, such as *MespA, MespB, PapC* and *MyoD* (Chapter 5).

However, somites of *Greb1* morphants loose their typical chevron shape, a phenotype reminiscent of failed specification of muscle fibres. Loss of chevron shape and failure of muscle type specification occur when Hedgehog signalling is over-activated (Koudijs et al., 2008), implying that Hedgehog signalling is somehow deregulated in *Greb1* embryos, a possibility which deserves more investigations. For example, one shall analyse whether Hedgehog target genes (e.g. *Gli* genes) are induced in *Greb1*

morphants. Injection of *Greb1* morpholino results in *MyoD* induction in the somitic compartment, premising complete conversion of myotome to slow muscle cells versus fast muscle cells (Wolff et al., 2003). Thus, it would be interesting to test this hypothesis by looking at markers of slow muscle differentiation (e.g. *Prdm1*) in *Greb1* morphants (Baxendale et al., 2004). In support of the possibility that a link exists between *Greb1* and Hedgehog signalling, Xu et al. (2006) have identified *Greb1* in a genome wide screen for Hedgehog target genes.

Alternatively, it is possible that Hedgehog signalling is not perturbed in *Greb1* morphants, and that the putative muscle phenotype might be due to defective convergent extension movements (as hypothesized). Consistent with this possibility, Yin et al. (2007) have shown that, although the development of slow muscle fibres is impaired in *knypek;trilobite* double mutants, Hedgehog signalling is not altered. In the *knypek;trilobite* double mutants, the defective convergent extension movements prevent adaxial cells, the precursors of slow muscle fibres, to reach the notochord where they receive the Hedgehog signal necessary for maintaining their identity. Therefore, the *knypek;trilobite* phenotype is due to impaired cell movements, rather than perturbed Hedgehog signalling.

The research described in this thesis supports the notion that the correct dose of key genes is required for maintaining tissue lengthening and somite formation, their deregulation causing premature termination of axial elongation and segmentation. Insights have been provided into the link between cellular events (such as convergent extension) and embryonic processes (such as axial elongation). Further analysis will reveal the genetic interactions and the molecular networks underlying such link.

Reference List

ABU-ABED, S., DOLLE, P., METZGER, D., BECKETT, B., CHAMBON, P. & PETKOVICH, M. 2001. The retinoic acid-metabolizing enzyme, CYP26A1, is essential for normal hindbrain patterning, vertebral identity, and development of posterior structures. *Genes Dev,* 15**,** 226-40.

AERNE, B. & ISH-HOROWICZ, D. 2004. Receptor tyrosine phosphatase psi is required for Delta/Notch signalling and cyclic gene expression in the presomitic mesoderm. *Development,* 131**,** 3391-9.

AKIMENKO, M. A., EKKER, M., WEGNER, J., LIN, W. & WESTERFIELD, M. 1994. Combinatorial expression of three zebrafish genes related to distal-less: part of a homeobox gene code for the head. *J Neurosci,* 14**,** 3475-86.

ALBAZERCHI, A. & STERN, C. D. 2007. A role for the hypoblast (AVE) in the initiation of neural induction, independent of its ability to position the primitive streak. *Dev Biol,* 301**,** 489-503.

AMACHER, S. L., DRAPER, B. W., SUMMERS, B. R. & KIMMEL, C. B. 2002. The zebrafish T-box genes no tail and spadetail are required for development of trunk and tail mesoderm and medial floor plate. *Development,* 129**,** 3311-23.

AULEHLA, A. & POURQUIE, O. 2010. Signaling gradients during paraxial mesoderm development. *Cold Spring Harb Perspect Biol,* 2**,** a000869.

AULEHLA, A., WEHRLE, C., BRAND-SABERI, B., KEMLER, R., GOSSLER, A., KANZLER, B. & HERRMANN, B. G. 2003. Wnt3a plays a major role in the segmentation clock controlling somitogenesis. *Dev Cell,* 4**,** 395-406.

AULEHLA, A., WIEGRAEBE, W., BAUBET, V., WAHL, M. B., DENG, C., TAKETO, M., LEWANDOSKI, M. & POURQUIE, O. 2008. A beta-catenin gradient links the clock and wavefront systems in mouse embryo segmentation. *Nat Cell Biol,* 10**,** 186-93.

BAXENDALE, S., DAVISON, C., MUXWORTHY, C., WOLFF, C., INGHAM, P. W. & ROY, S. 2004. The B-cell maturation factor Blimp-1 specifies vertebrate slow-twitch muscle fiber identity in response to Hedgehog signaling. *Nat Genet,* 36**,** 88-93.

BEDDINGTON, R. S., RASHBASS, P. & WILSON, V. 1992. Brachyury--a gene affecting mouse gastrulation and early organogenesis. *Dev Suppl***,** 157-65.

BESSHO, Y., SAKATA, R., KOMATSU, S., SHIOTA, K., YAMADA, S. & KAGEYAMA, R. 2001. Dynamic expression and essential functions of Hes7 in somite segmentation. *Genes Dev,* 15**,** 2642-7.

BLADER, P., FISCHER, N., GRADWOHL, G., GUILLEMOT, F. & STRAHLE, U. 1997. The activity of neurogenin1 is controlled by local cues in the zebrafish embryo. *Development,* 124**,** 4557-69.

BLENTIC, A., GALE, E. & MADEN, M. 2003. Retinoic acid signalling centres in the avian embryo identified by sites of expression of synthesising and catabolising enzymes. *Dev Dyn,* 227**,** 114-27.

BOLOGNESI, R., FARZANA, L., FISCHER, T. D. & BROWN, S. J. 2008. Multiple Wnt genes are required for segmentation in the short-germ embryo of Tribolium castaneum. *Curr Biol,* 18**,** 1624-9.

BOTTCHER, R. T. & NIEHRS, C. 2005. Fibroblast growth factor signaling during early vertebrate development. *Endocr Rev,* 26**,** 63-77.

BRISCOE, J., PIERANI, A., JESSELL, T. M. & ERICSON, J. 2000. A homeodomain protein code specifies progenitor cell identity and neuronal fate in the ventral neural tube. *Cell,* 101**,** 435-45.

BRONNER-FRASER, M. & FRASER, S. E. 1997. Differentiation of the vertebrate neural tube. *Curr Opin Cell Biol,* 9**,** 885-91.

BUCHBERGER, A., SEIDL, K., KLEIN, C., EBERHARDT, H. & ARNOLD, H. H. 1998. cMeso-1, a novel bHLH transcription factor, is involved in somite formation in chicken embryos. *Dev Biol,* 199**,** 201-15.

BURKE, A. C., NELSON, C. E., MORGAN, B. A. & TABIN, C. 1995. Hox genes and the evolution of vertebrate axial morphology. *Development,* 121**,** 333-46.

CAMBRAY, N. & WILSON, V. 2002. Axial progenitors with extensive potency are localised to the mouse chordoneural hinge. *Development,* 129**,** 4855-66.

CAMBRAY, N. & WILSON, V. 2007. Two distinct sources for a population of maturing axial progenitors. *Development,* 134**,** 2829-40.

CARREIRA-BARBOSA, F., CONCHA, M. L., TAKEUCHI, M., UENO, N., WILSON, S. W. & TADA, M. 2003. Prickle 1 regulates cell movements during gastrulation and neuronal migration in zebrafish. *Development,* 130**,** 4037-46.

CHAWENGSAKSOPHAK, K., JAMES, R., HAMMOND, V. E., KONTGEN, F. & BECK, F. 1997. Homeosis and intestinal tumours in Cdx2 mutant mice. *Nature,* 386**,** 84-7.

CHIA, I. V. & COSTANTINI, F. 2005. Mouse axin and axin2/conductin proteins are functionally equivalent in vivo. *Mol Cell Biol,* 25**,** 4371-6.

CHIANG, C., LITINGTUNG, Y., LEE, E., YOUNG, K. E., CORDEN, J. L., WESTPHAL, H. & BEACHY, P. A. 1996. Cyclopia and defective axial patterning in mice lacking Sonic hedgehog gene function. *Nature,* 383**,** 407-13.

CONLON, R. A. 1995. Retinoic acid and pattern formation in vertebrates. *Trends Genet,* 11**,** 314-9.

CONLON, R. A., REAUME, A. G. & ROSSANT, J. 1995. Notch1 is required for the coordinate segmentation of somites. *Development,* 121**,** 1533-45.

CONNOLLY, D., MCNAUGHTON, L. A., KRUMLAUF, R. & COOKE, J. 1995. Improved in vitro development of the chick embryo using roller-tube culture. *Trends Genet,* 11**,** 259-60.

COOKE, J. & ZEEMAN, E. C. 1976. A clock and wavefront model for control of the number of repeated structures during animal morphogenesis. *J Theor Biol,* 58**,** 455-76.

DAGGETT, D. F., BOYD, C. A., GAUTIER, P., BRYSON-RICHARDSON, R. J., THISSE, C., THISSE, B., AMACHER, S. L. & CURRIE, P. D. 2004. Developmentally restricted actin-regulatory molecules control morphogenetic cell movements in the zebrafish gastrula. *Curr Biol,* 14**,** 1632-8.

DAHMANN, C., OATES, A. C. & BRAND, M. 2011. Boundary formation and maintenance in tissue development. *Nat Rev Genet,* 12**,** 43-55.

DALE, J. K., MAROTO, M., DEQUEANT, M. L., MALAPERT, P., MCGREW, M. & POURQUIE, O. 2003. Periodic notch inhibition by lunatic fringe underlies the chick segmentation clock. *Nature,* 421**,** 275-8.

DAS, R. M., VAN HATEREN, N. J., HOWELL, G. R., FARRELL, E. R., BANGS, F. K., PORTEOUS, V. C., MANNING, E. M., MCGREW, M. J., OHYAMA, K., SACCO, M. A., HALLEY, P. A., SANG, H. M., STOREY, K. G., PLACZEK, M., TICKLE, C., NAIR, V. K. & WILSON, S. A. 2006. A robust system for

RNA interference in the chicken using a modified microRNA operon. *Dev Biol,* 294**,** 554-63.
DAVIS, R. L. & KIRSCHNER, M. W. 2000. The fate of cells in the tailbud of Xenopus laevis. *Development,* 127**,** 255-67.
DELFINI, M. C., DUBRULLE, J., MALAPERT, P., CHAL, J. & POURQUIE, O. 2005. Control of the segmentation process by graded MAPK/ERK activation in the chick embryo. *Proc Natl Acad Sci U S A,* 102**,** 11343-8.
DEQUEANT, M. L., GLYNN, E., GAUDENZ, K., WAHL, M., CHEN, J., MUSHEGIAN, A. & POURQUIE, O. 2006. A complex oscillating network of signaling genes underlies the mouse segmentation clock. *Science,* 314**,** 1595-8.
DEQUEANT, M. L. & POURQUIE, O. 2008. Segmental patterning of the vertebrate embryonic axis. *Nat Rev Genet,* 9**,** 370-82.
DIEZ DEL CORRAL, R., OLIVERA-MARTINEZ, I., GORIELY, A., GALE, E., MADEN, M. & STOREY, K. 2003. Opposing FGF and retinoid pathways control ventral neural pattern, neuronal differentiation, and segmentation during body axis extension. *Neuron,* 40**,** 65-79.
DODD, J., JESSELL, T. M. & PLACZEK, M. 1998. The when and where of floor plate induction. *Science,* 282**,** 1654-7.
DUBRULLE, J., MCGREW, M. J. & POURQUIE, O. 2001. FGF signaling controls somite boundary position and regulates segmentation clock control of spatiotemporal Hox gene activation. *Cell,* 106**,** 219-32.
DUBRULLE, J. & POURQUIE, O. 2004a. Coupling segmentation to axis formation. *Development,* 131**,** 5783-93.
DUBRULLE, J. & POURQUIE, O. 2004b. fgf8 mRNA decay establishes a gradient that couples axial elongation to patterning in the vertebrate embryo. *Nature,* 427**,** 419-22.
DUNTY, W. C., JR., BIRIS, K. K., CHALAMALASETTY, R. B., TAKETO, M. M., LEWANDOSKI, M. & YAMAGUCHI, T. P. 2008. Wnt3a/beta-catenin signaling controls posterior body development by coordinating mesoderm formation and segmentation. *Development,* 135**,** 85-94.
DUNWOODIE, S. L., CLEMENTS, M., SPARROW, D. B., SA, X., CONLON, R. A. & BEDDINGTON, R. S. 2002. Axial skeletal defects caused by mutation in the spondylocostal dysplasia/pudgy gene Dll3 are associated with disruption of the segmentation clock within the presomitic mesoderm. *Development,* 129**,** 1795-806.
DURBIN, L., SORDINO, P., BARRIOS, A., GERING, M., THISSE, C., THISSE, B., BRENNAN, C., GREEN, A., WILSON, S. & HOLDER, N. 2000. Anteroposterior patterning is required within segments for somite boundary formation in developing zebrafish. *Development,* 127**,** 1703-13.
ECONOMIDES, K. D., ZELTSER, L. & CAPECCHI, M. R. 2003. Hoxb13 mutations cause overgrowth of caudal spinal cord and tail vertebrae. *Dev Biol,* 256**,** 317-30.
EVRARD, Y. A., LUN, Y., AULEHLA, A., GAN, L. & JOHNSON, R. L. 1998. lunatic fringe is an essential mediator of somite segmentation and patterning. *Nature,* 394**,** 377-81.
FERJENTSIK, Z., HAYASHI, S., DALE, J. K., BESSHO, Y., HERREMAN, A., DE STROOPER, B., DEL MONTE, G., DE LA POMPA, J. L. & MAROTO, M.

2009. Notch is a critical component of the mouse somitogenesis oscillator and is essential for the formation of the somites. *PLoS Genet,* 5**,** e1000662.

GIAMPIETRO, P. F., DUNWOODIE, S. L., KUSUMI, K., POURQUIE, O., TASSY, O., OFFIAH, A. C., CORNIER, A. S., ALMAN, B. A., BLANK, R. D., RAGGIO, C. L., GLURICH, I. & TURNPENNY, P. D. 2009. Progress in the understanding of the genetic etiology of vertebral segmentation disorders in humans. *Ann N Y Acad Sci,* 1151**,** 38-67.

GIBB, S., ZAGORSKA, A., MELTON, K., TENIN, G., VACCA, I., TRAINOR, P., MAROTO, M. & DALE, J. K. 2009. Interfering with Wnt signalling alters the periodicity of the segmentation clock. *Dev Biol,* 330**,** 21-31.

GOLDMAN, D. C., MARTIN, G. R. & TAM, P. P. 2000. Fate and function of the ventral ectodermal ridge during mouse tail development. *Development,* 127**,** 2113-23.

GOMEZ, C., OZBUDAK, E. M., WUNDERLICH, J., BAUMANN, D., LEWIS, J. & POURQUIE, O. 2008. Control of segment number in vertebrate embryos. *Nature,* 454**,** 335-9.

GRUNEBERG, H. 1958. Genetical studies on the skeleton of the mouse. XXIII. The development of brachyury and anury. *J Embryol Exp Morphol,* 6**,** 424-43.

HALPERN, M. E., HO, R. K., WALKER, C. & KIMMEL, C. B. 1993. Induction of muscle pioneers and floor plate is distinguished by the zebrafish no tail mutation. *Cell,* 75**,** 99-111.

HAMBURGER, V. & HAMILTON, H. L. 1992. A series of normal stages in the development of the chick embryo. 1951. *Dev Dyn,* 195**,** 231-72.

HATADA, Y. & STERN, C. D. 1994. A fate map of the epiblast of the early chick embryo. *Development,* 120**,** 2879-89.

HEISENBERG, C. P., TADA, M., RAUCH, G. J., SAUDE, L., CONCHA, M. L., GEISLER, R., STEMPLE, D. L., SMITH, J. C. & WILSON, S. W. 2000. Silberblick/Wnt11 mediates convergent extension movements during zebrafish gastrulation. *Nature,* 405**,** 76-81.

HENRIQUE, D., ADAM, J., MYAT, A., CHITNIS, A., LEWIS, J. & ISH-HOROWICZ, D. 1995. Expression of a Delta homologue in prospective neurons in the chick. *Nature,* 375**,** 787-90.

HENRY, C. A., HALL, L. A., BURR HILLE, M., SOLNICA-KREZEL, L. & COOPER, M. S. 2000. Somites in zebrafish doubly mutant for knypek and trilobite form without internal mesenchymal cells or compaction. *Curr Biol,* 10**,** 1063-6.

HOFMANN, M., SCHUSTER-GOSSLER, K., WATABE-RUDOLPH, M., AULEHLA, A., HERRMANN, B. G. & GOSSLER, A. 2004. WNT signaling, in synergy with T/TBX6, controls Notch signaling by regulating Dll1 expression in the presomitic mesoderm of mouse embryos. *Genes Dev,* 18**,** 2712-7.

HOLLEY, S. A., JULICH, D., RAUCH, G. J., GEISLER, R. & NUSSLEIN-VOLHARD, C. 2002. her1 and the notch pathway function within the oscillator mechanism that regulates zebrafish somitogenesis. *Development,* 129**,** 1175-83.

HOMBURGER, S. A. & FEKETE, D. M. 1996. High efficiency gene transfer into the embryonic chicken CNS using B-subgroup retroviruses. *Dev Dyn,* 206**,** 112-20.

HORIKAWA, K., ISHIMATSU, K., YOSHIMOTO, E., KONDO, S. & TAKEDA, H. 2006. Noise-resistant and synchronized oscillation of the segmentation clock. *Nature,* 441**,** 719-23.

ITASAKI, N., BEL-VIALAR, S. & KRUMLAUF, R. 1999. 'Shocking' developments in chick embryology: electroporation and in ovo gene expression. *Nat Cell Biol,* 1**,** E203-7.

JESSELL, T. M. 2000. Neuronal specification in the spinal cord: inductive signals and transcriptional codes. *Nat Rev Genet,* 1**,** 20-9.

JESSEN, J. R., TOPCZEWSKI, J., BINGHAM, S., SEPICH, D. S., MARLOW, F., CHANDRASEKHAR, A. & SOLNICA-KREZEL, L. 2002. Zebrafish trilobite identifies new roles for Strabismus in gastrulation and neuronal movements. *Nat Cell Biol,* 4**,** 610-5.

JIANG, Y. J., AERNE, B. L., SMITHERS, L., HADDON, C., ISH-HOROWICZ, D. & LEWIS, J. 2000. Notch signalling and the synchronization of the somite segmentation clock. *Nature,* 408**,** 475-9.

JOUVE, C., PALMEIRIM, I., HENRIQUE, D., BECKERS, J., GOSSLER, A., ISH-HOROWICZ, D. & POURQUIE, O. 2000. Notch signalling is required for cyclic expression of the hairy-like gene HES1 in the presomitic mesoderm. *Development,* 127**,** 1421-9.

KANKI, J. P. & HO, R. K. 1997. The development of the posterior body in zebrafish. *Development,* 124**,** 881-93.

KAWAKAMI, Y., RODRIGUEZ-LEON, J., KOTH, C. M., BUSCHER, D., ITOH, T., RAYA, A., NG, J. K., ESTEBAN, C. R., TAKAHASHI, S., HENRIQUE, D., SCHWARZ, M. F., ASAHARA, H. & IZPISUA BELMONTE, J. C. 2003. MKP3 mediates the cellular response to FGF8 signalling in the vertebrate limb. *Nat Cell Biol,* 5**,** 513-9.

KELLER, P. J., SCHMIDT, A. D., WITTBRODT, J. & STELZER, E. H. 2008. Reconstruction of zebrafish early embryonic development by scanned light sheet microscopy. *Science,* 322**,** 1065-9.

KELLER, R. 2002. Shaping the vertebrate body plan by polarized embryonic cell movements. *Science,* 298**,** 1950-4.

KIBAR, Z., VOGAN, K. J., GROULX, N., JUSTICE, M. J., UNDERHILL, D. A. & GROS, P. 2001. Ltap, a mammalian homolog of Drosophila Strabismus/Van Gogh, is altered in the mouse neural tube mutant Loop-tail. *Nat Genet,* 28**,** 251-5.

KILIAN, B., MANSUKOSKI, H., BARBOSA, F. C., ULRICH, F., TADA, M. & HEISENBERG, C. P. 2003. The role of Ppt/Wnt5 in regulating cell shape and movement during zebrafish gastrulation. *Mech Dev,* 120**,** 467-76.

KIM, W., MATSUI, T., YAMAO, M., ISHIBASHI, M., TAMADA, K., TAKUMI, T., KOHNO, K., OBA, S., ISHII, S., SAKUMURA, Y. & BESSHO, Y. 2011. The period of the somite segmentation clock is sensitive to Notch activity. *Mol Biol Cell,* 22**,** 3541-3549.

KIMMEL, C. B., BALLARD, W. W., KIMMEL, S. R., ULLMANN, B. & SCHILLING, T. F. 1995. Stages of embryonic development of the zebrafish. *Dev Dyn,* 203**,** 253-310.

KIMMEL, C. B., WARGA, R. M. & SCHILLING, T. F. 1990. Origin and organization of the zebrafish fate map. *Development,* 108**,** 581-94.

KNEZEVIC, V., DE SANTO, R. & MACKEM, S. 1997. Two novel chick T-box genes related to mouse Brachyury are expressed in different, non-overlapping mesodermal domains during gastrulation. *Development,* 124**,** 411-9.

KNEZEVIC, V., DE SANTO, R. & MACKEM, S. 1998. Continuing organizer function during chick tail development. *Development,* 125**,** 1791-801.

KOIZUMI, K., NAKAJIMA, M., YUASA, S., SAGA, Y., SAKAI, T., KURIYAMA, T., SHIRASAWA, T. & KOSEKI, H. 2001. The role of presenilin 1 during somite segmentation. *Development,* 128**,** 1391-402.

KOUDIJS, M. J., DEN BROEDER, M. J., GROOT, E. & VAN EEDEN, F. J. 2008. Genetic analysis of the two zebrafish patched homologues identifies novel roles for the hedgehog signaling pathway. *BMC Dev Biol,* 8**,** 15.

KRAUS, F., HAENIG, B. & KISPERT, A. 2001. Cloning and expression analysis of the mouse T-box gene Tbx18. *Mech Dev,* 100**,** 83-6.

KROL, A. J., ROELLIG, D., DEQUEANT, M. L., TASSY, O., GLYNN, E., HATTEM, G., MUSHEGIAN, A., OATES, A. C. & POURQUIE, O. 2011. Evolutionary plasticity of segmentation clock networks. *Development,* 138**,** 2783-92.

KUSUMI, K., SUN, E. S., KERREBROCK, A. W., BRONSON, R. T., CHI, D. C., BULOTSKY, M. S., SPENCER, J. B., BIRREN, B. W., FRANKEL, W. N. & LANDER, E. S. 1998. The mouse pudgy mutation disrupts Delta homologue Dll3 and initiation of early somite boundaries. *Nat Genet,* 19**,** 274-8.

LAI, E. C. 2004. Notch signaling: control of cell communication and cell fate. *Development,* 131**,** 965-73.

LAUFER, E., DAHN, R., OROZCO, O. E., YEO, C. Y., PISENTI, J., HENRIQUE, D., ABBOTT, U. K., FALLON, J. F. & TABIN, C. 1997. Expression of Radical fringe in limb-bud ectoderm regulates apical ectodermal ridge formation. *Nature,* 386**,** 366-73.

LAWSON, A. & SCHOENWOLF, G. C. 2001. New insights into critical events of avian gastrulation. *Anat Rec,* 262**,** 238-52.

LAWSON, K. A., MENESES, J. J. & PEDERSEN, R. A. 1991. Clonal analysis of epiblast fate during germ layer formation in the mouse embryo. *Development,* 113**,** 891-911.

LEWIS, J. 2003. Autoinhibition with transcriptional delay: a simple mechanism for the zebrafish somitogenesis oscillator. *Curr Biol,* 13**,** 1398-408.

LEWIS, J. 2008. From signals to patterns: space, time, and mathematics in developmental biology. *Science,* 322**,** 399-403.

LITTLE, S. C. & MULLINS, M. C. 2009. Bone morphogenetic protein heterodimers assemble heteromeric type I receptor complexes to pattern the dorsoventral axis. *Nat Cell Biol,* 11**,** 637-43.

LUMSDEN, A. & KRUMLAUF, R. 1996. Patterning the vertebrate neuraxis. *Science,* 274**,** 1109-15.

MADEN, M. 2006. Retinoids and spinal cord development. *J Neurobiol,* 66**,** 726-38.

MAKITA, R., MIZUNO, T., KOSHIDA, S., KUROIWA, A. & TAKEDA, H. 1998. Zebrafish wnt11: pattern and regulation of the expression by the yolk cell and No tail activity. *Mech Dev,* 71**,** 165-76.

MANSOUR, S. L., GODDARD, J. M. & CAPECCHI, M. R. 1993. Mice homozygous for a targeted disruption of the proto-oncogene int-2 have developmental defects in the tail and inner ear. *Development,* 117**,** 13-28.

MANSOURI, A., YOKOTA, Y., WEHR, R., COPELAND, N. G., JENKINS, N. A. & GRUSS, P. 1997. Paired-related murine homeobox gene expressed in the developing sclerotome, kidney, and nervous system. *Dev Dyn,* 210**,** 53-65.

MARA, A., SCHROEDER, J., CHALOUNI, C. & HOLLEY, S. A. 2007. Priming, initiation and synchronization of the segmentation clock by deltaD and deltaC. *Nat Cell Biol,* 9**,** 523-30.

MARLOW, F., TOPCZEWSKI, J., SEPICH, D. & SOLNICA-KREZEL, L. 2002. Zebrafish Rho kinase 2 acts downstream of Wnt11 to mediate cell polarity and effective convergence and extension movements. *Curr Biol,* 12**,** 876-84.

MARTIN, B. L. & KIMELMAN, D. 2008. Regulation of canonical Wnt signaling by Brachyury is essential for posterior mesoderm formation. *Dev Cell,* 15**,** 121-33.

MARTIN, B. L. & KIMELMAN, D. 2009. Wnt signaling and the evolution of embryonic posterior development. *Curr Biol,* 19**,** R215-9.

MARTIN, B. L. & KIMELMAN, D. 2010. Brachyury establishes the embryonic mesodermal progenitor niche. *Genes Dev,* 24**,** 2778-83.

MCGREGOR, A. P., PECHMANN, M., SCHWAGER, E. E., FEITOSA, N. M., KRUCK, S., ARANDA, M. & DAMEN, W. G. 2008. Wnt8 is required for growth-zone establishment and development of opisthosomal segments in a spider. *Curr Biol,* 18**,** 1619-23.

MCGREW, M. J., SHERMAN, A., LILLICO, S. G., ELLARD, F. M., RADCLIFFE, P. A., GILHOOLEY, H. J., MITROPHANOUS, K. A., CAMBRAY, N., WILSON, V. & SANG, H. 2008. Localised axial progenitor cell populations in the avian tail bud are not committed to a posterior Hox identity. *Development,* 135**,** 2289-99.

MENDE, M., CHRISTOPHOROU, N. A. & STREIT, A. 2008. Specific and effective gene knock-down in early chick embryos using morpholinos but not pRFPRNAi vectors. *Mech Dev,* 125**,** 947-62.

MINOWADA, G., JARVIS, L. A., CHI, C. L., NEUBUSER, A., SUN, X., HACOHEN, N., KRASNOW, M. A. & MARTIN, G. R. 1999. Vertebrate Sprouty genes are induced by FGF signaling and can cause chondrodysplasia when overexpressed. *Development,* 126**,** 4465-75.

MOMOSE, T., TONEGAWA, A., TAKEUCHI, J., OGAWA, H., UMESONO, K. & YASUDA, K. 1999. Efficient targeting of gene expression in chick embryos by microelectroporation. *Dev Growth Differ,* 41**,** 335-44.

MOON, R. T., CAMPBELL, R. M., CHRISTIAN, J. L., MCGREW, L. L., SHIH, J. & FRASER, S. 1993. Xwnt-5A: a maternal Wnt that affects morphogenetic movements after overexpression in embryos of Xenopus laevis. *Development,* 119**,** 97-111.

MORENO, T. A. & KINTNER, C. 2004. Regulation of segmental patterning by retinoic acid signaling during Xenopus somitogenesis. *Dev Cell,* 6**,** 205-18.

MORIMOTO, M., SASAKI, N., OGINUMA, M., KISO, M., IGARASHI, K., AIZAKI, K., KANNO, J. & SAGA, Y. 2007. The negative regulation of Mesp2 by mouse Ripply2 is required to establish the rostro-caudal patterning within a somite. *Development,* 134**,** 1561-9.

MYERS, D. C., SEPICH, D. S. & SOLNICA-KREZEL, L. 2002a. Bmp activity gradient regulates convergent extension during zebrafish gastrulation. *Dev Biol,* 243**,** 81-98.

MYERS, D. C., SEPICH, D. S. & SOLNICA-KREZEL, L. 2002b. Convergence and extension in vertebrate gastrulae: cell movements according to or in search of identity? *Trends Genet,* 18**,** 447-55.

NAKAJIMA, Y., MORIMOTO, M., TAKAHASHI, Y., KOSEKI, H. & SAGA, Y. 2006. Identification of Epha4 enhancer required for segmental expression and the regulation by Mesp2. *Development,* 133**,** 2517-25.

NASEVICIUS, A. & EKKER, S. C. 2000. Effective targeted gene 'knockdown' in zebrafish. *Nat Genet,* 26**,** 216-20.

NIEDERREITHER, K., MCCAFFERY, P., DRAGER, U. C., CHAMBON, P. & DOLLE, P. 1997. Restricted expression and retinoic acid-induced downregulation of the retinaldehyde dehydrogenase type 2 (RALDH-2) gene during mouse development. *Mech Dev,* 62**,** 67-78.

NIEDERREITHER, K., SUBBARAYAN, V., DOLLE, P. & CHAMBON, P. 1999. Embryonic retinoic acid synthesis is essential for early mouse post-implantation development. *Nat Genet,* 21**,** 444-8.

NIEDERREITHER, K., VERMOT, J., SCHUHBAUR, B., CHAMBON, P. & DOLLE, P. 2002. Embryonic retinoic acid synthesis is required for forelimb growth and anteroposterior patterning in the mouse. *Development,* 129**,** 3563-74.

NIKAIDO, M., KAWAKAMI, A., SAWADA, A., FURUTANI-SEIKI, M., TAKEDA, H. & ARAKI, K. 2002. Tbx24, encoding a T-box protein, is mutated in the zebrafish somite-segmentation mutant fused somites. *Nat Genet,* 31**,** 195-9.

NIWA, Y., MASAMIZU, Y., LIU, T., NAKAYAMA, R., DENG, C. X. & KAGEYAMA, R. 2007. The initiation and propagation of Hes7 oscillation are cooperatively regulated by Fgf and notch signaling in the somite segmentation clock. *Dev Cell,* 13**,** 298-304.

OATES, A. C. & HO, R. K. 2002. Hairy/E(spl)-related (Her) genes are central components of the segmentation oscillator and display redundancy with the Delta/Notch signaling pathway in the formation of anterior segmental boundaries in the zebrafish. *Development,* 129**,** 2929-46.

OATES, A. C., MORELLI, L. G. & ARES, S. 2012. Patterning embryos with oscillations: structure, function and dynamics of the vertebrate segmentation clock. *Development,* 139**,** 625-39.

OGINUMA, M., NIWA, Y., CHAPMAN, D. L. & SAGA, Y. 2008. Mesp2 and Tbx6 cooperatively create periodic patterns coupled with the clock machinery during mouse somitogenesis. *Development,* 135**,** 2555-62.

OHTA, S., SUZUKI, K., TACHIBANA, K., TANAKA, H. & YAMADA, G. 2007. Cessation of gastrulation is mediated by suppression of epithelial-mesenchymal transition at the ventral ectodermal ridge. *Development,* 134**,** 4315-24.

OTTO, D. M., HENDERSON, C. J., CARRIE, D., DAVEY, M., GUNDERSEN, T. E., BLOMHOFF, R., ADAMS, R. H., TICKLE, C. & WOLF, C. R. 2003. Identification of novel roles of the cytochrome p450 system in early embryogenesis: effects on vasculogenesis and retinoic Acid homeostasis. *Mol Cell Biol,* 23**,** 6103-16.

PALMEIRIM, I., HENRIQUE, D., ISH-HOROWICZ, D. & POURQUIE, O. 1997. Avian hairy gene expression identifies a molecular clock linked to vertebrate segmentation and somitogenesis. *Cell,* 91**,** 639-48.

PARK, M. & MOON, R. T. 2002. The planar cell-polarity gene stbm regulates cell behaviour and cell fate in vertebrate embryos. *Nat Cell Biol,* 4**,** 20-5.

PLACZEK, M., TESSIER-LAVIGNE, M., YAMADA, T., JESSELL, T. & DODD, J. 1990. Mesodermal control of neural cell identity: floor plate induction by the notochord. *Science,* 250**,** 985-8.

POURQUIE, O. 2011. Vertebrate segmentation: from cyclic gene networks to scoliosis. *Cell,* 145**,** 650-63.

RESENDE, T. P., FERREIRA, M., TEILLET, M. A., TAVARES, A. T., ANDRADE, R. P. & PALMEIRIM, I. 2010. Sonic hedgehog in temporal control of somite formation. *Proc Natl Acad Sci U S A,* 107**,** 12907-12.

ROBU, M. E., LARSON, J. D., NASEVICIUS, A., BEIRAGHI, S., BRENNER, C., FARBER, S. A. & EKKER, S. C. 2007. p53 activation by knockdown technologies. *PLoS Genet,* 3**,** e78.

ROELINK, H., AUGSBURGER, A., HEEMSKERK, J., KORZH, V., NORLIN, S., RUIZ I ALTABA, A., TANABE, Y., PLACZEK, M., EDLUND, T., JESSELL, T. M. & ET AL. 1994. Floor plate and motor neuron induction by vhh-1, a vertebrate homolog of hedgehog expressed by the notochord. *Cell,* 76**,** 761-75.

ROELLIG, D., MORELLI, L. G., ARES, S., JULICHER, F. & OATES, A. C. 2011. SnapShot: the segmentation clock. *Cell,* 145**,** 800-800 e1.

ROSSANT, J., ZIRNGIBL, R., CADO, D., SHAGO, M. & GIGUERE, V. 1991. Expression of a retinoic acid response element-hsplacZ transgene defines specific domains of transcriptional activity during mouse embryogenesis. *Genes Dev,* 5**,** 1333-44.

SAGA, Y. 1998. Genetic rescue of segmentation defect in MesP2-deficient mice by MesP1 gene replacement. *Mech Dev,* 75**,** 53-66.

SAGA, Y. 2007. Segmental border is defined by the key transcription factor Mesp2, by means of the suppression of Notch activity. *Dev Dyn,* 236**,** 1450-5.

SAGA, Y., HATA, N., KOBAYASHI, S., MAGNUSON, T., SELDIN, M. F. & TAKETO, M. M. 1996. MesP1: a novel basic helix-loop-helix protein expressed in the nascent mesodermal cells during mouse gastrulation. *Development,* 122**,** 2769-78.

SAGA, Y., HATA, N., KOSEKI, H. & TAKETO, M. M. 1997. Mesp2: a novel mouse gene expressed in the presegmented mesoderm and essential for segmentation initiation. *Genes Dev,* 11**,** 1827-39.

SAGA, Y. & TAKAHASHI, Y. 2008. Mesp-family genes are required for segmental patterning and segmental border formation. *Adv Exp Med Biol,* 638**,** 113-23.

SAGA, Y. & TAKEDA, H. 2001. The making of the somite: molecular events in vertebrate segmentation. *Nat Rev Genet,* 2**,** 835-45.

SAIKI, R. K., GELFAND, D. H., STOFFEL, S., SCHARF, S. J., HIGUCHI, R., HORN, G. T., MULLIS, K. B. & ERLICH, H. A. 1988. Primer-directed enzymatic amplification of DNA with a thermostable DNA polymerase. *Science,* 239**,** 487-91.

SAKAI, Y., MENO, C., FUJII, H., NISHINO, J., SHIRATORI, H., SAIJOH, Y., ROSSANT, J. & HAMADA, H. 2001. The retinoic acid-inactivating enzyme CYP26 is essential for establishing an uneven distribution of retinoic acid along the anterio-posterior axis within the mouse embryo. *Genes Dev,* 15**,** 213-25.

SANDERS, E. J., KHARE, M. K., OOI, V. C. & BELLAIRS, R. 1986. An experimental and morphological analysis of the tail bud mesenchyme of the chick embryo. *Anat Embryol (Berl),* 174**,** 179-85.

SASSOON, D., LYONS, G., WRIGHT, W. E., LIN, V., LASSAR, A., WEINTRAUB, H. & BUCKINGHAM, M. 1989. Expression of two myogenic regulatory factors myogenin and MyoD1 during mouse embryogenesis. *Nature,* 341**,** 303-7.

SATO, Y., KASAI, T., NAKAGAWA, S., TANABE, K., WATANABE, T., KAWAKAMI, K. & TAKAHASHI, Y. 2007. Stable integration and conditional expression of electroporated transgenes in chicken embryos. *Dev Biol,* 305**,** 616-24.

SAVORY, J. G., BOUCHARD, N., PIERRE, V., RIJLI, F. M., DE REPENTIGNY, Y., KOTHARY, R. & LOHNES, D. 2009. Cdx2 regulation of posterior development through non-Hox targets. *Development,* 136**,** 4099-110.

SAVORY, J. G., MANSFIELD, M., RIJLI, F. M. & LOHNES, D. 2011. Cdx mediates neural tube closure through transcriptional regulation of the planar cell polarity gene Ptk7. *Development,* 138**,** 1361-70.

SAWADA, A., FRITZ, A., JIANG, Y. J., YAMAMOTO, A., YAMASU, K., KUROIWA, A., SAGA, Y. & TAKEDA, H. 2000. Zebrafish Mesp family genes, mesp-a and mesp-b are segmentally expressed in the presomitic mesoderm, and Mesp-b confers the anterior identity to the developing somites. *Development,* 127**,** 1691-702.

SCHROTER, C. & OATES, A. C. 2010. Segment number and axial identity in a segmentation clock period mutant. *Curr Biol,* 20**,** 1254-8.

SCHULTE-MERKER, S., HO, R. K., HERRMANN, B. G. & NUSSLEIN-VOLHARD, C. 1992. The protein product of the zebrafish homologue of the mouse T gene is expressed in nuclei of the germ ring and the notochord of the early embryo. *Development,* 116**,** 1021-32.

SELLECK, M. A. & STERN, C. D. 1991. Fate mapping and cell lineage analysis of Hensen's node in the chick embryo. *Development,* 112**,** 615-26.

SEPICH, D. S., MYERS, D. C., SHORT, R., TOPCZEWSKI, J., MARLOW, F. & SOLNICA-KREZEL, L. 2000. Role of the zebrafish trilobite locus in gastrulation movements of convergence and extension. *Genesis,* 27**,** 159-73.

SEWELL, W. & KUSUMI, K. 2007. Genetic analysis of molecular oscillators in mammalian somitogenesis: clues for studies of human vertebral disorders. *Birth Defects Res C Embryo Today,* 81**,** 111-20.

SHUM, A. S., POON, L. L., TANG, W. W., KOIDE, T., CHAN, B. W., LEUNG, Y. C., SHIROISHI, T. & COPP, A. J. 1999. Retinoic acid induces down-regulation of Wnt-3a, apoptosis and diversion of tail bud cells to a neural fate in the mouse embryo. *Mech Dev,* 84**,** 17-30.

SOLNICA-KREZEL, L. 2005. Conserved patterns of cell movements during vertebrate gastrulation. *Curr Biol,* 15**,** R213-28.

SOLNICA-KREZEL, L., STEMPLE, D. L., MOUNTCASTLE-SHAH, E., RANGINI, Z., NEUHAUSS, S. C., MALICKI, J., SCHIER, A. F., STAINIER, D. Y., ZWARTKRUIS, F., ABDELILAH, S. & DRIEVER, W. 1996. Mutations affecting cell fates and cellular rearrangements during gastrulation in zebrafish. *Development,* 123**,** 67-80.

SPARROW, D. B., JEN, W. C., KOTECHA, S., TOWERS, N., KINTNER, C. & MOHUN, T. J. 1998. Thylacine 1 is expressed segmentally within the paraxial mesoderm of the Xenopus embryo and interacts with the Notch pathway. *Development,* 125**,** 2041-51.

STAMATAKI, D., ULLOA, F., TSONI, S. V., MYNETT, A. & BRISCOE, J. 2005. A gradient of Gli activity mediates graded Sonic Hedgehog signaling in the neural tube. *Genes Dev,* 19**,** 626-41.

STAUBER, M., SACHIDANANDAN, C., MORGENSTERN, C. & ISH-HOROWICZ, D. 2009. Differential axial requirements for lunatic fringe and Hes7 transcription during mouse somitogenesis. *PLoS One,* 4**,** e7996.

STEMPLE, D. L. 2005. Structure and function of the notochord: an essential organ for chordate development. *Development,* 132**,** 2503-12.

STEMPLE, D. L., SOLNICA-KREZEL, L., ZWARTKRUIS, F., NEUHAUSS, S. C., SCHIER, A. F., MALICKI, J., STAINIER, D. Y., ABDELILAH, S., RANGINI, Z., MOUNTCASTLE-SHAH, E. & DRIEVER, W. 1996. Mutations affecting development of the notochord in zebrafish. *Development,* 123**,** 117-28.

STERN, C. D. 1998. Detection of multiple gene products simultaneously by in situ hybridization and immunohistochemistry in whole mounts of avian embryos. *Curr Top Dev Biol,* 36**,** 223-43.

STOLLEWERK, A., SCHOPPMEIER, M. & DAMEN, W. G. 2003. Involvement of Notch and Delta genes in spider segmentation. *Nature,* 423**,** 863-5.

SUMANAS, S., KIM, H. J., HERMANSON, S. & EKKER, S. C. 2001. Zebrafish frizzled-2 morphant displays defects in body axis elongation. *Genesis,* 30**,** 114-8.

SUN, X., MEYERS, E. N., LEWANDOSKI, M. & MARTIN, G. R. 1999. Targeted disruption of Fgf8 causes failure of cell migration in the gastrulating mouse embryo. *Genes Dev,* 13**,** 1834-46.

SWINDELL, E. C., THALLER, C., SOCKANATHAN, S., PETKOVICH, M., JESSELL, T. M. & EICHELE, G. 1999. Complementary domains of retinoic acid production and degradation in the early chick embryo. *Dev Biol,* 216**,** 282-96.

TADA, M. & KAI, M. 2009. Noncanonical Wnt/PCP signaling during vertebrate gastrulation. *Zebrafish,* 6**,** 29-40.

TAKADA, S., STARK, K. L., SHEA, M. J., VASSILEVA, G., MCMAHON, J. A. & MCMAHON, A. P. 1994. Wnt-3a regulates somite and tailbud formation in the mouse embryo. *Genes Dev,* 8**,** 174-89.

TAKAHASHI, J., OHBAYASHI, A., OGINUMA, M., SAITO, D., MOCHIZUKI, A., SAGA, Y. & TAKADA, S. 2010. Analysis of Ripply1/2-deficient mouse embryos reveals a mechanism underlying the rostro-caudal patterning within a somite. *Dev Biol,* 342**,** 134-45.

TAKAHASHI, Y., INOUE, T., GOSSLER, A. & SAGA, Y. 2003. Feedback loops comprising Dll1, Dll3 and Mesp2, and differential involvement of Psen1 are essential for rostrocaudal patterning of somites. *Development,* 130**,** 4259-68.

TAKAHASHI, Y., KOIZUMI, K., TAKAGI, A., KITAJIMA, S., INOUE, T., KOSEKI, H. & SAGA, Y. 2000. Mesp2 initiates somite segmentation through the Notch signalling pathway. *Nat Genet,* 25**,** 390-6.

TAKKE, C. & CAMPOS-ORTEGA, J. A. 1999. her1, a zebrafish pair-rule like gene, acts downstream of notch signalling to control somite development. *Development,* 126**,** 3005-14.

TAM, P. P. 1981. The control of somitogenesis in mouse embryos. *J Embryol Exp Morphol,* 65 Suppl**,** 103-28.

TENIN, G., WRIGHT, D., FERJENTSIK, Z., BONE, R., MCGREW, M. J. & MAROTO, M. 2010. The chick somitogenesis oscillator is arrested before all paraxial mesoderm is segmented into somites. *BMC Dev Biol,* 10**,** 24.

TOMASINI, A. J., SCHULER, A. D., ZEBALA, J. A. & MAYER, A. N. 2009. PhotoMorphs: a novel light-activated reagent for controlling gene expression in zebrafish. *Genesis,* 47**,** 736-43.

TONEGAWA, A. & TAKAHASHI, Y. 1998. Somitogenesis controlled by Noggin. *Dev Biol,* 202**,** 172-82.

TOPCZEWSKI, J., SEPICH, D. S., MYERS, D. C., WALKER, C., AMORES, A., LELE, Z., HAMMERSCHMIDT, M., POSTLETHWAIT, J. & SOLNICA-KREZEL, L. 2001. The zebrafish glypican knypek controls cell polarity during gastrulation movements of convergent extension. *Dev Cell,* 1**,** 251-64.

TURNPENNY, P. D., ALMAN, B., CORNIER, A. S., GIAMPIETRO, P. F., OFFIAH, A., TASSY, O., POURQUIE, O., KUSUMI, K. & DUNWOODIE, S. 2007. Abnormal vertebral segmentation and the notch signaling pathway in man. *Dev Dyn,* 236**,** 1456-74.

TZOUANACOU, E., WEGENER, A., WYMEERSCH, F. J., WILSON, V. & NICOLAS, J. F. 2009. Redefining the progression of lineage segregations during mammalian embryogenesis by clonal analysis. *Dev Cell,* 17**,** 365-76.

VAN EEDEN, F. J., GRANATO, M., SCHACH, U., BRAND, M., FURUTANI-SEIKI, M., HAFFTER, P., HAMMERSCHMIDT, M., HEISENBERG, C. P., JIANG, Y. J., KANE, D. A., KELSH, R. N., MULLINS, M. C., ODENTHAL, J., WARGA, R. M., ALLENDE, M. L., WEINBERG, E. S. & NUSSLEIN-VOLHARD, C. 1996. Mutations affecting somite formation and patterning in the zebrafish, Danio rerio. *Development,* 123**,** 153-64.

VERMOT, J. & POURQUIE, O. 2005. Retinoic acid coordinates somitogenesis and left-right patterning in vertebrate embryos. *Nature,* 435**,** 215-20.

VOICULESCU, O., PAPANAYOTOU, C. & STERN, C. D. 2008. Spatially and temporally controlled electroporation of early chick embryos. *Nat Protoc,* 3**,** 419-26.

WAHL, M. B., DENG, C., LEWANDOSKI, M. & POURQUIE, O. 2007. FGF signaling acts upstream of the NOTCH and WNT signaling pathways to control segmentation clock oscillations in mouse somitogenesis. *Development,* 134**,** 4033-41.

WALLINGFORD, J. B., ROWNING, B. A., VOGELI, K. M., ROTHBACHER, U., FRASER, S. E. & HARLAND, R. M. 2000. Dishevelled controls cell polarity during Xenopus gastrulation. *Nature,* 405**,** 81-5.

WEINBERG, E. S., ALLENDE, M. L., KELLY, C. S., ABDELHAMID, A., MURAKAMI, T., ANDERMANN, P., DOERRE, O. G., GRUNWALD, D. J. & RIGGLEMAN, B. 1996. Developmental regulation of zebrafish MyoD in wild-type, no tail and spadetail embryos. *Development,* 122**,** 271-80.

WEISER, D. C., PYATI, U. J. & KIMELMAN, D. 2007. Gravin regulates mesodermal cell behavior changes required for axis elongation during zebrafish gastrulation. *Genes Dev,* 21**,** 1559-71.

WENINGER, W. J., GEYER, S. H., MOHUN, T. J., RASSKIN-GUTMAN, D., MATSUI, T., RIBEIRO, I., COSTA LDA, F., IZPISUA-BELMONTE, J. C. & MULLER, G. B. 2006. High-resolution episcopic microscopy: a rapid technique for high detailed 3D analysis of gene activity in the context of tissue architecture and morphology. *Anat Embryol (Berl),* 211**,** 213-21.

WILKINSON, D. G., BHATT, S. & HERRMANN, B. G. 1990. Expression pattern of the mouse T gene and its role in mesoderm formation. *Nature,* 343**,** 657-9.

WILSON, V. & BEDDINGTON, R. S. 1996. Cell fate and morphogenetic movement in the late mouse primitive streak. *Mech Dev,* 55**,** 79-89.

WILSON, V., OLIVERA-MARTINEZ, I. & STOREY, K. G. 2009. Stem cells, signals and vertebrate body axis extension. *Development,* 136**,** 1591-604.

WINNIER, G., BLESSING, M., LABOSKY, P. A. & HOGAN, B. L. 1995. Bone morphogenetic protein-4 is required for mesoderm formation and patterning in the mouse. *Genes Dev,* 9**,** 2105-16.

WOLFF, C., ROY, S. & INGHAM, P. W. 2003. Multiple muscle cell identities induced by distinct levels and timing of hedgehog activity in the zebrafish embryo. *Curr Biol,* 13**,** 1169-81.

WRIGHT, D., FERJENTSIK, Z., CHONG, S. W., QIU, X., JIANG, Y. J., MALAPERT, P., POURQUIE, O., VAN HATEREN, N., WILSON, S. A., FRANCO, C., GERHARDT, H., DALE, J. K. & MAROTO, M. 2009. Cyclic Nrarp mRNA expression is regulated by the somitic oscillator but Nrarp protein levels do not oscillate. *Dev Dyn,* 238**,** 3043-55.

WU, M. Y., RAMEL, M. C., HOWELL, M. & HILL, C. S. 2011. SNW1 is a critical regulator of spatial BMP activity, neural plate border formation, and neural crest specification in vertebrate embryos. *PLoS Biol,* 9**,** e1000593.

XU, J., SRINIVAS, B. P., TAY, S. Y., MAK, A., YU, X., LEE, S. G., YANG, H., GOVINDARAJAN, K. R., LEONG, B., BOURQUE, G., MATHAVAN, S. & ROY, S. 2006. Genomewide expression profiling in the zebrafish embryo identifies target genes regulated by Hedgehog signaling during vertebrate development. *Genetics,* 174**,** 735-52.

YAMAGUCHI, T. P., BRADLEY, A., MCMAHON, A. P. & JONES, S. 1999. A Wnt5a pathway underlies outgrowth of multiple structures in the vertebrate embryo. *Development,* 126**,** 1211-23.

YAMAGUCHI, T. P., HARPAL, K., HENKEMEYER, M. & ROSSANT, J. 1994. fgfr-1 is required for embryonic growth and mesodermal patterning during mouse gastrulation. *Genes Dev,* 8**,** 3032-44.

YAMAMOTO, A., AMACHER, S. L., KIM, S. H., GEISSERT, D., KIMMEL, C. B. & DE ROBERTIS, E. M. 1998. Zebrafish paraxial protocadherin is a downstream target of spadetail involved in morphogenesis of gastrula mesoderm. *Development,* 125**,** 3389-97.

YASUHIKO, Y., HARAGUCHI, S., KITAJIMA, S., TAKAHASHI, Y., KANNO, J. & SAGA, Y. 2006. Tbx6-mediated Notch signaling controls somite-specific Mesp2 expression. *Proc Natl Acad Sci U S A,* 103**,** 3651-6.

YIN, C. & SOLNICA-KREZEL, L. 2007. Convergence and extension movements mediate the specification and fate maintenance of zebrafish slow muscle precursors. *Dev Biol,* 304**,** 141-55.

YOON, J. K. & WOLD, B. 2000. The bHLH regulator pMesogenin1 is required for maturation and segmentation of paraxial mesoderm. *Genes Dev,* 14**,** 3204-14.

YOUNG, T., ROWLAND, J. E., VAN DE VEN, C., BIALECKA, M., NOVOA, A., CARAPUCO, M., VAN NES, J., DE GRAAFF, W., DULUC, I., FREUND, J. N., BECK, F., MALLO, M. & DESCHAMPS, J. 2009. Cdx and Hox genes differentially regulate posterior axial growth in mammalian embryos. *Dev Cell,* 17**,** 516-26.

ZENG, L., FAGOTTO, F., ZHANG, T., HSU, W., VASICEK, T. J., PERRY, W. L., 3RD, LEE, J. J., TILGHMAN, S. M., GUMBINER, B. M. & COSTANTINI, F.

1997. The mouse Fused locus encodes Axin, an inhibitor of the Wnt signaling pathway that regulates embryonic axis formation. *Cell,* 90**,** 181-92.